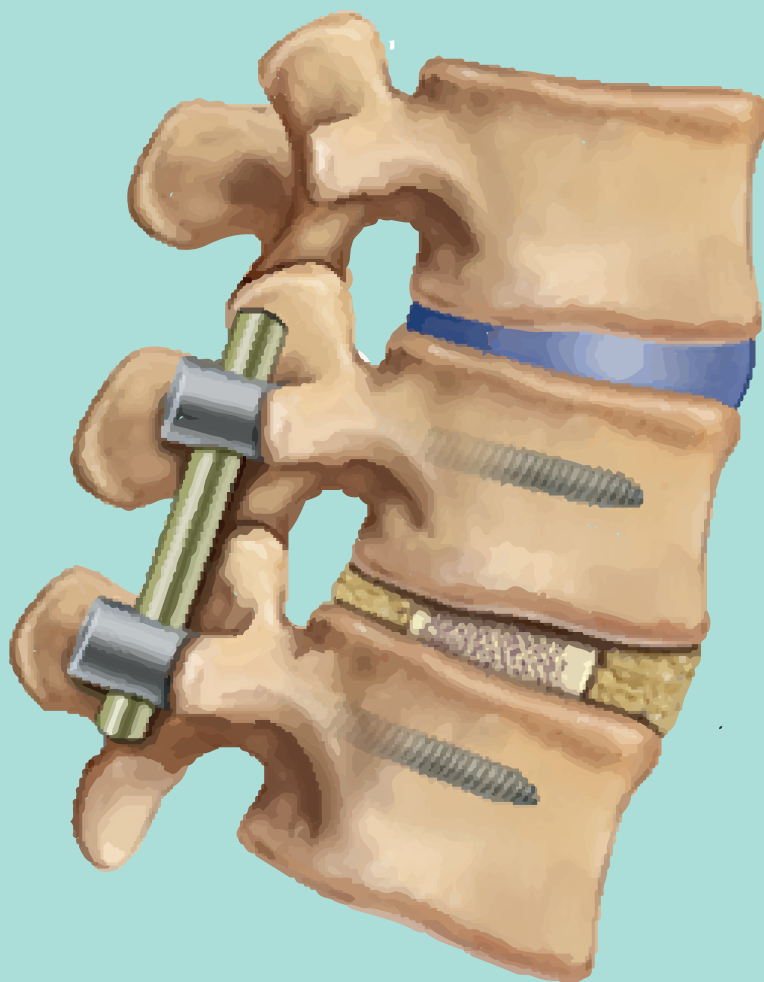


Applicability of Diffuse Reflectance Spectroscopy in accurate guidance of pedicle screws

Master Thesis



STUDENT | Akash Swamy
(4417682)

DATE | August 2016

SUPERVISION | Prof. Dr. J. Dankelman

Prof. Dr. B. H. W. Hendriks

Dr. Drazenko Babic

 **TU Delft**

PHILIPS

“Thanks to my solid academic training, today I can write hundreds of words on virtually any topic without possessing a shred of information, which is how I got a good job in journalism.”

Dave Barry

Contents

1	Project strategy	1
1.0.1	Research Objectives	2
	The clinical investigation	2
	The technical investigation	2
I	Phase 1 research: The clinical investigation	3
2	Is inaccuracy in pedicle screw placement a clinically relevant problem?	5
2.1	Abstract	5
2.2	Introduction	5
2.2.1	Spine anatomy	6
	Intervertebral disc	7
2.2.2	Spine Fusion Surgery	7
2.2.3	Reasons for Spine Instrumentation	9
2.2.4	Screw Insertion in Spinal Fusion surgery	10
2.3	Materials and methods	10
2.3.1	Scientific literature	10
2.3.2	Clinical perspective: Surgeons interviews	11
2.3.3	Market	11
2.4	State of art in pedicle screw placement	11
2.4.1	Pedicle screw placement techniques: A workflow analysis	11
	Free hand technique	11
	2D fluoroscopy-guided technique	12
	Computer-assisted technique	17
	Electrical conductivity measurement technique	21
	Neurophysiological monitoring technique	22
	Discussion	29
	Conclusion	29
2.4.2	Challenges in pedicle screw placement surgical procedure	29
	Breach definition problem	30
	Pedicle screw placement accuracy: Analysis of literature	31
	Dangers of radiation	34
	Pedicle screw-related complication rate: Analysis of literature	34
	Discussion	36
	Conclusion	37
2.4.3	Pedicle screw placement guidance techniques: A Trade-off analysis	38
	Conventional techniques	38
	3D Computer-assisted technique	40
	Assistive devices	40
	Surgeons interviews: Survey questionnaire of 67 spine surgeons	42
	Spinal fusion market analysis	44
2.4.4	Design requirements	45
2.5	Discussion	46
2.6	Conclusion	47
2.6.1	Secondary clinical research questions	47
2.6.2	Primary clinical research question	47

II	Phase 2 research: The technical investigation	49
3	Fundamental background into Diffuse Reflectance Spectroscopy	51
3.1	Absorption	51
3.2	Scattering	52
3.3	The measurement setup	52
3.4	Analysis of the spectra	53
	Diffusion theory fit model	54
4	The experimental investigation	57
4.1	Geometry mapping experiment of <i>ex vivo</i> swine vertebral tissue	57
4.1.1	Abstract	57
4.1.2	Introduction	57
4.1.3	Materials and methods	61
4.1.4	Results	62
	Structural features of bone and spinal canal	63
	Thickness of cortical bone	63
4.1.5	Discussion	64
4.1.6	Conclusion	65
4.2	Optical mapping experiment of <i>ex vivo</i> swine vertebral tissue	66
4.2.1	Abstract	66
4.2.2	Introduction	66
	Composition of bone	66
	Contents of epidural space	67
4.2.3	Materials and methods	67
	Experiment setup	67
	Experiment methods	68
	Statistical analysis	68
4.2.4	Results	69
4.2.5	Discussion	72
4.2.6	Conclusion	73
5	The simulation investigation: Building the Monte-Carlo model	75
5.1	Effect of fat concentration on insertion depth of the optical probe in vertebral swine tissue	75
5.1.1	Abstract	75
5.1.2	Introduction	75
	Fundamental background	75
	Optical properties of bone and spinal canal	78
5.1.3	Materials and methods	79
	Model input parameters	79
	Model geometry conventions	79
	Data Processing	80
	Validation protocol	81
	Multilayer geometry development	82
5.1.4	Results	82
	Model Validation	82
	Analysis of change in fat chromophore concentration during a medial breach scenario	83
5.1.5	Discussion	85
	Model Assumptions	86
5.1.6	Conclusion	86

6 Overall Conclusion	87
6.1 The clinical investigation	87
6.1.1 Secondary research questions	87
6.1.2 Primary research question	87
6.2 The technical investigation	88
6.2.1 Primary research question	88
Bibliography	89

List of Figures

1.1	Project strategy	1
2.1	Regions of the spine. Figure from [46]	6
2.2	Various views depicting the spine anatomy. Figure from [46]	7
2.3	Surgical treatment of herniated disc disease	8
2.4	Surgical workflow of Scoliosis surgery	9
2.5	Instrumentation for stabilization. Figure from [117]	9
2.6	Instrumentation for correction. Figure from [126]	9
2.7	Pedicle probe. Figure from [88]	12
2.8	Pedicle cannulation. Figure from [46]	12
2.9	Surgical workflow of Free-hand technique	13
2.10	Lateral and oblique 2D fluoroscopic views of lumbar spine during PSP. Figure from [12]	14
2.11	Cannulated Jamshidi needle. Figure from [3]	14
2.12	Surgical workflow of 2D fluoroscopic guided technique (Open)	15
2.13	Surgical workflow of 2D fluoroscopic guided technique (MIS)	16
2.14	Instrument with trackers used in CAS technique. Figure from [94]	17
2.15	Pedicle cannulation being performed using a Jamshidi needle with the aid of navigation. Figure from [12]	18
2.16	Surgical workflow of computer-assisted technique (Open)	19
2.17	Surgical workflow of computer-assisted technique (MIS)	20
2.18	Working principle of electrical conductivity measuring device. Figure from [50]	21
2.19	Electrical conductivity measurement device for open procedures. Figure from [50]	21
2.20	Electrical conductivity measurement device for MIS procedures. Figure from [50]	22
2.21	Surgical workflow of Electrical conductivity measurement technique (Open)	23
2.22	Surgical workflow of Electrical conductivity measurement technique (MIS)	24
2.23	Intraoperative monitoring using neuromonitoring system. Figure from [74]	25
2.24	Intraoperative monitoring using neuromonitoring system. Figure from [74]	25
2.25	Design modification of stimulation electrodes for MIS procedures	26
2.26	Surgical workflow of neurophysiological monitoring technique (Open)	27
2.27	Surgical workflow of neurophysiological monitoring technique (MIS)	28
2.28	Structural classification of pedicle screw placement techniques	29
2.29	Axial and coronal CT images illustrating various screw positions corresponding to breach definition of type 1. Figure from [82].	30
2.30	Anatomical grading system based on medial, lateral, superior, inferior or anterior screw penetration.	30
2.31	CT scans of severely malpositioned screws without patients suffering from neurological or vascular deficits. Screws not revised. Figures from [34]	35
2.32	CT scan showing an axial view of a right medially misplaced screw in L-4, which caused new on-set radiculopathy. Symptoms disappeared after screw replacement. Figure from [34].	35
2.33	Median accuracy and range for conventional techniques. (Error bars indicate min and max accuracy rates)	36
2.34	Median accuracy and range for CAS technique. (Error bars indicate min and max accuracy rates)	37
2.35	Lateral and oblique 2D fluoroscopic views of the lumbar spine during PSP. Figure from [12].	39
2.36	Response to Question 1: Do you think there is a need for a simple device to aid PS placement?	42

2.37	Response to Question 2: What spinal systems do you currently use to aid PS placement?	43
2.38	Response to Question 3: Have you experienced any problems with PS placement in patients?	43
2.39	Global spinal market share. Figure from [75].	44
3.1	Schematic representation of photon scattering and absorption in tissue. The left fiber emits broad-band white light, the right fiber collects photons and transports them to the spectrometer. Each arrow represents a photon, the black shapes are chromophores. The green photon is absorbed after two scattering events whilst the yellow photon is scattered twice and then leaves the tissue. Both the red and blue photon undergo several scattering events until they are collected by the right fiber.	51
3.2	Absorption spectra of Hb, HbO ₂ , water and fat over the whole wavelength area (left) and absorption spectra of water and fat from 800 to 1100 nm (right).	52
3.3	Schematic of the measurement setup of the optical probe	53
4.1	Axial view of thoracic vertebral bone. Figure from [89]	58
4.2	Axial view of thoracic vertebral bone. Cortical bone can be seen surrounding the vertebral body and the spinal canal	58
4.3	Various views showing the spinal canal cross-section and tissues surrounding it.	59
4.4	Surgical workflow of 2D fluoroscopic guided technique (Open)	60
4.5	Vertebral column extracted from a swine vertebra	61
4.6	Dividing the swine vertebrae into 6 regions in the axial view	61
4.7	The available optical microscope was used to zoom-in into the tissue under investigation	62
4.8	Whitish semi-fluidic material found in the spinal canal	62
4.9	Microscopic images of various regions of the extracted swine vertebra	63
4.10	Box plots of cortical bone thickness measurements across intravertebral regions	64
4.11	(A) Schematic representation of components of the measurement set-up; (B) Front view of dual-fiber probe	67
4.12	Axial view of a thoracic vertebra divided into five regions. Each region was mapped using the optical probe.	68
4.13	Optical probe placed perpendicular to the vertebral tissue surface during data acquisition.	69
4.14	Boxplot depicting the change in fat concentration across the six intravertebral regions probed.	70
4.15	Boxplot depicting the pooled data of the change in fat concentration across intravertebral regions for the three principal tissues under investigation.	70
4.16	Boxplot depicting the change in the scattering parameter across the six intravertebral regions probed.	71
4.17	Boxplot depicting the pooled data of the change in scattering parameter across intravertebral regions for the three principal tissues under investigation.	71
5.1	A scattering event is a function of deflection angle θ and azimuthal angle ψ	76
5.2	Flowchart depicting photon propagation in medium	77
5.3	Wavelength-dependent optical properties found experimentally by Bashkatov <i>et al</i> [7]. The symbols correspond to averaged experimental data found in literature.	79
5.4	Cylindrical grid system used to model a tissue layer in Monte-Carlo simulations	80
5.5	The diffuse reflectance information was extracted from the entire region represented in red (Figure not to scale).	80
5.6	Absorption and reduced scattering coefficients for the Monte-Carlo model	81
5.7	Workflow diagram of Monte-Carlo model validation protocol	82
5.8	Cylindrical grid system used to model a tissue layer in Monte-Carlo simulations	82
5.9	Comparison of experimentally measured spectra and Monte-Carlo model spectra for the three principal tissues under investigation.	83
5.10	3-layered Monte-Carlo model depicting the change in fat concentration with insertion depth during a medial breach scenario	84

List of Tables

2.1	Selected keywords and their results in Google Scholar	10
2.2	Accuracy table for conventional techniques	31
2.3	Breach definitions reported in literature	32
2.4	Trade-off analysis of the main techniques	39
2.5	Trade-off analysis of assistive devices	41
2.6	Most costly OR procedures performed in US hospitals in 2011. Table from [135]	45
2.7	Design requirements for smart assistive device	46
4.1	Thoracic vertebra-1	64
4.2	Thoracic vertebra-2	64
4.3	Descriptive statistics of fat concentration data	70
4.4	Descriptive statistics of scattering parameter data	71
5.1	Monte-Carlo validity checked via VAF	82

List of Abbreviations

PSP	Pedicle Screw Placement
DRS	Diffuse Reflectance Spectroscopy
MIS	Minimally Invasive Surgery
CAS	Computer Assisted Surgery
AP	Anterior Posterior
CT	Computer Tomography
EMG	Electro Myo Graphy
SSEP	Somato Sensory Evoked Potential
MEP	Motor Evoked Potential
K wire	Kirschner wire
CSF	Cerebro Spinal Fluid
US	United States
MC	Monte Carlo

Chapter 1

Project strategy

The overall project strategy has been summed up in a flowchart shown below.

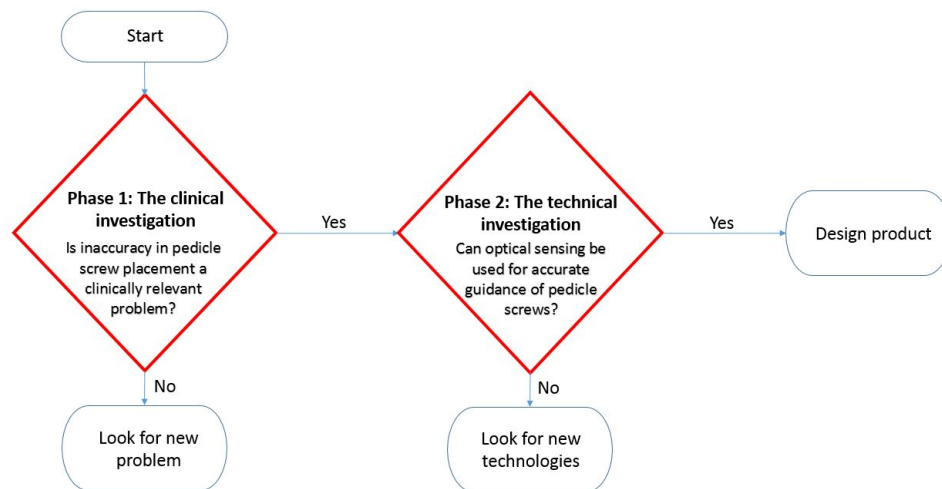


FIGURE 1.1: Project strategy

Over the years, several research groups and companies have developed various technologies in order to guide the surgeon to accurately place pedicle screws in the spinal vertebra in order to ensure a healthy spinal fusion of the concerned spinal levels. However, whether these technologies have been successful in optimizing the surgical workflow, and significantly help the surgeon in the guidance of the screws in the appropriate location, needs to be thoroughly investigated. Accurate guidance of pedicle screws has a direct impact on the complication rate, patient recovery time and radiation exposure, especially to the surgeon. Therefore, one of the central questions of this literature study is to investigate whether given the current state of advancement in the field, is inaccuracy in pedicle screw placement (PSP) a clinically relevant problem. In other words, is there a need to solve this problem. This constitutes the first phase of the project and serves as the central question of the clinical investigation as indicated in figure 1.1.

If the answer to the central question in phase 1 research based on critical analysis of unbiased sources does indicate a legitimate problem, phase 2 research would commence. The central question to be answered in the second phase of this project is whether Diffuse Reflectance Spectroscopy (DRS) technology can be used to improve the accuracy of the pedicle screw placement procedure. This phase has been modularized into two main parts namely, the experimental and the simulation investigations. The experimental investigation has been further subdivided into two studies which are intrinsically linked to the study to follow in the simulation investigation.

1.0.1 Research Objectives

The clinical investigation

To answer the primary question of phase 1, information was gathered and analyzed from three main sources, namely the scientific literature, surgeons interviews and the market reports.

One of the most important sources to study the phase 1 question is the scientific literature. A systematic literature search was thus performed, which was guided by the following secondary research questions:

1. *What are the current surgical techniques or technologies used for the guidance of pedicle screws?*
2. *What is the definition of accurate pedicle screw placement?*
3. *How accurate are the current surgical techniques or technologies in pedicle screw placement?*
4. *What is the complication rate associated with each technique?*

Since the primary user of the proposed solution is the surgeon, understanding the surgeons perspective and preferences is vital in evaluating the entire scope of the problem. This is done by interviewing surgeons and finding questionnaire based studies in literature focusing on PSP. The current state of the market could provide potentially useful information about the magnitude or scale of the problem in terms of various parameters such as frequency and costs of spine fusion surgery. The health of the market and future trends could help identify whether the need for better solutions exists from a commercial standpoint.

The technical investigation

In order to answer the primary technical research question as shown in the project strategy flowchart of figure 1.1, a secondary technical research question was developed in order to narrow down the scope of the problem pertaining to this thesis. The secondary technical research question is stated as follows:

Can DRS technology be used to detect and anticipate the presence of a tissue boundary during a medial breach scenario?

Information regarding the underlying DRS technology, type of tissue boundaries and the definition of a medial breach have been elaborated within the studies.

Part I

Phase 1 research: The clinical investigation

Chapter 2

Is inaccuracy in pedicle screw placement a clinically relevant problem?

2.1 Abstract

BACKGROUND CONTEXT: Pedicle screw placement is a critical step in spinal fusion surgery. The close proximity of vital neural and vascular structures and the added variability in patient and spinal region dependent morphology makes the misalignment of one or more pedicle screws to have direct effect on the surgical outcome. Due to this complex nature of the procedure, several navigational and trajectory verification approaches have been developed to provide some degree of guidance and to provide additional feedback during pedicle screw placement to the surgeon.

PURPOSE: To explore the current state art in pedicle screw placement guidance techniques and to investigate the existence of a clinically relevant problem of inaccuracy in pedicle screw placement.

STUDY DESIGN: Systematic literature review.

METHODS: In order to comprehensively establish the current of art, all publications after 2005 were studied after an optimized keyword search criteria selection. An exhaustive surgical workflow analysis was performed for each guidance technique in order to visualize the various instruments used at each step. The pedicle screw placement accuracy and complication rates of various techniques were compared based on the highest level of evidence available in literature such as meta-analysis and systematic reviews. This was followed by a trade-off analysis of different techniques in which the advantages and disadvantages of each technique was discussed. This part also includes a survey questionnaire, which reflects the clinical perspective of the surgeons.

CONCLUSIONS: This literature review establishes the current state of development in pedicle screw placement guidance techniques. Based on the analysis of the highest level of evidence it can be concluded that free-hand and 2D fluoroscopy-guided techniques exhibit high screw placement accuracy variability, which is indicative of the technically demanding nature of the procedure.

2.2 Introduction

It is estimated that 1.3 million spine surgeries are performed every year in the United States alone, 53% of these are categorized as spinal fusion surgeries [73, 115]. Rajaei *et al* [102] found a 2.4-fold or 137% increase of spinal fusion discharges between the year 1998 to 2008. It is estimated that due to the continued growth of the aging population, the global spinal surgical market is projected to reach almost \$6.5 billion by 2015 [115].

An important aspect of spinal fusion surgery involves the accurate placement of pedicle screws in the vertebrae to stabilize the spine after decompression or correction of spine alignment and to ensure healthy fusion of spine levels in question. This aspect of the surgery is especially considered to be highly complex and technically demanding with a steep learning curve [68, 128].

The first phase of my literature study focuses on investigating whether inaccuracy in pedicle screw placement is a clinically and commercially relevant problem. This was carried out by rigorously analyzing various sources of information such as scientific literature, surgeons interviews and the market to establish the current state of art in this domain.

The In-body Systems group at Philips Research has been working on a specific optical spectroscopy technology namely Diffusive Reflectance Spectroscopy (DRS) for tissue identification. If the results of the phase 1 research do indeed indicate a clinical and commercial need for solving this problem, phase 2 research would commence. The second phase of my research would then focus on the applicability of DRS in improving the accuracy of pedicle screw placement (PSP). This research focus would also lie at the heart of my master thesis.

In order for the reader to understand the essence of the problem, the following sections serve as a necessary primer.

2.2.1 Spine anatomy

The human spine is an integrated complex of bones, nerves, muscles, tendons and ligaments. The vertebrae are the bony building blocks of the spine. There are 33 individual bones that interlock with each other to form the spinal column. These are divided into 5 regions namely cervical, thoracic, lumbar, sacral and coccyx as shown in figure 2.1.

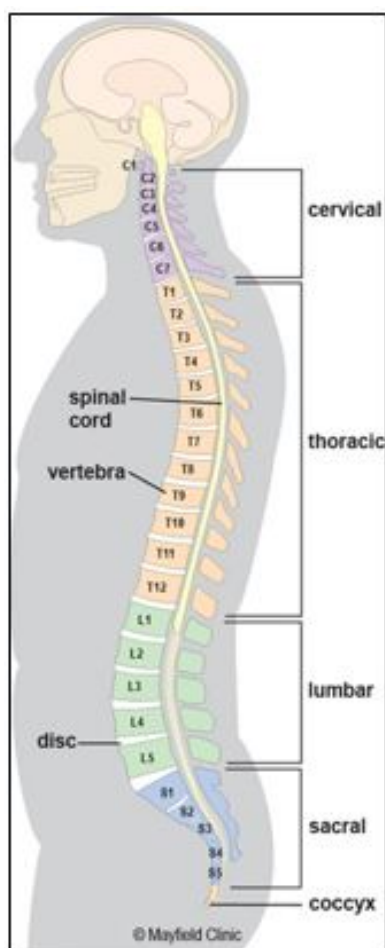


FIGURE 2.1: Regions of the spine. Figure from [46]

Each vertebrae consists of three main parts namely the body, vertebral arch and the processes. Each vertebral arch is made up of two supporting pedicles and two laminae as shown in the axial view of figure 2.2a. The hollow spinal canal contains the spinal cord, fat, ligaments

and blood vessels. Under each of the pedicles, a pair of spinal nerves exits the spinal cord and passes through the intervertebral foramen to branch out to the rest of the body as shown in figure 2.2a and figure 2.2b.

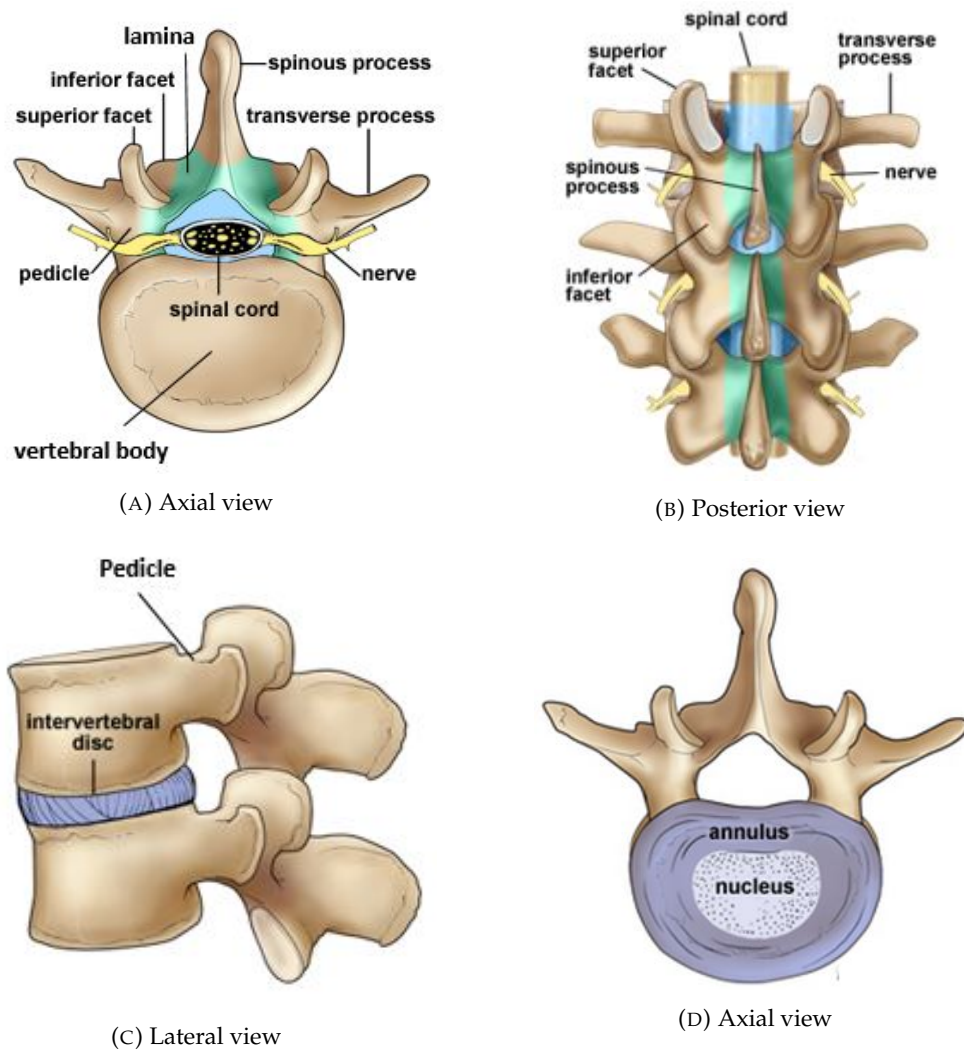


FIGURE 2.2: Various views depicting the spine anatomy. Figure from [46]

Intervertebral disc

Each vertebrae is separated and cushioned by an inter-vertebral disc as illustrated in figure 2.2c. The disc consists of an outer fibrous ring called the annulus fibrosus, which surrounds an inner gel-like center, namely the nucleus pulposus as depicted in figure 2.2d. They have three extremely important functions which fundamentally ensure proper functioning of the spine. They help provide mobility to the spine by preventing the bones from rubbing against each other; they act as shock absorbers which function like coiled springs to bear the necessary dynamic loads during various activities; and they also act like spacers, to help maintain a constant gap between vertebrae and to allow the branching out of then nerves as shown in figure 2.2b [129, 46].

2.2.2 Spine Fusion Surgery

Spinal fusion surgery involves a surgical technique in which two or more vertebrae are fused together using surgical instrumentation and bone graft material [142]. Spinal fusion is performed to eliminate any relative motion between the affected vertebrae in order to reduce pain indications and to improve the stability of the spine. There are several indications for the need of spinal fusion surgery namely:

1. Spondylosis, a degenerative osteoarthritis of the joints of the joints between the centers of the spinal vertebrae and intervertebral foramen.
2. Spondylolisthesis, a condition in which one vertebrae slips forward relative to the vertebrae above or below it.
3. Instability and pain caused due to excessive motion between vertebrae
4. Bulging or herniated disc, which can cause compression of the spinal nerves.
5. Spinal deformities such as Scoliosis or Kyphosis
6. Trauma to the vertebrae

Spinal fusion surgery is performed in two main steps. The first step is to perform the necessary decompression due to diseases mentioned above such as herniated disc, Spondylolisthesis etc. This step usually involves dissection or removal of the inter-vertebral disc in question and placement of bone graft material in the particular segment of the spine. The second step usually involves installing the spine instrumentation (pedicle screws and rods) for adequate spinal fusion. Taking the condition of herniated disc as an example, the broad workflow of the surgical treatment is shown in figure 2.3

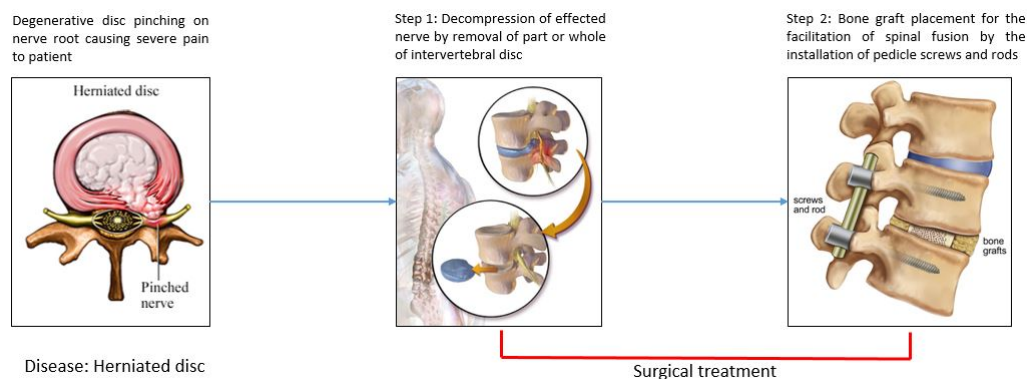


FIGURE 2.3: Surgical treatment of herniated disc disease

In case of spinal deformity cases like Scoliosis and Kyphosis, spine instrumentation is first installed which serves as an anchor for the application of corrective and distractive maneuvers in order to correct the deformity. In the second step, more often than not a few vertebrae are also fused to prevent movement of the particular segment and thereby also prevent the progression of the curve deformity [125]. The broad surgical workflow of Scoliosis surgery has been described in figure 2.4.

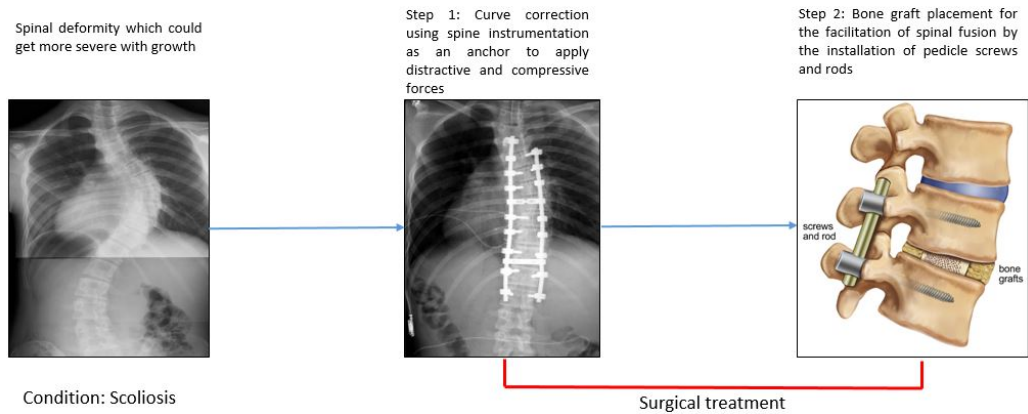
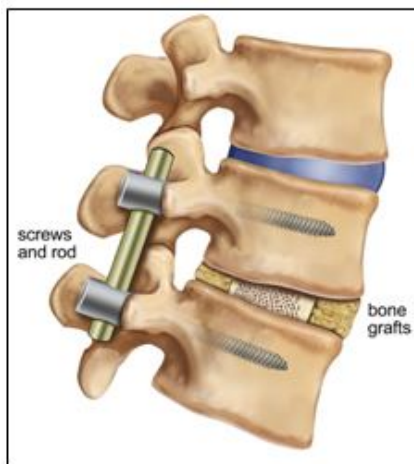
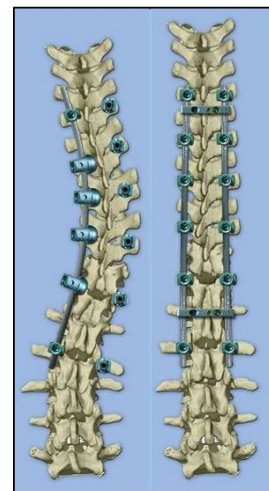


FIGURE 2.4: Surgical workflow of Scoliosis surgery

2.2.3 Reasons for Spine Instrumentation

There are two main reasons for spinal instrumentation. The first one involves stabilization of the spine after spinal fusion surgery. Pedicle screws and rods are placed to ensure no relative movement exists between the vertebrae until they are completely fused as shown in figure 2.5. After complete fusion of the vertebrae, the role of the spinal instrumentation gradually decreases but is not removed barring patient discomfort or other complications. This concept of load sharing between the spinal column and the instrumentation and its importance in maintaining stability has been studied extensively in several biomechanical studies [14, 33, 59, 72, 25, 41, 67, 100, 6, 110].

FIGURE 2.5: Instrumentation for stabilization.
Figure from [117]FIGURE 2.6: Instrumentation for correction.
Figure from [126]

Spinal instrumentation is also required for the correction of deformity due to conditions like Scoliosis or Kyphosis as shown in figure 2.6. In these cases, the screws and rods are inserted and used to reduce the amount of curvature. Compressive and distractive forces are applied via the instrumentation in order to get a suitable correction of the spine [42]. It may or may not involve spinal fusion.

From section 1.2 and 1.3 it becomes quite clear that an extremely important aspect of spinal fusion surgery is the placement of the pedicle screws into the vertebrae in order to get a good fusion of the vertebrae, and thereby relieve pain or to ensure permanent correction of deformity.

2.2.4 Screw Insertion in Spinal Fusion surgery

The procedure for pedicle screw placement is known to be highly complex and technically demanding with a steep learning curve [68, 36, 121]. There is a limited visibility of spinal anatomical landmarks during surgery which makes it extremely important to gain a sound understanding of the spine anatomy that are hidden from direct view. Adding to the problem is the extremely small sizes of the pedicles itself. The inner diameter of the pedicles can be as small as 2 millimeters. [144]. Moreover, the close proximity of vital neural and vascular structures and the added variability in patient and region dependent morphology contribute significantly to the difficulties in accurate placement. The complexity of the procedure can also be roughly estimated based on the delicate nature of the spine anatomy as shown in figure 2.2.

Therefore, the implication of perforation of vertebral wall due to improperly placed screws could place the neural and vascular structures at serious risk of damage. It comes as no surprise then that an array of techniques aided by various technologies have been developed to improve accuracy rates.

2.3 Materials and methods

A total of three sources were used to answer the primary research question of phase 1, these being the scientific literature, surgeon interviews and the market.

2.3.1 Scientific literature

One of the most reliable sources of information is the scientific literature relative to questionnaires and market reports, although it often has certain types of biases associated with it.

The strategy followed here involves using unique keywords for each of the techniques used in pedicle screw placement. After performing several unstructured arbitrary google searches to get acquainted with the field and formulating research questions, the most appropriate and broad keywords were selected. Google Scholar was used as the primary academic search engine which has one of the most robust search algorithms containing range of sources including articles, books, technical notes and theses etc.

TABLE 2.1: Selected keywords and their results in Google Scholar

Search string	Number of hits	Number of relevant articles
pedicle (screw OR screws) "free hand"	71	59
pedicle (screw OR screws) intraoperative fluoroscopy	9	8
pedicle (screw OR screws) ("computer assisted"OR "computer navigation")	61	47
pedicle (screw OR screws) pediguard	61	20
pedicle (screw OR screws) (electrical OR electronic OR conductivity)	19	3
pedicle (screw OR screws) (neurophysiological OR electrophysiological OR EMG OR electromyography OR SEEP OR motor evoked potential)	62	26
Total	283	163

Table 2.1 gives a list of all search strings used to filter out relevant articles. In total, out of 283 hits, 163 relevant articles were found. The inclusion criteria included several factors: articles dated from 2005 to 2015 were included, only english articles were filtered. Cadaveric studies were excluded from the search. Articles that did not focus specifically on PSP were also excluded. Some exceptions regarding the date of publication were made if the article was highly cited and helped in the growth of the field.

2.3.2 Clinical perspective: Surgeons interviews

Since the whole problem revolves around optimizing a surgical procedure which is primarily performed and lead by a surgeon, his/her clinical perspective would be of great importance in understanding the subtle aspects of the issue that might have been entirely missed while researching the scientific literature.

Interviews were gathered in two ways. The first approach involved scanning databases for relevant survey questionnaires performed by fellow researchers. A relatively large, extremely relevant survey questionnaire of 67 surgeons from UK and Ireland was found and would be discussed in detail in the future chapters. Actual interviews taken in person or via internet services like Skype would constitute the second approach. The latter approach would not be discussed in this report as the process is still ongoing.

2.3.3 Market

Given that no medical device is developed in an isolated environment, understanding the health of the spine device market in terms of market size, market shares based on region, technology and industries, cost of surgery and reimbursement policies etc. would help go a long way in understanding the magnitude of the problem, especially from a commercial standpoint. This data is acquired from published market reports, reliable blog articles by market analysts and from the websites of well-known market research companies.

2.4 State of art in pedicle screw placement

2.4.1 Pedicle screw placement techniques: A workflow analysis

This chapter tries to answer the first of the four secondary research questions pertaining to this phase. To do so, a detailed overview of the various currently used techniques in pedicle screw placement would be elaborated via a surgical workflow analysis. The important medical devices crucial to accurate PSP used along various steps of the surgical workflow would also be discussed.

Free hand technique

One the oldest and still a widely used technique for pedicle screw placement is the free hand technique. The goal of the free-hand technique is to accurately and safely place screws in the vertebrae without the use of any intraoperative fluoroscopy, radiography, and/or image-guided techniques, as described in the study by kim *et al* [51]. A step by step account of the surgical workflow right from the initial incision to the confirmation of screw placement is shown in figure 2.9.

Since this is an open technique, the first step involves making a midline incision exposing the entire surgical area of interest. It must be noted that this step involves stripping the muscles in order to gain exposure.

One of the crucial next step is the entry point selection. This step is heavily dependent on the surgeons experience on identifying anatomical landmarks and using them as a reference to select appropriate entry point and trajectory. Although ideally no image guidance is used, surgeons do occasionally take fluoroscopy shots to confirm the vertebral levels of interest [13].

In the third step of the process the surgeon creates a shallow, roughly 5 mm deep pilot hole. This is done using a high speed burr breaching into the cortical bone.

The next step involves pedicle cannulation, which is one of the most crucial and technically demanding steps as it involves the advancement of the pedicle probe into the pedicle. The correct cannulation is crucial in order to avoid the perforation of the spinal canal as shown in figure 2.8.



FIGURE 2.7: Pedicle probe. Figure from [88]

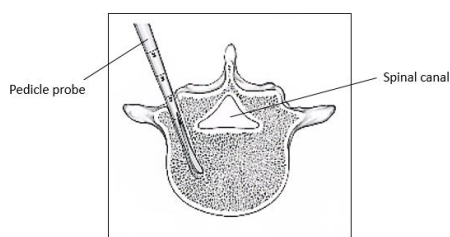


FIGURE 2.8: Pedicle cannulation. Figure from [46]

This step is performed in order to create a preliminary guide hole for future steps such as tapping and screw placement. The design of the pedicle probe is shown in figure 2.7. The surgeons rely only on tactile feedback based on the difference in insertion resistance between Cortical and Cancellous bone to safely advance the probe without impinging into any neural or vascular elements.

The hole trajectory is then checked by palpating the walls of the hole manually using a blunt ball-tipped probe. The length of the hole is also confirmed in a rather crude way by measuring the distance traveled by the ball-tipped probe using an ordinary scale as shown in the fifth step of the surgical workflow elaborated in figure 2.9. The length of the hole is used to select the length of the tap and the screw.

After confirming that no violations have been performed and ensuring the safety of all neural and vascular structures, preparation of the previously made hole is performed using an undersized tap. The final screw diameter is roughly estimated using preoperative CT images or radiographs. A tap with a diameter usually 0.5 mm less than the intended screw is used [51, 52]. The tapped hole is again checked for any perforations or violations using a ball tipped probe which constitutes as the sixth step of the procedure.

The pedicle screw is then placed into the tapped hole. The final step involves the confirmation of the hole via anterior/posterior (AP) and/or lateral fluoroscopy shots.

2D fluoroscopy-guided technique

In the 2D fluoroscopy-guided technique surgeons often acquire fluoroscopy images via the C-arm image intensifier system in order to guide them through the various stages during PSP. Different surgeons use the fluoroscopy images at various steps depending upon the type of patient case, approach (Open or MIS) and level of experience.

Open surgical approach The open 2D fluoroscopy-guided technique surgical workflow has been depicted in figure 4.4. It can be observed that the workflow is very similar to the free-hand technique as shown in the previous section [43, 82, 48, 78]. The only major difference is in the number of fluoroscopic images acquired. In this technique for most of the relatively crucial steps fluoroscopic images are taken. As shown in figure 4.4, for the entry point selection, pilot hole creation and pedicle cannulation, a number of fluoroscopy shots are acquired to check for any breaches. Lateral and AP images are also taken to guide placement and confirmation of pedicle screws into the pedicle and vertebral body.

Minimally invasive surgical (MIS) approach The workflow analysis for the minimally invasive surgical (MIS) technique has been described in figure 2.13. It is important to note that it is a different approach both from a workflow standpoint and from the instrumentation involved, which has also been observed in the studies by Raley *et al* [104] and Park *et al* [93]. The first step involves the identification of entry point via AP and lateral fluoroscopy shots. Surgeons often mark the entry point on the skin for each vertebral level to be instrumented.

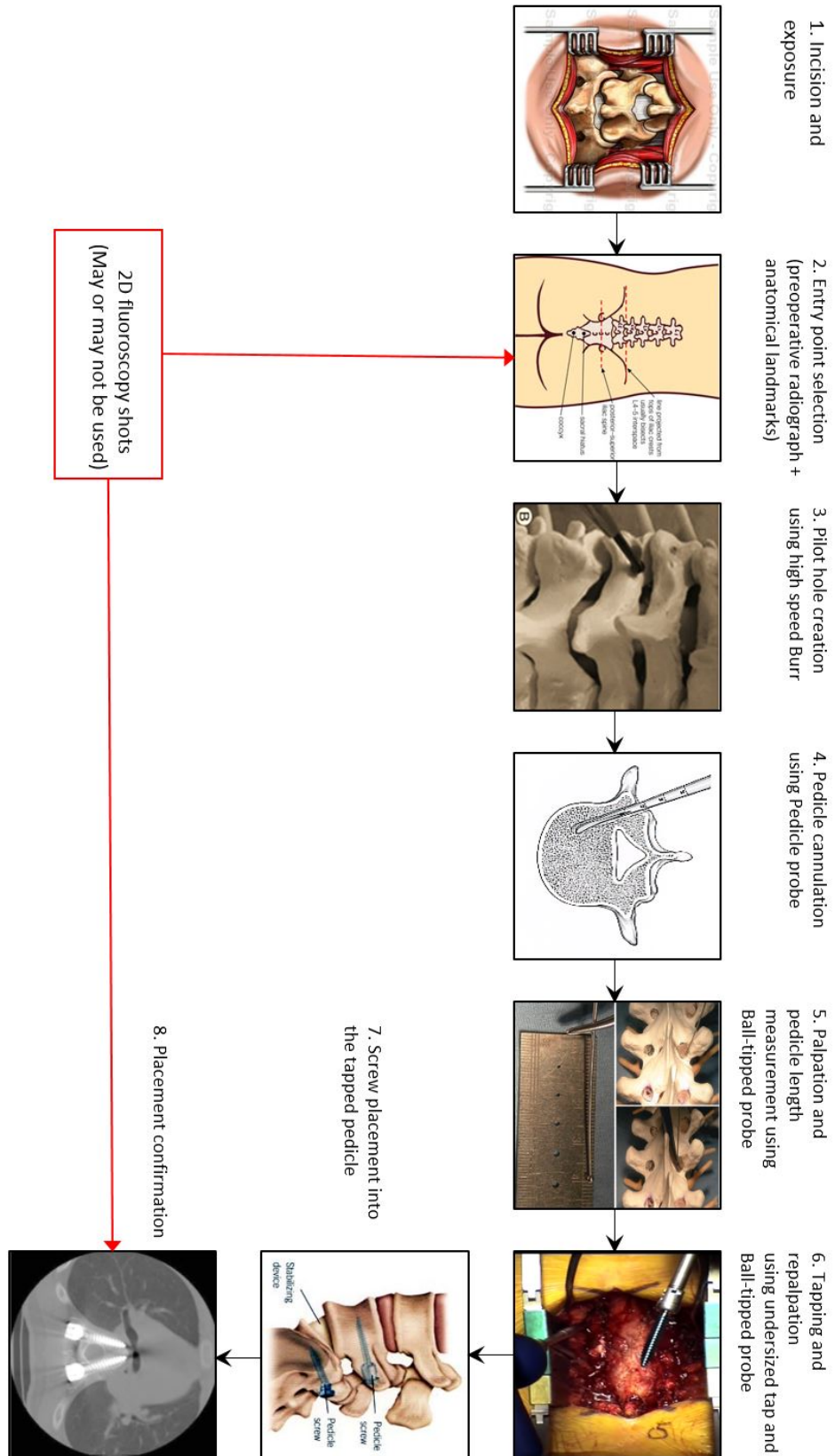


FIGURE 2.9: Surgical workflow of Free-hand technique

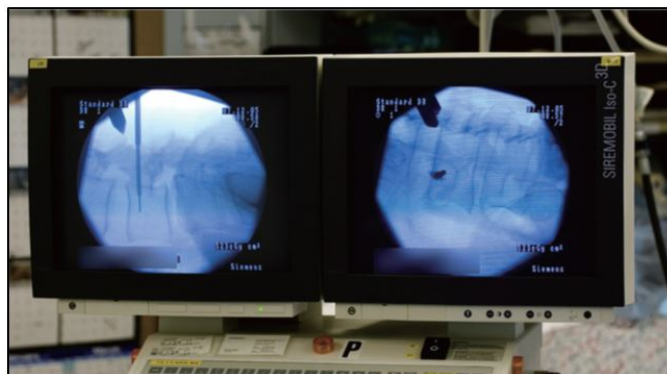


FIGURE 2.10: Lateral and oblique 2D fluoroscopic views of lumbar spine during PSP.
Figure from [12]

The next step involves making small incisions of no more than an inch in diameter. Since the approach is supposed to be minimally invasive, no large mid line incision is made. Due to the small exposure of the surgical site the instruments used have also been modified. The second step involves inserting flexible k-wires through a rigid cannulated Jamshidi needle through the previously made incision in order to make a brief entry into the pedicle of the vertebrae. An example of a cannulated Jamshidi needle can be seen in figure 2.11. The trajectory of the inserted K-wire is checked by acquiring AP and lateral fluoroscopy images. Once the K-wire is found to be in its intended position, the Jamshidi needle is retracted. In the subsequent steps all the instrumentation would be placed over these K-wires.

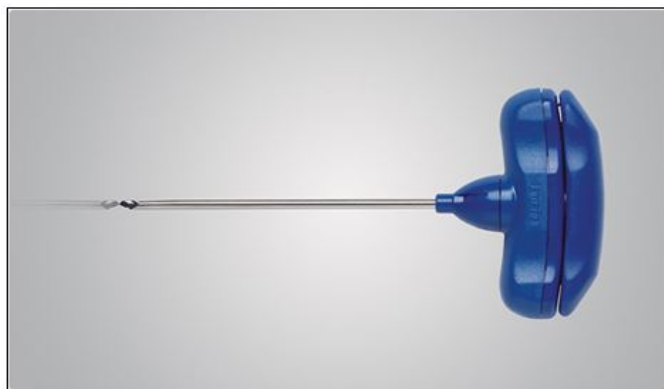


FIGURE 2.11: Cannulated Jamshidi needle. Figure from [3]

In the third step as shown in figure 2.13, the pedicle of the vertebrae is cannulated. This is one of the crucial steps of the process. Before the cannulation can be performed the narrow entry hole created needs to be widened. This is done by splitting and not stripping the muscles as was done in the open 2D fluoroscopic-guided technique. Therefore to gain access to the surgical area, serial tubular dilators are inserted over the K-wires. Once adequate exposure is made, an awl or Jamshidi needle might be used to further cannulate the pedicle.

After the retraction of the awl, the cannulated hole is further prepared using an undersized tap over the K-wires. 2D fluoroscopy images are then acquired to confirm safe tapping.

The final step involves placing the pedicle screw into the desired location over the K-wire. Lateral and AP fluoroscopy shots are taken again to confirm accurate placement.

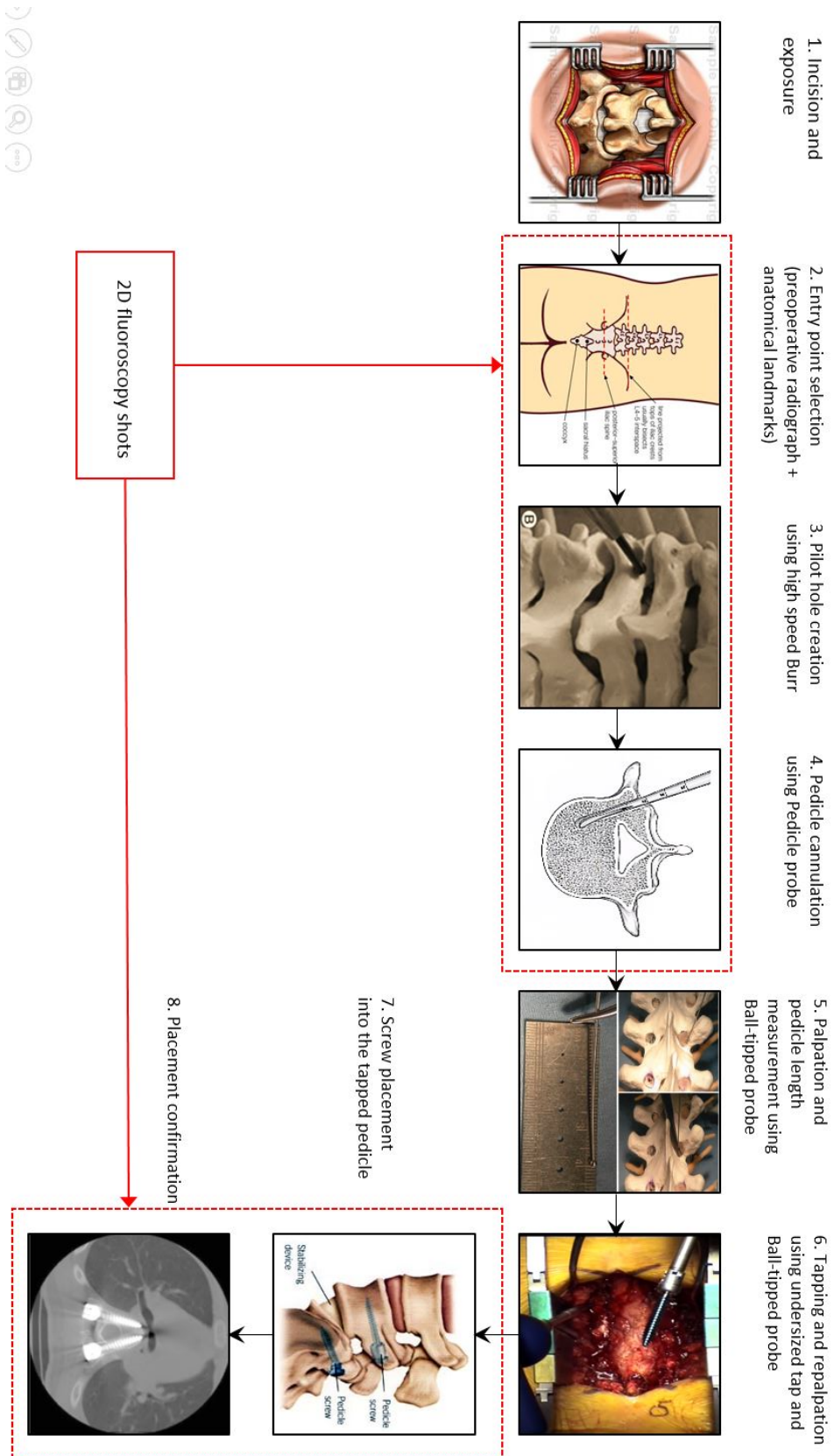


FIGURE 2.12: Surgical workflow of 2D fluoroscopic guided technique (Open)

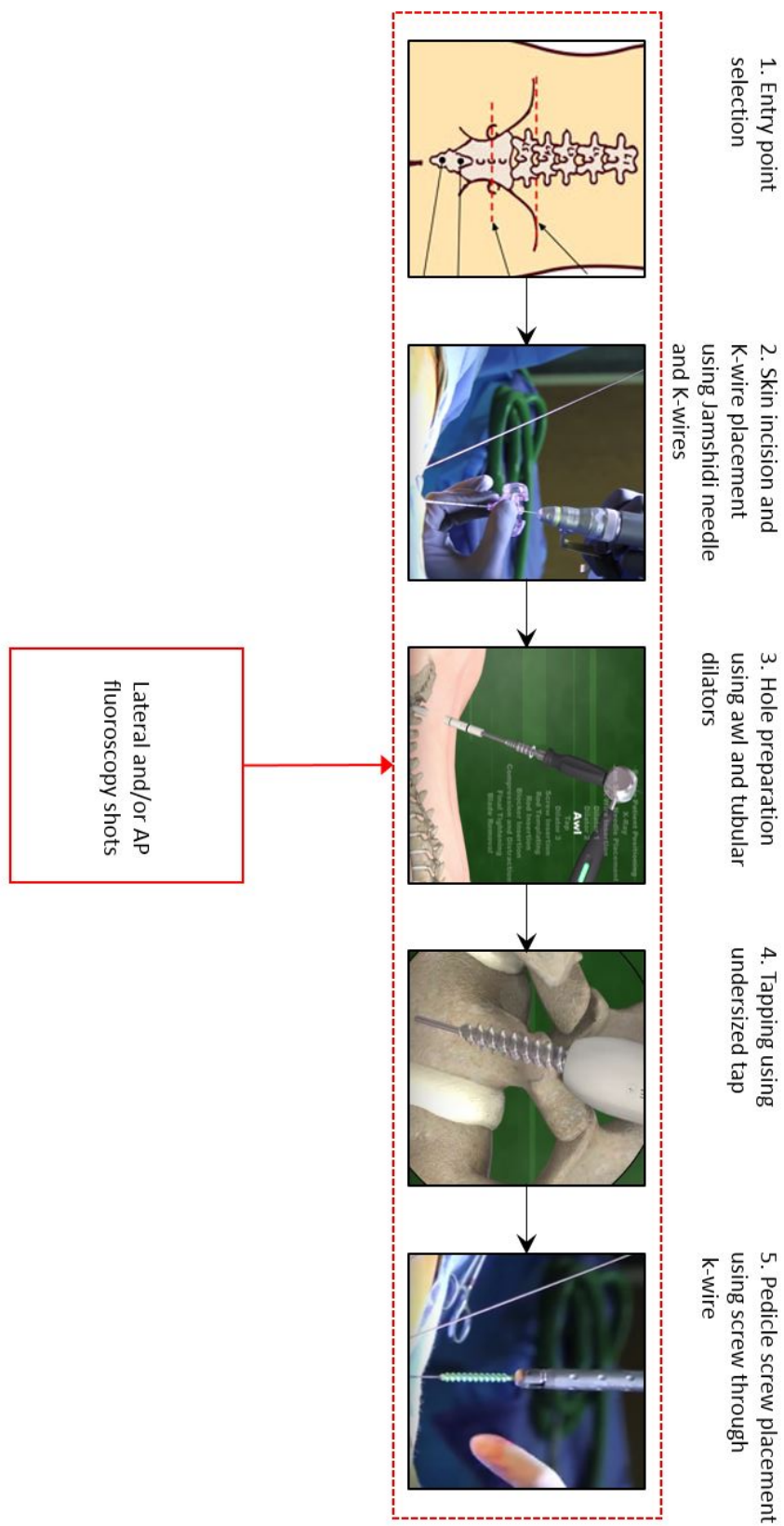


FIGURE 2.13: Surgical workflow of 2D fluoroscopic guided technique (MIS)

Computer-assisted technique

The computer-assisted surgical (CAS) technique for pedicle screw placement relies on a navigation software along with fluoroscopy and/or CT images to plan screw trajectory and navigate through the anatomical obstacles in real-time. It has an added advantage of displaying the images in 3D which leads to a more enhanced and intuitive visualization. The basic principle of the computer-assisted system is very similar to the way a car is navigated with the help of global positioning system technology [68]. The navigation system uses cameras to track the instruments via instrument and patient trackers to obtain real time information about the instrument position relative to the patient.

Open surgical approach Preoperative CT images are taken to roughly estimate the entry point and the levels to be instrumented. A rough estimate of the diameter of the final screw is also made.

The next step involves attaching the dynamic reference frame array to either the iliac crest or the spinous process. As the name of the instrument suggests, the frame clamped to the patient acts as a reference so that the instrument tracking is performed relative to the patient tracker. The navigated instruments are then calibrated via the camera and the navigation software.

After the attachment of the dynamic reference frame and calibration of instruments, the entire OR team leave the operation theatre while the imaging system (C-arm or CT scanner) performs image acquisition. Auto-registration and merging of pre-operative and intra-operative images is also performed and the data is transferred to the navigation software. The navigation system is now ready. All the steps from five to eight as shown in figure 2.16 are performed under real time image guidance with the aid of the navigation system.

As discussed before, since it is an open approach a midline incision is made by stripping the muscles and ligaments to expose the entire surgical area.

A crucial step of screw trajectory planning and pilot hole creation is performed using instruments which are tracked by the navigation system. The instrument trackers attached to the instruments itself are shown in the figure 2.14

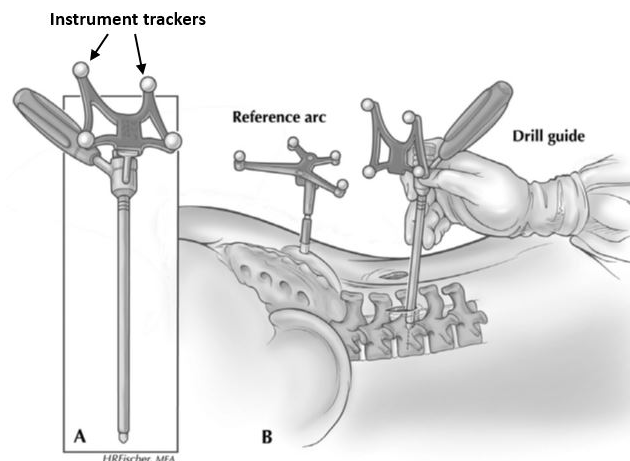


FIGURE 2.14: Instrument with trackers used in CAS technique. Figure from [94]

Subsequently, pedicle cannulation using the probe, tapping and screw insertion are all performed under real-time navigation with 3D visualization.

Minimally invasive surgical (MIS) approach Shown in figure 2.17 is the workflow analysis of the MIS approach of CAS technique. The initial preparation steps to set-up the navigation system are exactly the same as in the open approach. As seen in the previously discussed techniques transitioning from open to MIS approach leads to change in instrument design to accommodate the reduced surgical exposure.

The completion of the auto-registration signifies that the navigation software is now functional. Inch-sized skin incisions are then made and the screw trajectory planning is performed under real time image guidance using the navigation system.

Based on the selection of the screw trajectory, Jamshidi needle is used to find the pedicle and make a shallow cannulation as shown in figure 2.15. A flexible K-wire is then passed through this rigid Jamshidi needle which will now serve as a guide for further hole preparation, tapping and screw placement. The K-wire placement process is repeated for all levels to be instrumented.

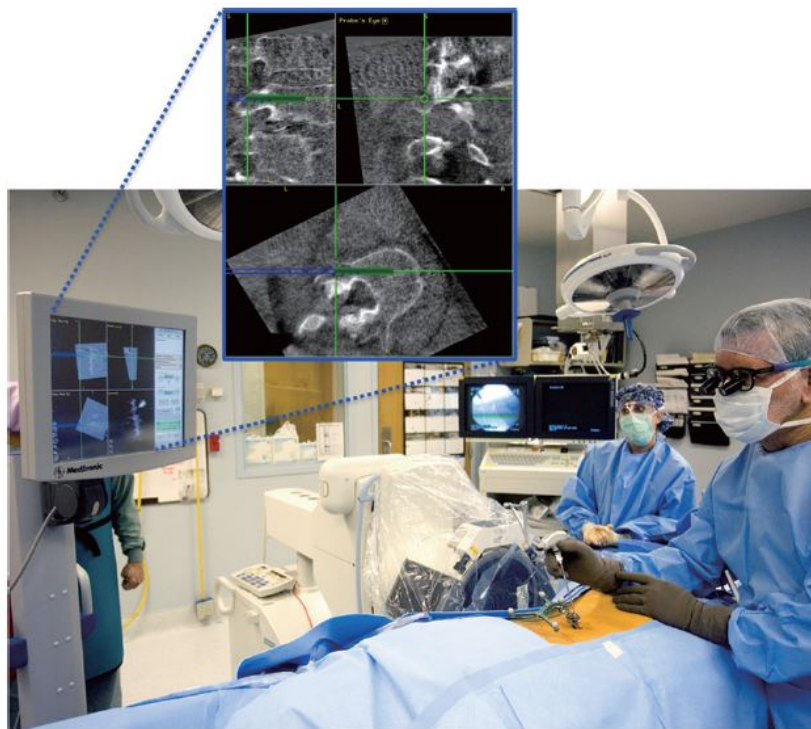


FIGURE 2.15: Pedicle cannulation being performed using a Jamshidi needle with the aid of navigation. Figure from [12]

To allow the relatively large diameter of the tap and screw from passing through the muscles and ligaments and into the pedicle, muscle splitting is performed by the use of serial dilators. These dilators of increasing diameters are serially inserted over the K-wire in order to increase surgical exposure. An awl is then inserted to adequately cannulate the pedicle before tapping and screw insertion can be performed.

Finally, again under real-time image guided 3D navigation, tapping and screw insertion is conducted.

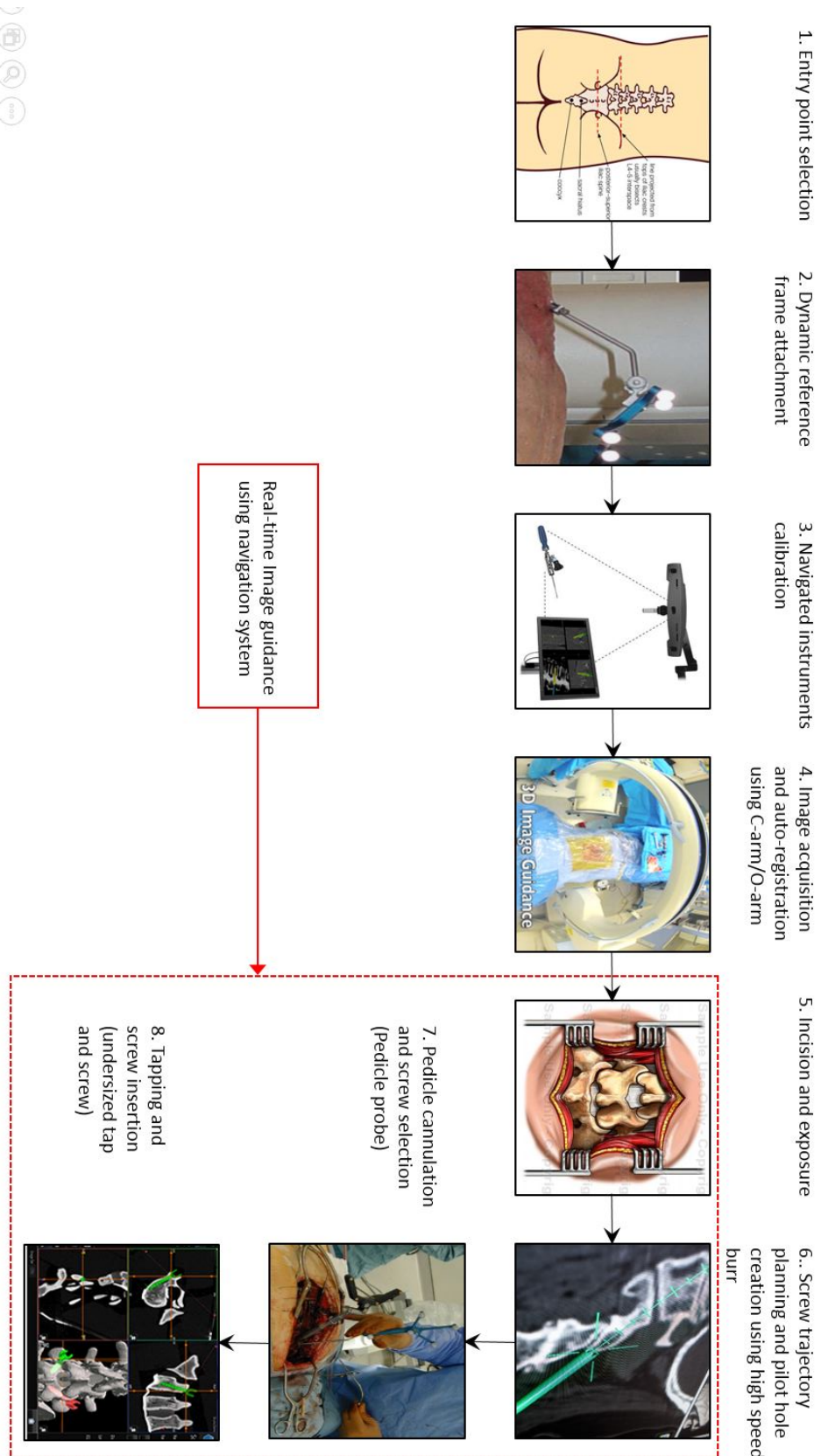


FIGURE 2.16: Surgical workflow of computer-assisted technique (Open)

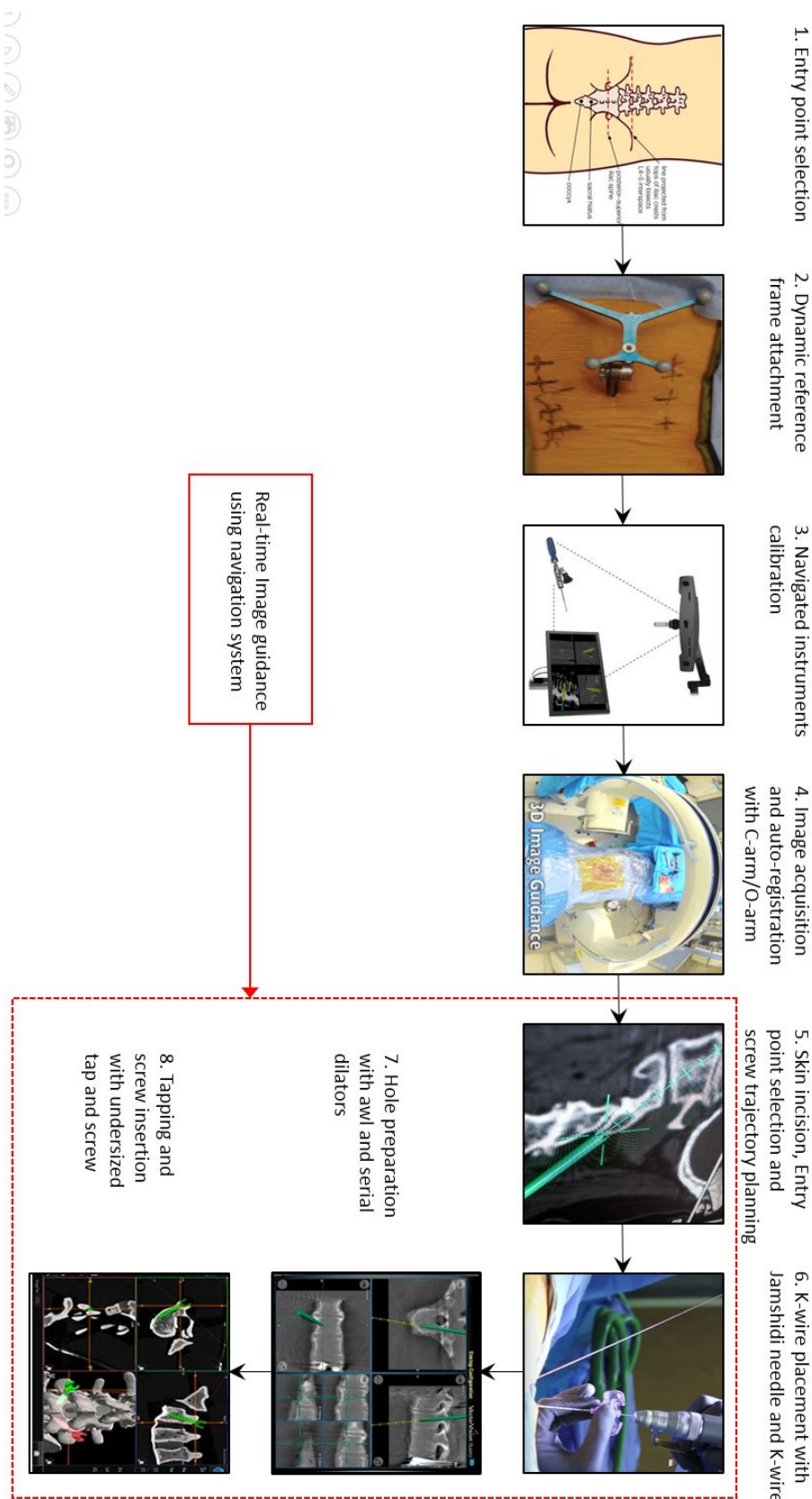


FIGURE 2.17: Surgical workflow of computer-assisted technique (MIS)

Electrical conductivity measurement technique

The electrical conductivity measurement technique is as such not an entirely unique technique. Central to this technique is the PediGuard probe device which is a flagship product developed relatively recently by the company named SpineGuard [50]. The PediGuard[®] measures the electrical conductivity of different tissue types such as blood, cortical and cancellous bone using a bipolar sensor. By measuring the differences in electrical conductivity between these tissues, cortical breaches can be anticipated by warning the surgeon via an audio and visual feedback. As the surgeon advances the PediGuard[®] probe, the sensor continuously measures the electrical conductivity of the tissue right in front of it. It gives out a medium pitched sound when sensing cancellous bone. The pitch lowers as the sensor encounters cortical bone. This signifies an impending breach. As the surgeon pushes the device further, blood starts to gush in, which is detected by the sensor producing a high pitched alarm as shown in figure 2.18.

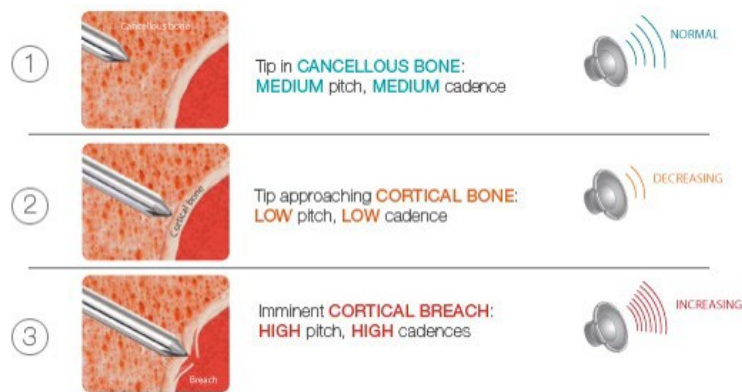


FIGURE 2.18: Working principle of electrical conductivity measuring device. Figure from [50]

Open surgical approach The surgical workflow of the electrical conductivity measurement technique as shown in figure 2.21 is very similar to that of the open 2D fluoroscopy-guided technique as shown in figure 4.4. The difference mainly lies in the fourth step involving pedicle cannulation. Instead of using the traditional pedicle probe as shown in figure 2.7, the surgeon uses the PediGuard[®] device, as shown in figure 2.19.



FIGURE 2.19: Electrical conductivity measurement device for open procedures. Figure from [50]

Minimally invasive surgical (MIS) approach The surgical workflow of the electrical conductivity measurement technique using the MIS approach as shown in figure 2.22 is very similar to that of the MIS 2D fluoroscopy-guided technique as shown in figure 2.13. The working principle of the PediGuard[®] for tissue differentiation is also identical. The difference lies in the

design of the tool. Instead of the traditional Jamshidi needle, the PediGuard bipolar sensor is incorporated in the starter stylet. In the disassembled cannulated PediGuard as shown in figure 2.20, it can be seen that the starter stylet containing the sensor is inserted into the Jamshidi needle while cannulation is performed.

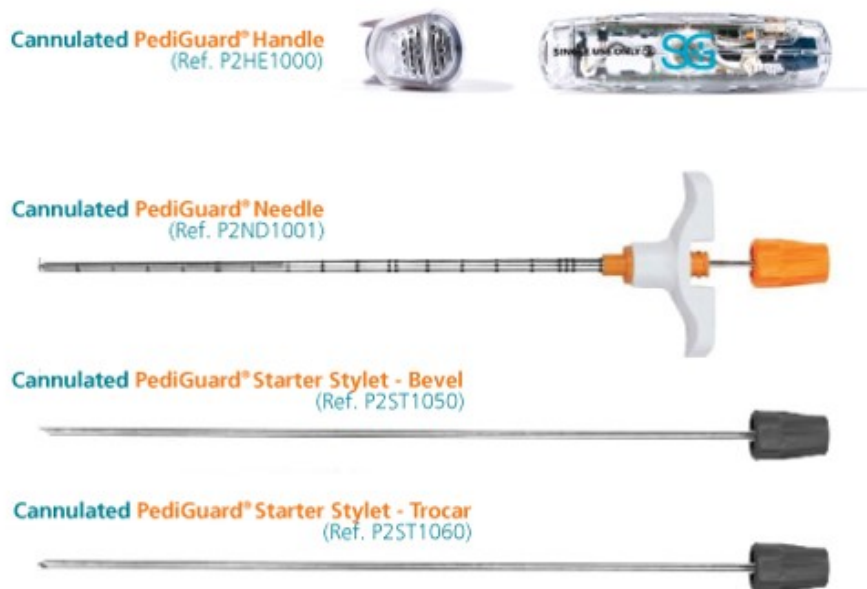


FIGURE 2.20: Electrical conductivity measurement device for MIS procedures.
Figure from [50]

Neurophysiological monitoring technique

The Neurophysiological monitoring technique is also a slight modification of the traditional approach. The goal of neurophysiological monitoring is to evaluate the integrity of the nervous system continuously during the critical steps of the procedure which have the potential to cause injury to the nervous system, particularly the spinal cord and spinal nerves [92]. There are several monitoring techniques or modalities available. The selection of the appropriate monitoring protocol by the surgeon and the neuromonitoring team depends upon the neural structures at risk.

One of the most common technique used for monitoring pedicle screw placement is the stimulated or triggered EMG monitoring [92]. Central to most techniques are the anode electrode, cathode electrode and the display monitor as shown in figure 2.23. The anode acts as the recording electrode usually placed at various locations of the body depending upon the monitoring modality chosen. The cathode acts at the stimulating electrode which is used to produce a fixed amount of current at the specific location of interest.

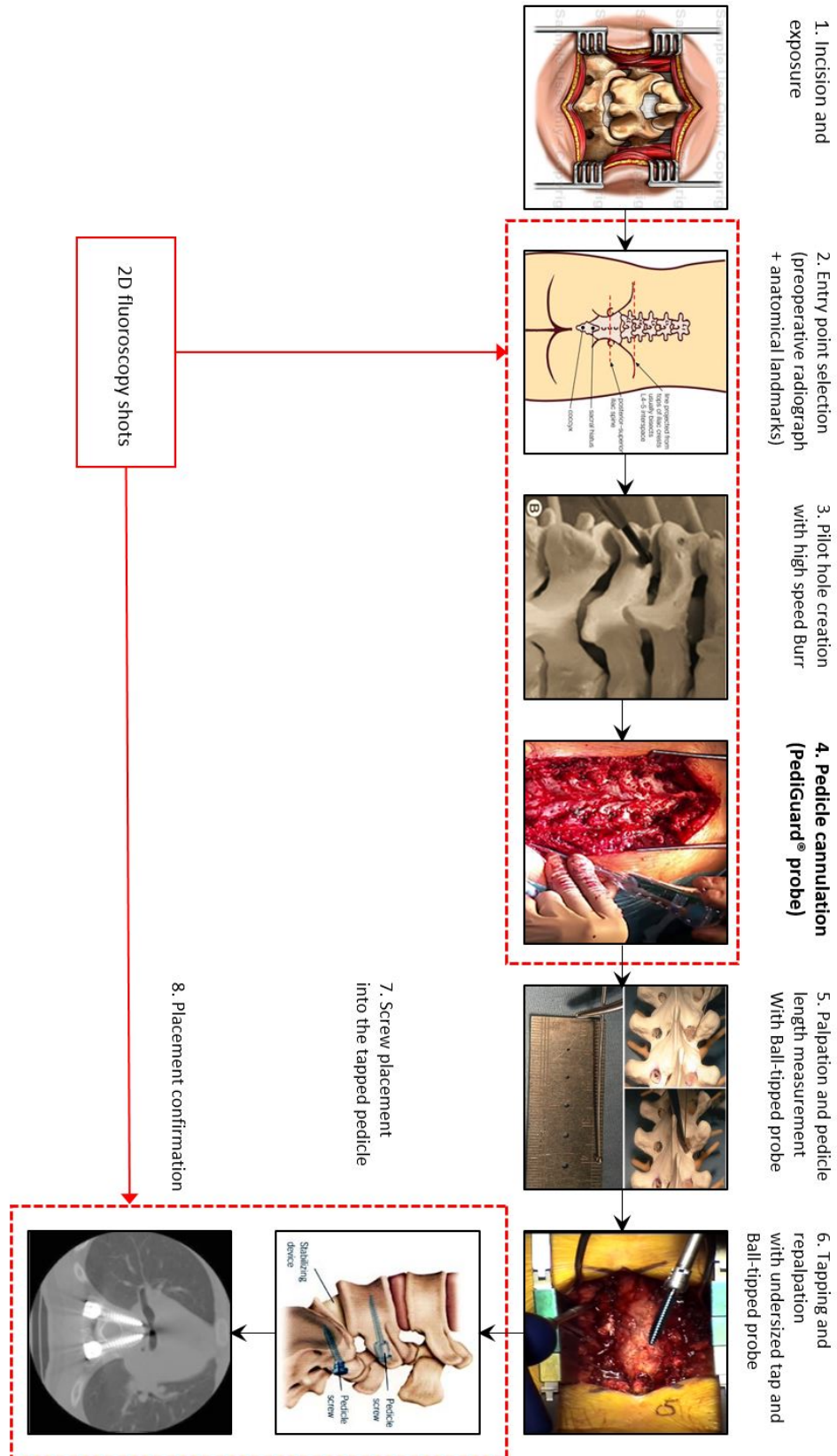


FIGURE 2.21: Surgical workflow of Electrical conductivity measurement technique (Open)

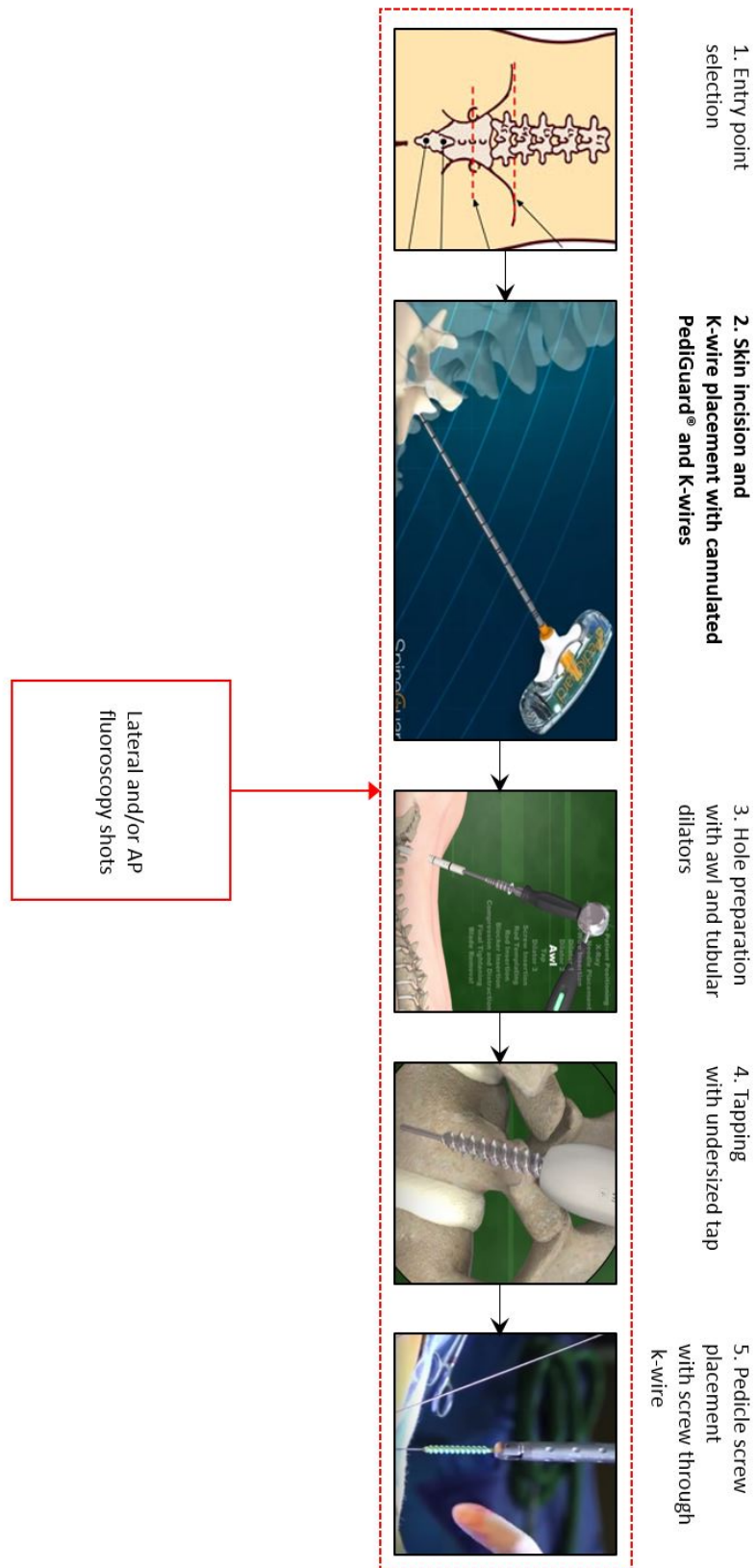


FIGURE 2.22: Surgical workflow of Electrical conductivity measurement technique (MIS)

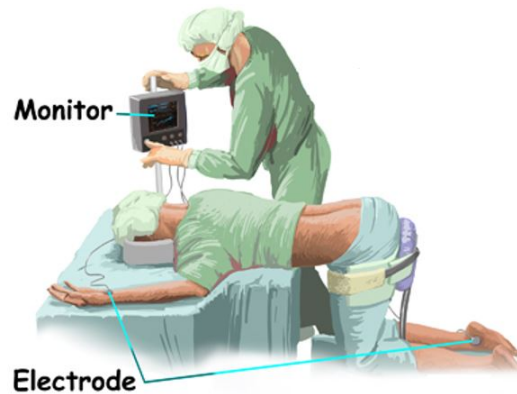


FIGURE 2.23: Intraoperative monitoring using neuromonitoring system.
Figure from [74]

The various neurophysiological monitoring modalities used in clinical practice are briefly discussed below.

Somatosensory evoked potential (SSEP) monitoring As the name suggests, SSEP recordings are used to assess the integrity of sensory pathways that traverse the spinal cord in the areas which are at the risk of injury. It is done by stimulating the peripheral nerves while recording from multiple sites. The level of surgery determines the choice of stimulation and recording sites. A loss or absence of recordings at the peripheral site, alerts the monitoring staff the presence of abnormality in the peripheral conduction pathways. A new SSEP recording can be generated at roughly 5 min intervals [92].

Motor evoked potential (MEP) monitoring This technique involves the monitoring of descending motor pathways which are sometimes used to check the results of SSEP monitoring. One of the most common MEP monitoring technique is the transcranial electrical stimulation [16, 119]. Corkscrew electrodes are placed on the scalp overlying the cortical motor areas which are used for stimulation to produce transcranial electrical MEPs (tceMEP). Recordings are made from subcutaneous or intramuscular needle electrodes placed in multiple muscles in the arms and legs [92].

Stimulated EMG monitoring This nerve-monitoring modality involves the recording and monitoring of spontaneous electromyographic (EMG) activity as shown in figure 2.24.

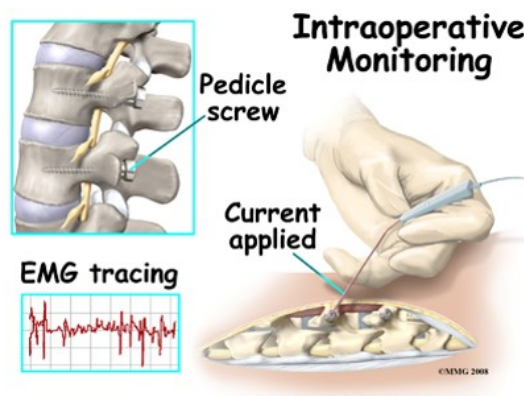


FIGURE 2.24: Intraoperative monitoring using neuromonitoring system.
Figure from [74]

Irritation of the nerves by stretching or compression can cause them to spontaneously discharge, producing trains of motor unit potential discharges in the muscles they innervate. By

watching the EMG tracings on the console, these neurotonic discharges can be detected. The stimulating electrodes are used to depolarize or stimulate the nearby nerves by applying a certain amount of current. The recording electrodes are used to pick up the EMG signal transferred through the nerve pathways. The stimulus intensity provided by the stimulating electrodes is directly dependent on their proximity to the nerves. If a low stimulus intensity is required to depolarize the nerves, it implies that the nerves are in close vicinity. This produces compound muscle action potentials (CMAPs). Therefore, the threshold stimulus intensity provided, is crucial in detecting a potential nerve injury.

Regardless of the type of modality, nerve-monitoring techniques slightly differ when it applying them using the open or MIS approach.

Open surgical approach The workflow of the open approach of the neuromonitoring technique for pedicle screw placement has been described in figure 2.26. It must be noted that the most popular modality, namely the stimulated EMG monitoring technique has been used as an example from here on.

The first step involves placing of the reference or recording electrodes at various locations in the body. This task needs a trained neuromonitoring team who understand the anatomical distribution of the various nerve pathways. Once this step is performed the neuromonitoring system is ready for use.

The next steps of making a midline incision, entry point selection, pilot hole creation and pedicle cannulation are identical to the free-hand technique. Palpation with a traditional ball-tipped probe to check for breaches might also be performed.

The cannulated pedicle is checked again by a monopolar ball-tipped stimulating probe. The triggered EMG reading is then recorded and observed in real time by the neuromonitoring team via the console or monitor.

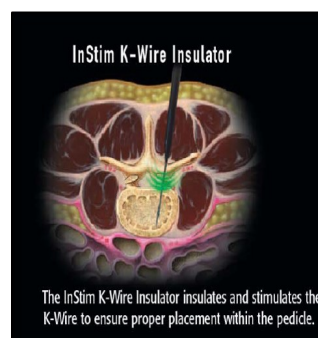
Tapping using an undersized tap is performed as usual. The prepared hole might be checked again using the monopolar stimulation probe.

Screw placement is then performed. Screw placement is then confirmed by directly stimulating the screw itself. 2D fluoroscopy images might also be acquired for reconfirmation.

Minimally invasive surgical (MIS) approach As shown from the workflow analysis described in figure 2.27, this MIS approach is a slight modification of the 2D fluoroscopy guided technique as shown in figure 2.13. Essentially, neuromonitoring via the stimulation probe is performed at every crucial step to ensure no nerves have been impinged. Like most MIS approaches, the nerve-monitoring electrodes have had to undergo a design modification. In order to stimulate the k-wire, tap or the pedicle screw, the surgeon has to now pass the electrode through various layers of fat, muscles and ligaments in order to check for nerve impingement locally. This presents a unique problem as it leads to significant loss in current density via the adjacent conductive soft tissue [91]. To mitigate this issue companies have modified the design by adding an insulator sleeve as shown in figure 2.28.



(A) Insulator sleeve used in a MIS approach.
Figure from [91]



(B) K-wire insulator used to stimulate the k-wire locally. Figure from [85]

FIGURE 2.25: Design modification of stimulation electrodes for MIS procedures

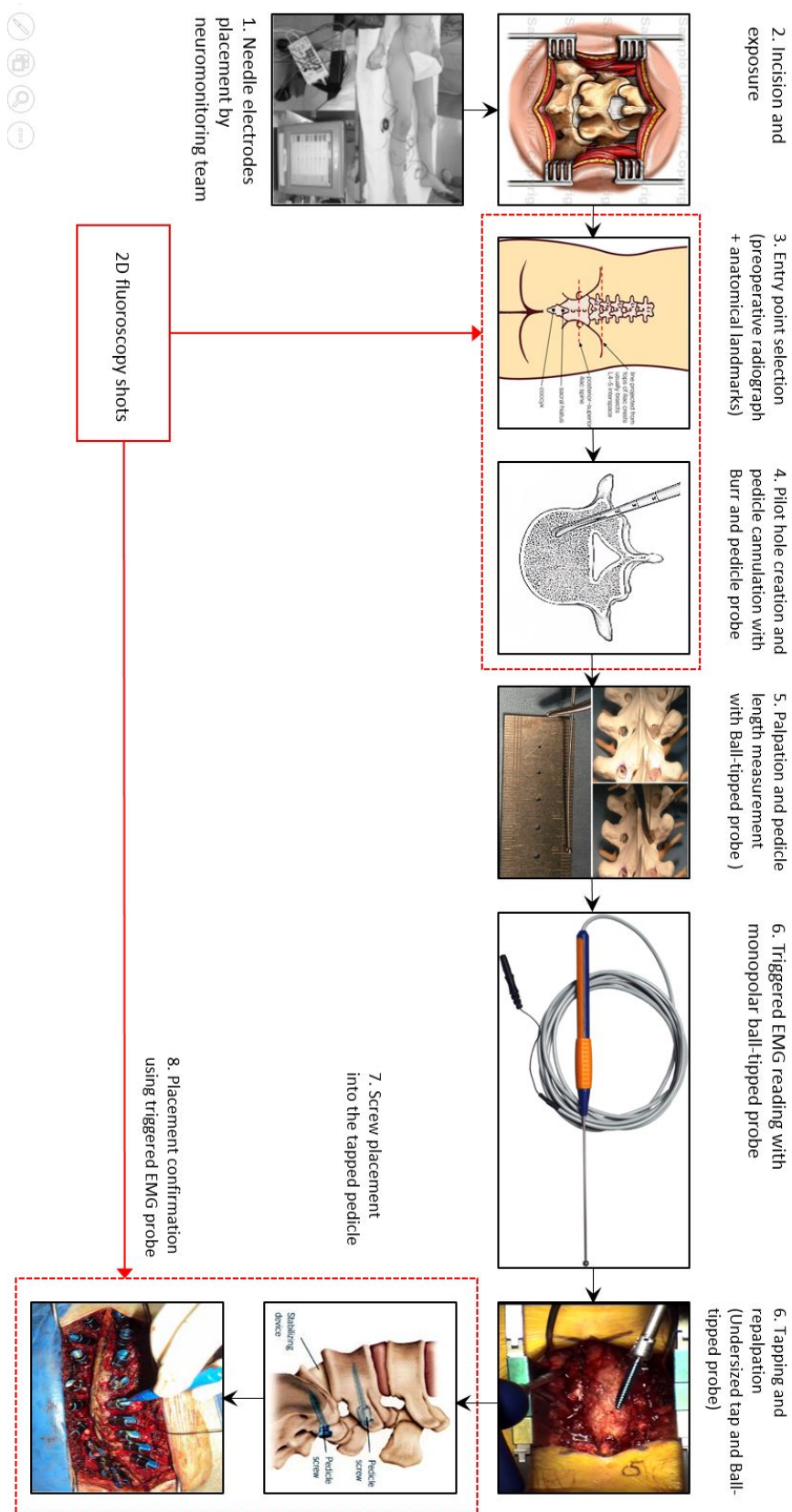


FIGURE 2.26: Surgical workflow of neurophysiological monitoring technique (Open)

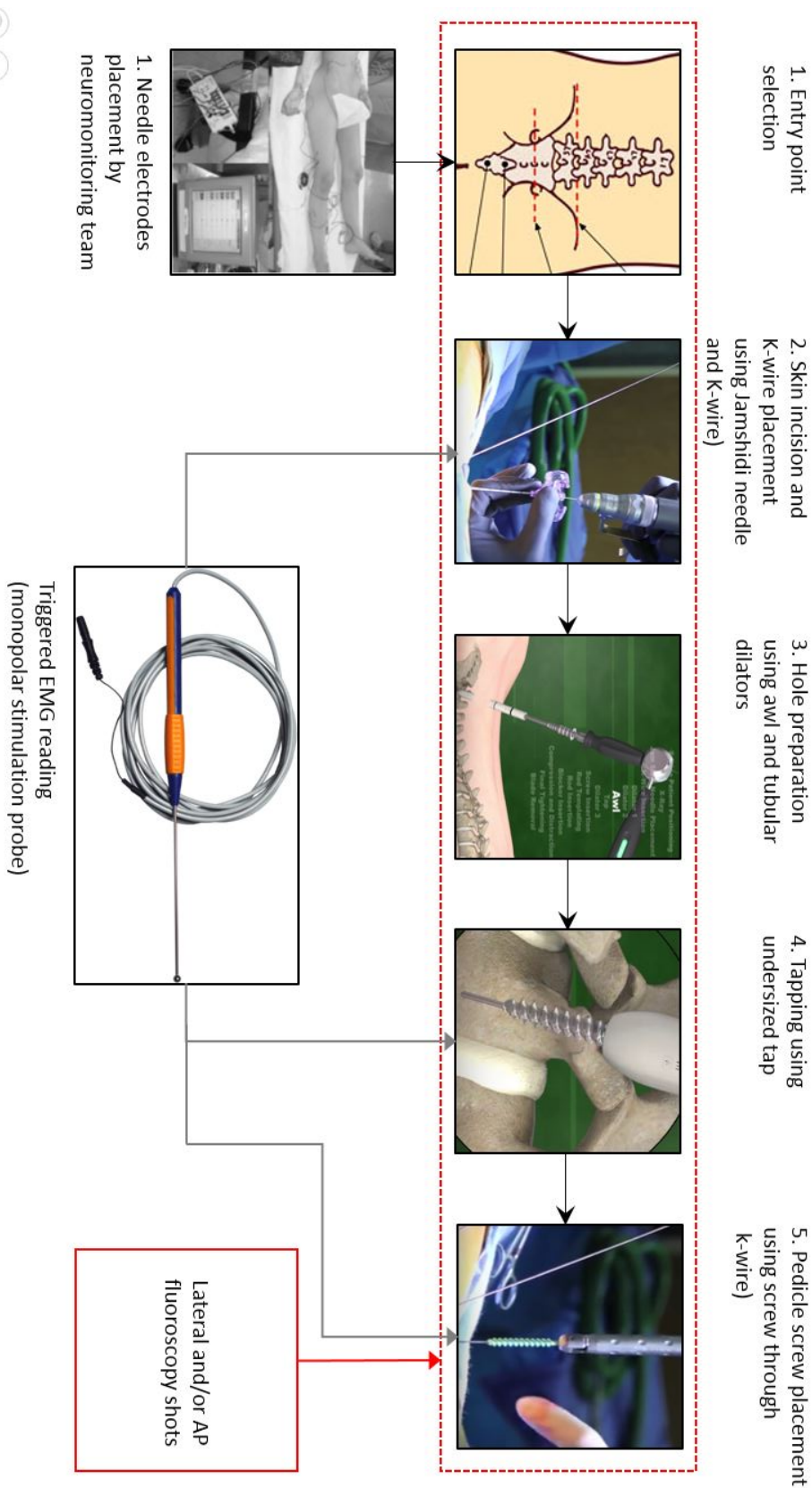


FIGURE 2.27: Surgical workflow of neurophysiological monitoring technique (MIS)

Discussion

The workflow analysis elaborated above was performed in order to meticulously visualize each step of the pedicle screw placement process. This analysis also helps to pinpoint the instruments used at each step of the process. It is important to note that the focus of this report is on the pedicle screw placement guidance techniques and the medical devices which are specifically used for guidance. Therefore, instruments such as the tap, retractors and K-wires etc. itself are not given special attention. A classification map was thus created to structurally sum up all the techniques as shown in figure 2.28.

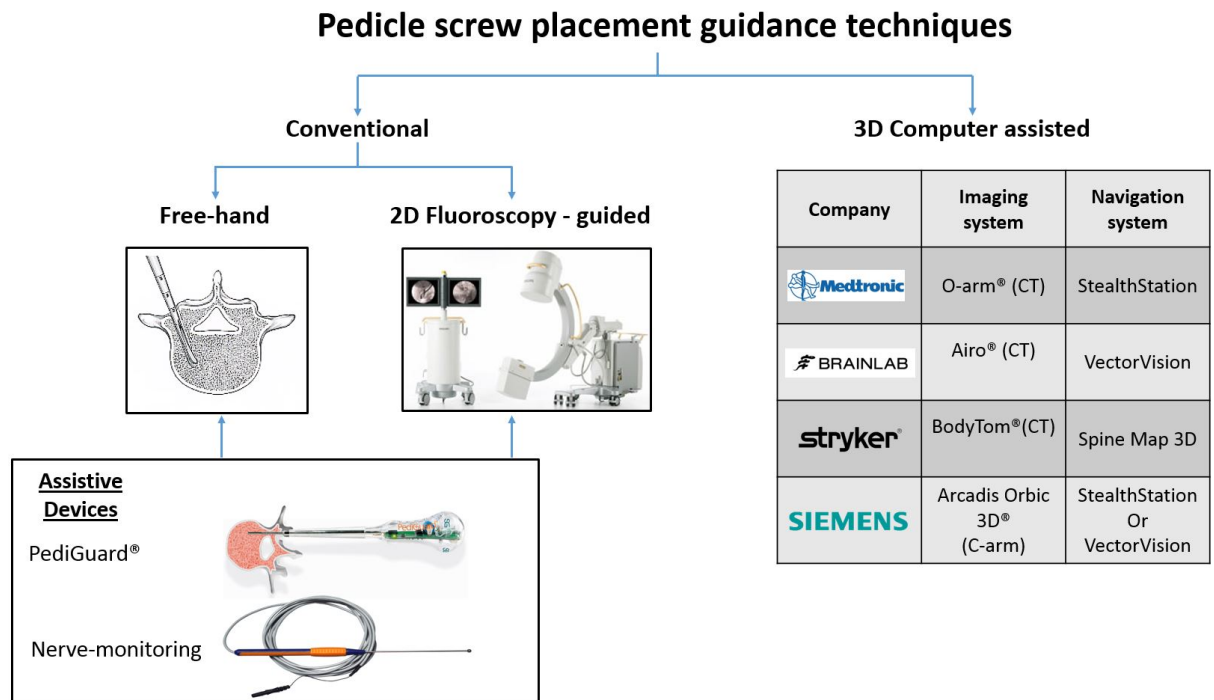


FIGURE 2.28: Structural classification of pedicle screw placement techniques

From the classification map it can be seen that there are three main techniques namely the free-hand, 2D fluoroscopy-guided and 3D computer assisted. Central to the electrical conductivity measurement and neurophysiological monitoring technique are the PediGuard and nerve-monitoring devices respectively. After careful analysis of the workflows it was found that these devices play more of an assistive role at the crucial steps of pedicle screw placement especially for the free-hand and 2D-fluoroscopy guided techniques. This was confirmed by visualizing the similarities between the workflows of conventional techniques with both electrical conductivity measurement and neurophysiological monitoring technique.

Conclusion

The workflow analysis described above helps answer the first of the four secondary research questions mentioned in subsection 1.0.1. Details of current techniques serve as a primer in answering the remaining research questions discussed in the following chapters.

2.4.2 Challenges in pedicle screw placement surgical procedure

This chapter focuses on the challenges of PSP faced by the surgeons while using the various techniques discussed in the previous chapter.

One of the most crucial parameters which has a direct impact on the outcome of the spinal fusion surgery is PSP accuracy. Malpositioned screws even without clinical symptoms can be directly linked to screw loosening [61] or pedicle break out [2], which can result in improper

fusion leading to spinal instability. In the worst case scenario a revision surgery might have to be performed.

Moreover, due to close proximity of vital neural and vascular structures, malposition of pedicle screws can put these vital elements at serious risk. To investigate this very risk, complication rate reported in literature was also studied. The dangers of radiation exposure especially to spine surgeons and OR staff due to repeated imaging would also be explored.

However, to calculate the accuracy rate, a well defined definition of a breach, perforation or malposition is essential. The findings from the literature search for a standardized breach definition is discussed in the subsequent section.

Breach definition problem

After an exhaustive literature review it was found that there exists a large amount of heterogeneity in coining the definition of a breach or malposition of a pedicle screw. This was concluded after finding approximately 8 unique accuracy definition types as elaborated in table 2.3. Despite the heterogeneity, two breach definitions seems to have gained high popularity among literature based on the number of citations. Breach definition corresponding to type 1 as described in table 2.3 is shown in figure 2.29

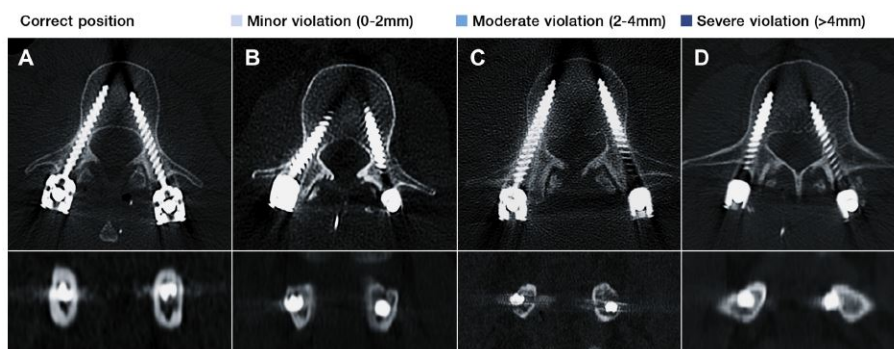
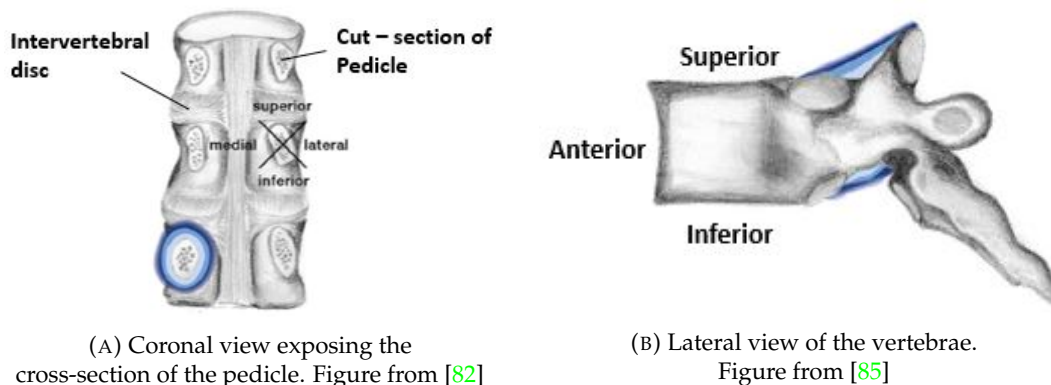


FIGURE 2.29: Axial and coronal CT images illustrating various screw positions corresponding to breach definition of type 1. Figure from [82].

Apart from a quantitative grading scheme as described in figure 2.29, researchers very often also use an anatomical grading scheme. This is based on screw penetration of either of the 4 walls of the pedicle located laterally, medially, superiorly, inferiorly as shown in figure 2.30a. An anterior penetration out of the vertebral body is also a possibility as shown from the lateral view of the vertebrae in figure 2.31b. This could occur for example due to an overestimated screw length selection.



(A) Coronal view exposing the cross-section of the pedicle. Figure from [82]

(B) Lateral view of the vertebrae. Figure from [85]

FIGURE 2.30: Anatomical grading system based on medial, lateral, superior, inferior or anterior screw penetration.

The type 1 definition is based on the notion of the existence of an 'anatomical safe zone' around the spinal canal. A study conducted by Laine *et al* [58] found that screw perforations by less than 4 mm did not cause any neurological problems. A meta-analysis conducted recently by Tang *et al* [120] used the type 1 definition as a basis for comparison of accuracy rates. Based on the 'anatomical safe zone' principle he defined grade 1 screws as 'perfect'; grade 2 screws as 'safe' zone screws; grade 3 screws as 'potentially hazardous' and grade 4 screws as 'absolutely hazardous'. Such a classification often leads to underreporting of malposition rates as researchers only report a breach if it falls under grade 3 or higher even though a breach has occurred.

The criteria based on the anatomical safe zone has not been left unchallenged [27]. The debate for a standardized breach definition is still unresolved. This is due to several factors. For instance, there exists significant anatomical variations among patient population. To add to the complexity is the anatomical variation between various spine regions such as cervical, thoracic, lumbar and sacral. Moreover, different imaging modalities such as fluoroscopy images and CT images have varying magnifications and resolutions. Therefore, accurate and repeatable measurement of breach distance is often not straightforward. All of these factors have led to several non-validated breach definitions adding to the increasing heterogeneity in literature. The above points have also been argued by several researchers [56, 121]

This is a fundamental problem which naturally questions the validity of the accuracy rates discussed in the next section. Some possible solutions to this problem would be addressed in the later part of this chapter.

Pedicle screw placement accuracy: Analysis of literature

Comparison of free-hand, 2D fluoroscopy-guided and computer-assisted techniques As elaborated in the previous section, a high amount of heterogeneity was found in literature primarily due to ambiguity in the accuracy definition. In order to make a fair and a relatively unbiased comparison of accuracy rates between techniques, highest level of evidence was chosen namely, meta-analysis and systematic reviews. A total of 7 articles were found between the years 2007 and 2014 based on the search criteria discussed in chapter 2. The median accuracy and the minimum and maximum placement accuracy (range) reported in each of these articles has been summarized in table 2.2.

TABLE 2.2: Accuracy table for conventional techniques

Source	Technique	Number of screws placed	Median accuracy (%)	Accuracy range (%)
Kosmopoulos 2007	Conventional	12299	90.3	27.6-100
Verma 2010	Conventional	2437	84.7	-
Tian 2011	Conventional	1358	82.6	-
Gelalis 2012	Free-hand	2412	-	69-94
Mason 2014	2D fluoroscopy-guided	3719	68.1	49.7-91.7
Gelalis 2012	2D fluoroscopy-guided	1902	-	28-85
Tian 2009	2D fluoroscopy-guided	1219	85.5	72.7-96

TABLE 2.3: Breach definitions reported in literature

Type	Breach Definition	Source
1	Grade 1: Fully located within the pedicle (Correct) Grade 2: Perforated screws with up to 2mm displacement Grade 3: Perforated screws with up 2-4 mm displacement Grade 4: Perforated screws with >4 mm displacement	[76, 132, 94, 141, 77, 84, 116, 84, 138, 36, 120, 49, 103, 146, 82]
2	Grade 0 : Within the cortex (Correct) Grade 1: Malposition by less than half screw diameter(<2 mm) Grade 2: Malposition by more than half screw diameter(>2 mm)	[53, 48, 21, 60, 133, 22, 140, 43, 19, 104, 130]
3	Correct: Screw completely surrounding cortex Breach: Any part of screw outside cortex	[78, 143, 87]
4	Breach: >25 % screw dia outside pedicle or cortex	[96]
5	Grade 0: Non-breached screws (Correct) Grade 1: Screws perforating wall and exposing 0-90 of screw circumference Grade 2: Screws perforating wall and exposing 90-180 of screw circumference Grade 3: Screws perforating wall and exposing 180-270 of screw circumference Grade 4: Screws perforating wall and exposing 270-360 of screw circumference	[18]
6	Grade 1: Perforation of VA foramen but not violating largest dia of VA foramen Grade 2: Screw violating largest dia of VA foramen but not completely occluding it Grade 3: Complete occlusion of VA foramen	[93]
7	Grade 1: Screw completely within the vertebral body and pedicle Grade 2: Screw contained within pedicle rib complex with screw tip within VB Grade 3: Screw tip located laterally or anteriorly to VB Grade 4: Screw tip perforated inferior or medial pedicle border Grade 5: Neural or vascular structures at risk and require removal or revision	[109]
8	Encroachment: If the pedicle cortex could not be visualized Minor penetration: Screw <3 mm outside the pedicle boundaries Moderate penetration: Screw 3-6mm outside the pedicle boundaries Severe penetration: Screw >6mm outside the pedicle boundaries	[1]

The first meta-analysis on pedicle screw placement accuracy was conducted by Kosmopoulos *et al* [56]. After applying a rigorous search criteria and statistical analysis, two techniques were compared, namely, screw placement without (conventional) and with the aid of navigation. It was not made explicitly clear as to whether free-hand and 2D fluoroscopy-guided come under the gambit of screw placement without navigation. In any case, 12,299 pedicle screws placed in 32 *in vivo* patient studies were analysed in the non-navigated group. The median placement accuracy was found to be 90.3% with the minimum and maximum accuracy ranging between 27.6% and 100% respectively. This clearly illustrates an extremely high accuracy variability. A total of 3059 screws placed in 21 studies were analyzed for the navigation technique. The median accuracy was found to be 95.1% ranging between 72% and 100%.

The second comprehensive meta-analysis was conducted by Tian *et al* [121] specifically on image-guided pedicle screw insertion accuracy. Three groups or techniques were compared namely, 2D fluoroscopy-navigated (2D FluoroNav), 3D fluoroscopy-navigated (3D FluoroNav) and CT-navigated (CT Nav). It must be noted that 2D FluoroNav is not specified in the classification map shown in figure 2.28. This is because it can be considered under 2D-fluoroscopy-guided technique. As far as 3D FluoroNav and CT Nav groups are concerned, they both come under 3D Computer assisted techniques. Free-hand technique and other techniques using assistive devices were excluded. For the 2D FluoroNav group, 1219 pedicle screws were placed

with a median accuracy and range of 85.48% and 23.32% (minimum 72.73%, maximum 96.05%), respectively. In the 3D FluoroNav group, 1290 pedicle screws were placed. The median accuracy and range were 97 % and 18.44 % (minimum 80.85% maximum 99.29%), respectively. For the CT Nav group, the range in placement accuracy was 26.22% (minimum 72.03% ,maximum 98.25%) with a median accuracy of 90.76%.

The same author namely Tian *et al* [122] performed another systematic review and meta-analysis this time comparing conventional and navigation techniques. They also compared the groups within the navigation group namely, 2D and 3D Fluoroscopy-based navigation and 3D CT-based navigation. Results showed that the median accuracy rate of conventional versus navigation group was found to be 82.6 % and 96.4% respectively. Within the navigation group, 3D Fluoroscopy-based navigation was found to have the highest accuracy compared to CT-based and 2D Fluoroscopy-based navigation.

Verma *et al* [128] made a similar comparison like Kosmopoulos *et al* [56] by comparing techniques without (conventional) and with the aid of navigation. Again, the definition of 'conventional' was not explicitly stated. A total of 23 studies including 5992 screws met the inclusion criteria. Of the 2437 screws placed in the conventional group, 84.7% were found to be accurately placed. In the navigation group, out of 3555 screws placed in total, 93.3% were placed accurately. A statistically significant advantage of the navigation technique over the conventional technique was also shown.

The fifth study discussed here is a systematic review comparing accuracy of pedicle screw placement between free-hand, fluoroscopy-guided and navigation technique published recently by Gelalis *et al* [36]. It must be noted here that this is the first systematic review which clearly defined the groups being compared. A total of 26 prospective clinical studies were included in which 6,617 screws were placed. Results showed that using the free-hand technique, the accuracy rate ranged from 69 to 94%, with the aid of fluoroscopy from 25 to 85%, using CT-based navigation from 80 to 100 % and using fluoroscopy-based navigation from 81 to 92%. Unfortunately no parameter indicating the central tendency of the placement accuracy such as the mean, median or mode was specified.

One of the most recent systematic literature review was performed by Mason *et al* [71]. The author compared placement accuracy between conventional fluoroscopy-guided, 2D fluoroscopy-guided navigation and 3D fluoroscopy-guided navigation. The results showed that out of 3719 screws placed using 2D fluoroscopy guided technique, the median accuracy rate was found to be 68.1 % with a minimum and maximum rate of 49.7 and 91.7% respectively. In case of 2D-fluoroscopy-based navigation, a total of 1223 screws were placed with an accuracy rate of 84.3 (minimum 73.7 %, maximum 95 %). Lastly, 4368 screws were placed in total using the 3D fluoroscopy-guided navigation technique. The accuracy rate was found to be 95.5 % (minimum 80.9 %, maximum % 100).

Another recent meta-analysis was performed by Tang *et al* [120] who not only compared the placement accuracy between navigation and conventional techniques but also did a subgroup analysis based on type 1 definition of breach as shown in 2.3. He used one the most commonly used breach definitions cited in literature based on the safe zone principle described in section 4.1. For all of the subgroups he found that navigation had superior placement accuracy than conventional techniques. However, he also provided evidence that there is an obvious publication bias in reporting positive outcomes.

Assistive devices

Electrical conductivity measurement device: PediGuard[®] There are 4 articles published in literature using the PediGuard to cannulate the pedicle on human subjects [5, 19, 11, 90]. Bai *et al* [5] placed 694 screws in 42 patients and reported an accuracy rate of 95.9 %. Chaput *et al* [19] placed screws using the PediGuard and the standard pedicle probe. He placed 78 screws in 18 patients. Although the accuracy rate was found to be 97.5 %, he found no difference in accuracy rate between the PediGuard and pedicle probe. Other studies on human subjects were used only to perform pedicle cannulations. 3 cadaveric studies using the PediGuard were also found. Study by Koller *et al* reported an accuracy rate of 88.9 % after placing 60 screws in 5 cadavers.

Neurophysiological monitoring device A very recently published systematic review and meta-analysis by Lee *et al* [60] studied the diagnostic test accuracy of triggered electromyography (t-EMG) in pedicle screw placement. t-EMG is the most common modality used for neurophysiological monitoring [92]. Enrolled studies included 13,948 lumbar and 2070 thoracic screws. The overall sensitivity and specificity values of t-EMG were found to be 0.55 and 0.97 in the lumbar spine and 0.41 and 0.95 in thoracic spine respectively, indicating a weak diagnostic value. Blas *et al* [10] found the rate of malposition to be as high as 18.7 % using t-EMG. He also concluded that t-EMG has a low sensitivity in predicting screw malpositioning. Other studies also found a similar result [111, 57].

Dangers of radiation

One of the popular techniques for PSP placement among conventional techniques is 2D-fluoroscopy-guided technique. As the name suggests, the surgeon uses an image intensifier to acquire fluoroscopy shots in order to avoid violations. The radiation exposure as a result of these shots on the patient and more importantly on the surgeon cannot be underestimated.

Upon careful observation of the workflows specifically of 2D fluoroscopy-guided technique as shown in figure 4.4 and figure 2.13, it can be observed that surgeons acquire 2D fluoroscopy shots quite often especially at the crucial steps of the procedure. This aspect of high radiation dosage to the surgeons is also reflected in literature. Rampersaud *et al* [105] found that spine surgeon who perform fluoroscopy-guided pedicle screw insertion experience a 10 to 12 fold increase in radiation dosage than recommended.

Study by Haque *et al* [44] also found the high amount of radiation exposure on the spine surgeons as unacceptable. In fact, he estimated that spine surgeons beginning their career at the age of 30 would exceed the recommended life time limit in less than 10 years.

Adding to the concern is the fact that surgeons performing MIS procedures would inevitably acquire many more fluoroscopy shots due to limited visualization. The workflow for the 2D-fluoroscopy-guided MIS approach depicted in figure 2.13 clearly points to this growing problem. Bindal *et al* [9] also cautions against exceeding surgeons annual dose limits due to increasing trend towards the adoption of MIS approaches in spine surgery.

Pedicle screw-related complication rate: Analysis of literature

By determining the prevalence of complications associated with pedicle screw placement, the magnitude of the problem can be addressed. A recent systematic review of 35,630 pedicle screws by Gautschi *et al* [34] provides by far the most exhaustive analysis of the clinically relevant complications related to pedicle screw placement. The article makes it clear that no exact definition of complication exists. Distinction between clinically relevant complications and asymptomatic screw-related complications needs to be made as several malpositioned screws might lead to no complications an example of which is shown in figure 2.31.

It is also difficult to differentiate between screw related and general complications. It is important to make the distinction between intraoperative and postoperative complication rate as some surgeons might under-report intra-operative complications after making corrections. Therefore, it becomes clear that the exact quantification of screw-related complication rate is extremely difficult.

Having said that, the author divides screw-related complications into various types such as complications due to nerve root or spinal cord injury, vascular injury, cerebrospinal fluid leak, visceral injury, pedicle fracture, screw pullout, screw breakage and late spinal instability. Dural lesions and nerve root irritation were reported in a mean of 0.18 % and 0.19 % per pedicle screw, respectively.

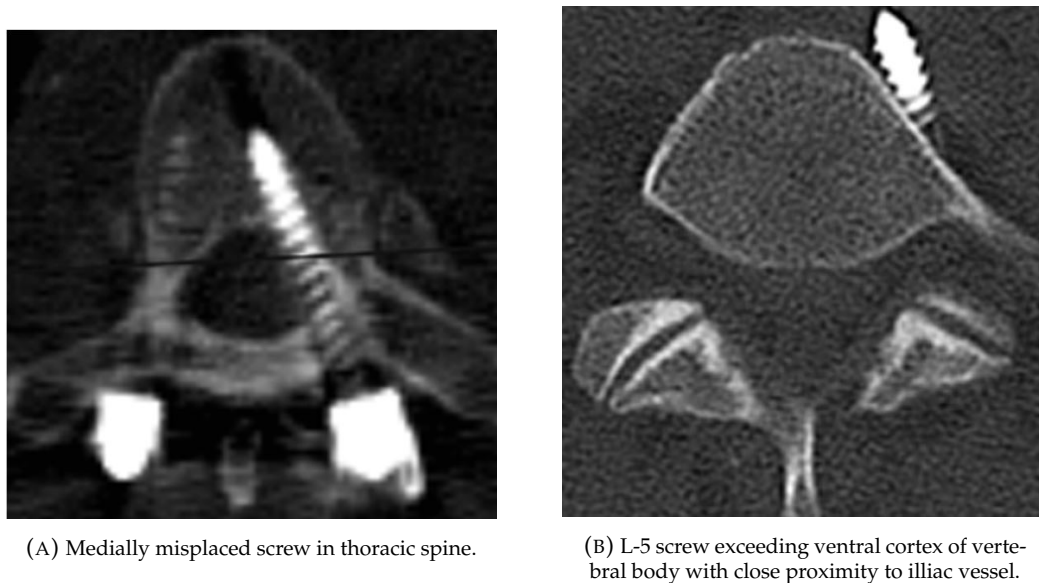


FIGURE 2.31: CT scans of severely malpositioned screws without patients suffering from neurological or vascular deficits. Screws not revised. Figures from [34]

Results show that clinically-relevant screw-related complication rates are low but serious, primarily because neural and vascular injuries could be potentially life threatening. However, these figures should be interpreted with caution as it is unclear whether these low reported numbers are due to low incidence of serious complications or whether they are subject to underreporting due to authors' medicolegal considerations.

A meta-analysis by Verma *et al* [128] compared the functional outcome of computer-assisted technique versus conventional techniques in pedicle screw placement. It was found that navigation using computer-assisted technique does not show statistically significant benefit in reducing neurological complications. He also concluded that neurological complications associated with pedicle screw placement is rare but a serious complication. This fact is also backed by other literature who have reported neurological problems as severe as ranging from numbness to lower-extremity paraplegia [2, 4, 66, 34]. figure 2.32 illustrates a case of new-onset radiculopathy due to a medially misplaced screw. It was confirmed that the complication was screw-related because the symptoms disappeared after screw replacement [34]. Vanischkachorn *et al* [127] presented a case of serious vessel injury in which one patient died and another underwent limb amputation.



FIGURE 2.32: CT scan showing an axial view of a right medially misplaced screw in L-4, which caused new on-set radiculopathy. Symptoms disappeared after screw replacement. Figure from [34].

Another recently published meta-analysis also compared complication rate associated with pedicle screw placement with and without navigation [120]. Based on their analysis of 4953 screws, they found that navigation techniques led to a significantly lower incidence of screw-related complications compared to conventional techniques. They also found fewer symptomatic complications relative to high perforation rate.

Discussion

Pedicle screw placement is a technically demanding procedure which has several challenges associated with it. There are several companies and research groups trying to develop better technologies in order to improve the clinical outcome of the procedure. In this chapter two crucial dependent outcome parameters were discussed in order to compare various techniques namely accuracy and complication rate. To compare accuracy rates of PSP of various techniques, a standardized and validated definition of accuracy or breach needs to be established. Unfortunately, such a definition is lacking in literature. This led to the creation of several accuracy definitions by researchers increasing the heterogeneity in this domain.

However, the definition based on anatomical safe zone principle has been cited widely. Even with this fundamental limitation, several meta-analysis and systematic reviews have been published with an attempt to homogenize articles and help draw legitimate conclusions. After an extensive analysis of the best evidence available in literature, high variability in accuracy rate for PSP was found in free-hand and fluoroscopy-guided techniques. The wide error bars in figure 2.33 clearly reflect this trend (The central tendency of the range specified by Gelalis *et al* [36] could not be found). This might help reiterate the fact that PSP is in fact a technically demanding procedure.

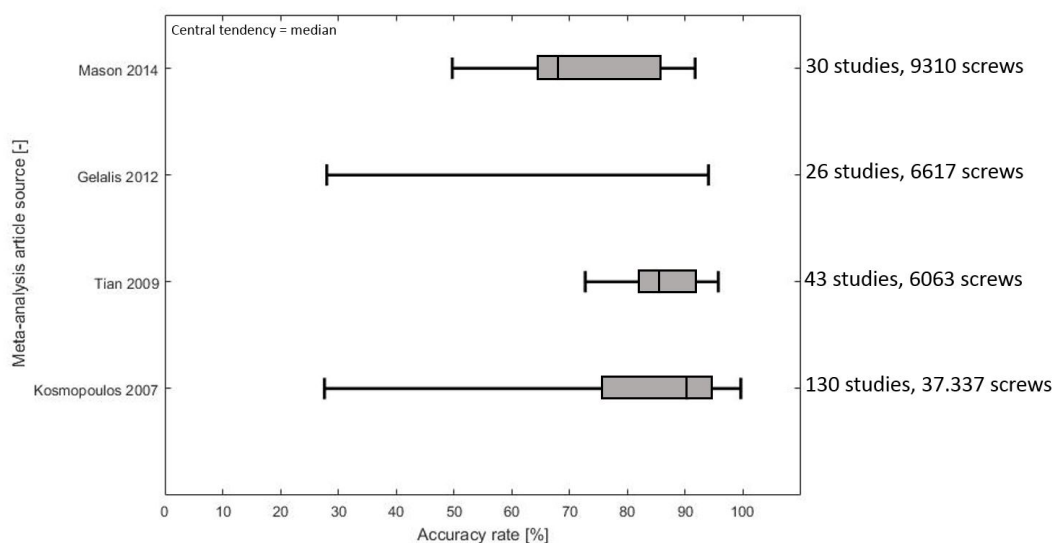


FIGURE 2.33: Median accuracy and range for conventional techniques.
(Error bars indicate min and max accuracy rates)

There is also a unanimous verdict on the superiority of the accuracy rate of computer-assisted technique over conventional techniques. The relatively shorter bars depicting range and median accuracy in figure 2.34, descriptively confirm this fact.

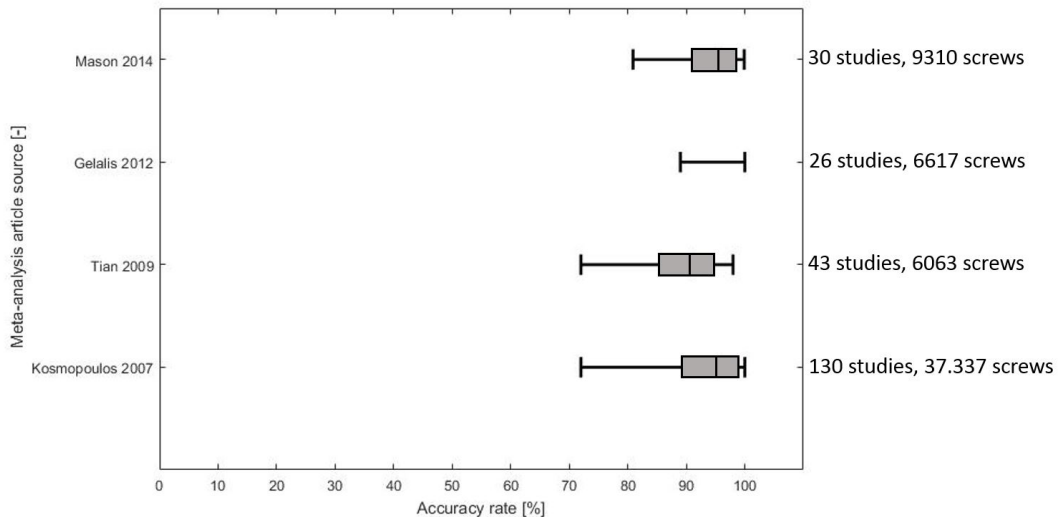


FIGURE 2.34: Median accuracy and range for CAS technique.
(Error bars indicate min and max accuracy rates)

Several assistive devices have also been developed in order to improve the accuracy rate of especially the free-hand and 2D-fluoroscopy-guided techniques. The neurophysiological monitoring devices come under this category. In literature there seems to be a clear trend signifying that these devices have low sensitivity to detect breaches which implies that the device has high false negative rates. In other words, there is a high probability that although the EMG tracings signify normal nerve activity, there is in fact nerve impingement or injury of some sort.

The PediGuard device has shown to have quite high PSP accuracy. However, there are very few articles which have confirmed this fact. As such, the PediGuard can be considered more superior to the nerve-monitoring devices in detecting breaches.

Radiation exposure especially to the surgeons has started to become an evergrowing problem. With the current frequency of fluoroscopy shots acquired during surgery coupled with the sharp rise of spinal fusion cases worldwide, surgeons exceeding the recommended lifetime dosage poses a serious health risk. The growing trend of adopting the MIS approach is only going to aggravate the problem.

Complication rates have only been extensively studied for the three main techniques. There does seem to be a trend suggesting that the complication rate associated with the pedicle screw placement is low. However, as discussed in the previous section, this low trend could be due to the surgeons' reluctance to report complications due to medicolegal considerations. Anyhow, although the complication rate reported in literature is low, they can be potentially life threatening and should not be underestimated.

Conclusion

A critical analysis based on the highest level of evidence found in literature has led to the following conclusions:

1. There is no standardized breach definition available in literature
2. High variability in accuracy rates were found especially in free-hand and 2D Fluoroscopy-guided techniques.
3. The Computer-assisted technique has a superior placement accuracy rate than free hand and 2D-Fluoroscopy-guided techniques.
4. PediGuard does exhibit higher accuracy than traditional pedicle probe. However, literature confirming its high placement accuracy is scarce.
5. Neurophysiological monitoring devices, especially the popular triggered EMG monitoring technique has low sensitivity in detecting nerve injury.

6. High radiation exposure experienced by surgeons is a serious and an ever growing concern.
7. Complication rates reported in literature are low but can be potentially life-threatening.

2.4.3 Pedicle screw placement guidance techniques: A Trade-off analysis

In this chapter the pros and cons of each technique based on the critical analysis of literature would be discussed in detail. The challenges of PSP elaborated in the previous chapter play a crucial role in building this trade-off analysis.

Apart from literature, clinical perspective of the surgeons was also gathered to help get a clearer picture of the problem. A survey questionnaire published by Patel *et al* [97] of 67 spine surgeons representing United Kingdom and Ireland would be discussed.

The chapter would conclude with a very brief look at the market specifically for assistive devices to investigate whether there exists a commercial need to solve the problem of PSP.

Conventional techniques

The classification map in figure 2.28 helps segregate the conventional techniques into Free-hand and 2D fluoroscopy-guided. The fundamental trade-offs associated with each of these techniques would be discussed in the following sections.

Free-hand technique

Advantages Given the fact that ideally the free-hand technique does not involve the use of any intra-operative imaging modality, the radiation exposure to the patient and OR staff is reduced to a bare minimum.

The increased surgical site exposure due to the open nature of this technique allows the surgeon to directly visualize the vital spine elements. This helps the surgeon to match the visual feedback with the tactile feedback of the instruments.

Due to the very limited use of imaging modalities, the surgical workflow is left uninterrupted. It also makes the procedure relatively inexpensive.

Disadvantages This technique relies heavily on meticulous identification of anatomical landmarks to identify the ideal entry point and screw trajectory. Thus, the success of this technique is extremely dependent on surgeons experience. This aspect is strongly reflected in the high variability in PSP accuracy rate mentioned earlier in section 4.4 and descriptively depicted in figure 2.33.

This technique relies on an open approach exposing the entire surgical area. This leads to large amount of muscle stripping. A study by Stevens *et al* [118] quantified the amount of paraspinal muscle damage and muscle edema due to the open approach by measuring the peak intramuscular pressure (IMP) in a lumbar fusion case. They concluded that the open approach lead to significantly more muscle damage than the MIS approach. This approach also leads to significantly higher blood loss, longer recovery time and hospital stays [95, 98]. The trade-offs involved have also been summarized in table 2.4.

TABLE 2.4: Trade-off analysis of the main techniques

Technique	Advantages	Disadvantages
Free-hand	<ul style="list-style-type: none"> • Minimized radiation exposure • Uninterrupted workflow • Low procedural costs 	<ul style="list-style-type: none"> • High accuracy rate variability • Muscle stripping due to high surgical exposure
2D Fluoroscopy-guided	<ul style="list-style-type: none"> • Uninterrupted workflow • Real-time image acquisition • Low procedural costs (Compared to CAS) 	<ul style="list-style-type: none"> • High accuracy rate variability • High radiation exposure • Limited visualization due to 2D images
3D Computer-assisted	<ul style="list-style-type: none"> • High placement accuracy • Relatively low radiation exposure • Allows for screw trajectory planning • Better handling of complex cases due to 3D visualization 	<ul style="list-style-type: none"> • High workflow interruption due to registration procedures • Longer operation time with increase in instrumented spine segments • Limited field of view • High cost of system

2D fluoroscopy-guided technique

Advantages One of the most common imaging modalities used in pedicle screw placement is the C-arm which acquires 2D fluoroscopy images. It has a big advantage of its ability to acquire real-time images which can be very useful to the surgeon during various stages of the procedure.

Also, due to the relatively quick image acquisition and visualization, the surgical workflow is left uninterrupted.

In case of MIS procedures, fluoroscopy images immensely enhance the visualization of surgical site. In fact, MIS procedures cannot be performed without the aid of an imaging system.

Disadvantages High accuracy variability found in literature in placing the pedicle screws in the appropriate location via this technique is major concern. It might be due to limited visualization due to 2D nature of the images as shown in figure 2.35. This is especially a problem while dealing with complex deformities and unusual anatomy.



FIGURE 2.35: Lateral and oblique 2D fluoroscopic views of the lumbar spine during PSP. Figure from [12].

One of the other important disadvantages is the high radiation dosage experienced by the surgeons. This problem has been given special attention in section 4.3. High radiation dosage is a serious long term problem especially in MIS and spine deformity cases where more visualization is warranted.

3D Computer-assisted technique

Advantages There is clear consensus in literature that 3D computer-assisted techniques are superior than free-hand and 2D fluoroscopy-guided in terms of PSP accuracy.

The surgical workflow has been optimized such that during the image acquisition process, the surgeon and the OR staff leave the OR and therefore receive limited radiation exposure. This fact has been confirmed by various studies [35, 114].

Another important advantage of the computer-assisted technique is that it allows for screw trajectory planning. The enhanced visualization accomplished with the help of the 3D images augmented by instrument tracking, allows the surgeon to plan the entry point as well as the screw trajectory before the actual perforation of the pedicle.

The ability of the surgeon to visualize instruments in multiple orientations simultaneously in real-time helps the surgeon to deal with cases with complex deformities and unusual anatomy. It also helps facilitate the MIS approach when needed.

Disadvantages Manbachi *et al* [68] in his review article clearly elucidated the potential disadvantages of the computer-assisted technique.

Discrepancies in patient positioning during preoperative and intra operative CT scans might influence placement accuracy. Marker movements during surgery due to a variety of reasons such as large skin deformations might necessitate the need for reregistration. This would mean that the entire registration process might have to be redone which might effect the operation time and cost significantly.

Due to registration inaccuracies, optical systems have an accuracy of around 0.3 mm [81] and electromagnetic systems have accuracies ranging from 0.5 to 0.9 mm [139, 64]. Cervical spines are much smaller in size and such errors are comparable to its pedicle sizes. This limits the use of instrumentation using computer-assisted technique in the cervical region.

Another important problem is the limited field of view. Each registration procedure normally takes into consideration three to five vertebrae at a time. In case of spinal deformities such as Scoliosis where longer segments are typically exposed, multiple registration procedures are required in order to obtain a full and accurate view of the operating area [68]. This can be a matter of great inconvenience especially in terms of workflow interruption and operation time.

Comparing the surgical workflows of the computer-assisted and fluoroscopic technique as shown in figure 4.4 and figure 2.16 respectively, it is observed that the actual procedure starts only in step 5. Therefore, the entire set-up procedure might significantly contribute in disruption of the traditional surgical workflow.

As Watkins *et al* [134] points out, the average cost of a navigation system is close to \$475,000. Such a high initial investment of close to half a million dollars does pose as a limitation. However, the author concludes that navigation systems may be cost-effective in spine cases with heavy volume, that perform surgery in difficult cases. This statement must be interpreted with great caution as the author is a paid consultant for BrainLAB and Siemens. Thus, there might be a significant bias due to the existence of a conflict of interest. Sanborn *et al* [112] compared the cost effectiveness of PSP techniques in confirming screw placement. He found the O-arm to be least costly than neurophysiological monitoring and postoperative CT scans in confirming location of screws.

Assistive devices

As discussed in section 3.6 and based on the classification map shown in figure 2.28, electrical conductivity measurement device and neurophysiological monitoring device are categorized together under assistive techniques. This is done so because these devices are used more in conjunction with palpation and 2D-fluoroscopy images to optimize safe pedicle screw placements.

The summary of the trade-off analysis performed on the assistive devices is shown in the table 2.5.

Electrical conductivity measurement device: PediGuard[®]

Advantages The device has shown to exhibit an accuracy rate as high as 95.9 % [5] Although a cadaveric study did report an accuracy rate as low as 88.9 %. In any case, since the device is designed to be a smarter version of the pedicle probe, it does seem to have superior accuracy than the traditional pedicle probe.

Due to the added sensing at the tip, one would expect the lowering of the reliance of 2D fluoroscopy images in pedicle cannulation. Study by Chaput *et al* [19] did find a 30 % reduction in fluoroscopy shots when the surgeon used the PediGuard instead of the standard probe.

The device has the ability to perform breach anticipation in real-time providing information to the surgeon in a timely manner to correct probe trajectory.

Since the device is designed like the pedicle probe for open approaches and like the Jamshidi needle for the MIS approaches, it seamlessly integrates into the traditional surgical workflow. The device is wireless and disposable, which is an added bonus.

TABLE 2.5: Trade-off analysis of assistive devices

Technique	Advantages	Disadvantages
PediGuard [®]	<ul style="list-style-type: none"> • Higher accuracy than conventional probe • Breach anticipation capability in real time • Reduced radiation exposure due to additional feedback • Hand-held disposable device 	<ul style="list-style-type: none"> • Technique dependent sensitivity in detecting breaches • Inability to plan probe trajectory before cannulation.
Neurophysiological monitoring devices	<ul style="list-style-type: none"> • High specificity in nerve injury detection • Real-time assessment of neurological deficits • Low nerve stimulation and recording time • Ability to perform multiple stimulations without workflow disruption 	<ul style="list-style-type: none"> • Low sensitivity in detecting breaches (Lumbar = 55 %, Thoracic = 41 %) • No consensus on critical threshold values • Cannot detect lateral breaches • Readings affected by factors such as anesthesia, body temperature, muscle relaxants, screw material properties etc. • Requires relatively well trained personnel

Disadvantages Studies have reported that the device has high technique dependent sensitivity in detecting breaches [145, 40]. Especially decreasing the pressure while cannulation causes blood to intervene leading to an inevitable false alarm. Also, variation in hand placement during advancement of the probe alters sound quality [40].

One study found that 31% of the screws placed using the PediGuard were longer than expected. They concluded that the device is not satisfactory in predicting length of screws [145].

An important fundamental limitation of the PediGuard was highlighted by Manchabi *et al* [68]. The PediGuard is essentially a trajectory verification device, which means that the surgeon essentially will always cannulate the pedicle blindly. Based on the sensing feedback the surgeon can then course correct the trajectory. This is distinctly different from computer-assisted technologies where the surgeon can plan the screw trajectory in advance.

Neurophysiological monitoring devices

Advantages As the name suggests, neurophysiological monitoring devices are dedicated towards safeguarding the normal functioning of the nervous system. This is also indicated by its high sensitivity in detecting nerve impingement or injuries. Since neural complications are by far the most serious and life-threatening complications, surgeons especially in deformity cases such as Scoliosis heavily rely on such modalities.

Once the entire nerve-monitoring system is set-up, the time required for stimulation using the stimulation probe is very brief. Also, multiple stimulations can be done without the interruption of the surgical workflow.

Disadvantages As discussed in the previous chapter, these devices have known to have a low sensitivity in the detection of breaches.

There is also no true cut-off value especially for triggered EMG modality which would guarantee accurate placement of pedicle screws [26]. This is because the readings are affected by a host of factors such as body temperature, blood pressure, muscle relaxants and screw material properties etc.

It cannot be used to detect lateral breaches as nerves of close proximity are found only medially. By extension, it cannot be used to detect vascular injuries as well.

Setting up the recording electrodes requires an in-depth understanding of the physiology and anatomical locations of the neural pathways. Therefore, well trained personnel are imperative to ensuring smooth installation, operation and reading interpretation.

Surgeons interviews: Survey questionnaire of 67 spine surgeons

The spine surgeon is the primary user of all the technologies used for PSP discussed in the previous chapters. Therefore, getting a clinical perspective of how the surgeon perceives the problem of PSP could provide crucial insights into the magnitude and seriousness of the issue. Patel *et al* [97] in his PhD thesis investigated the current practice of pedicle screw surgery in UK and Ireland via a questionnaire study. Accordingly, he interviewed a total of 67 surgeons who comprised of neurosurgeons, orthopedic surgeons and spine surgeons.

One of the first questions directed towards the surgeons was as follows:
"Do you think there is a need for a simple device to aid in pedicle screw placement?"
 Over half of the respondents answered "yes" to this question as shown in figure 2.36.

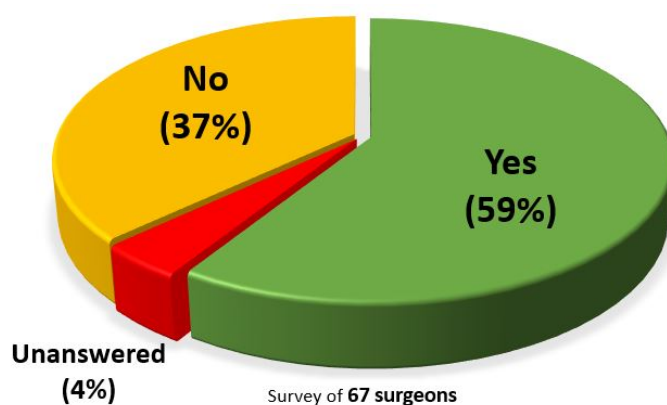


FIGURE 2.36: Response to Question 1: Do you think there is a need for a simple device to aid PS placement?

Increased accuracy, reduced X-ray exposure, reduced risk of neurological/vascular complications, use as a training tool for inexperienced surgeons and use of a supplement aid were highlighted as some of the potential benefits of using a simple device. Interestingly, surgeons

pointed out that in case of non-standard situations such as operating on deformed / degenerated spines or placing screws in thoracic or cervical regions, these cases would especially benefit from a simple assistive device.

The second question in the questionnaire was state as follows:
"What spinal systems do you currently used to aid PS placement?"

Interestingly, the majority of the respondents (55%) mentioned not using any commercially available spine systems. As shown in figure 2.37 the majority that used "other" systems (43%) used C-arm X-ray image intensifiers. This helps reiterate the fact that free-hand and 2D fluoroscopy-guided techniques are still highly popular.

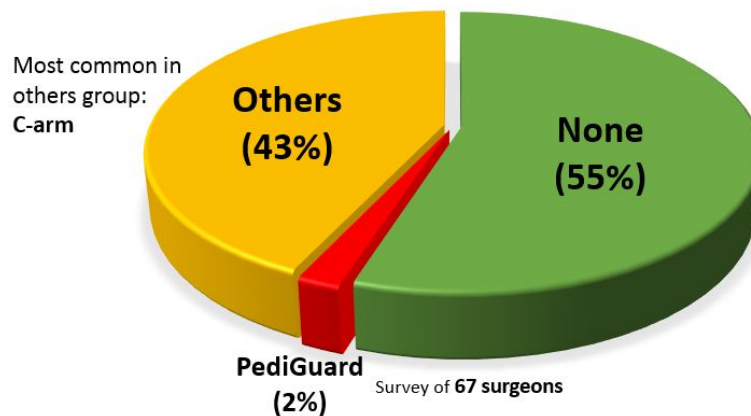


FIGURE 2.37: Response to Question 2: What spinal systems do you currently use to aid PS placement?

Another relevant question put forth was:
"Have you experienced any problems with PS placement in patients? If yes, please specify the problems."

An overwhelming majority of 78 % of the respondents admitted to having experienced problems with PS placement in their patients as shown in figure 2.38.

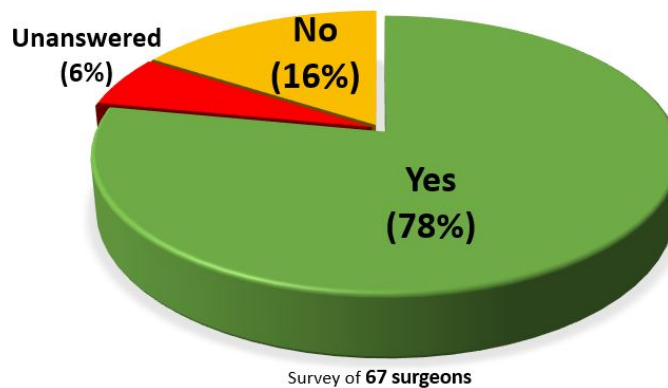


FIGURE 2.38: Response to Question 3: Have you experienced any problems with PS placement in patients?

Breaching the pedicle walls, screw malpositioning and finding difficulty in locating the pedicle were all problems specified by the surgeons. In fact, the most common error stated was the perforation of the lateral vertebral body wall and risking impingement of the descending nerve root. Other problems stated varied from CSF leaks, loss of fixation due to osteoporotic bone, difficulty in identifying landmarks in revision surgery and problems in operating on spinal deformity cases etc.

The outcomes of this survey should be interpreted with caution as it is often difficult to get rid of various biases especially associated with questionnaires.

Spinal fusion market analysis

The global spinal implants and devices market is expected to be worth over 15.73 billion USD by 2020 growing at a compound annual growth rate of 5.6% from 2015 to 2020 [70]. Another market report by ReportsnReports [107], projects the spinal fusion market to reach \$6.9 billion by 2020. It is estimated that over 1.3 million spine surgeries are performed every year in the United states, 53% of these are categorized as spinal fusion surgeries [73, 115]. Pfunter et al [99] in his study on the most frequent procedures performed in the US in 2010, found a whopping 115 % rise in spine fusion cases from 1997 to 2010. It comes as no surprise that one of the most common OR procedures performed in 2011 in the US was the excision of intervertebral disc [135]. It must be noted that the US by far has the biggest spine market as shown in figure 2.39.

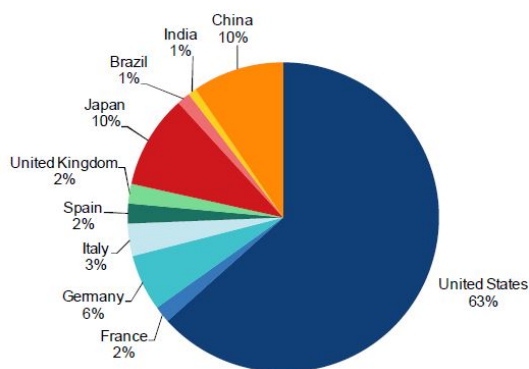


FIGURE 2.39: Global spinal market share. Figure from [75].

The second biggest spinal fusion market lies in China as also reflected in figure 2.39. China is expected to be the fastest growing market in the world, with an annual growth rate of 16.66%. This is estimated to account for a total market value of \$665 million by 2020 [37].

There are several factors associated with this exponential growth of the spinal fusion market, including:

- Expansion in indications of spinal fusion surgery from traditionally being restricted to Scoliosis to roughly 14 other indications such as Spondylosis, Spondylolisthesis, herniated disc etc.
- An immense rise in aging population especially in Europe and United States. The aging population today desires to retain activity and quality of life longer than in the past which is a major contributor of the rapid expansion of the spine market.
- Rising trend towards the preference of MIS techniques. This is due to the high cost of spine surgery. The Agency for Healthcare research and Quality rated spinal fusion surgery as incurring the highest aggregate cost for hospital stays in 2011, costing a massive \$12.8 billion [135], as also shown in table 2.6.

This clearly points to the need for new innovative, cost-effective devices to especially aid MIS procedures. It is a win-win situation not only for the surgeons who would benefit greatly from new technologies that enhance visualization, but also the insurance companies who might benefit from lowered costs due to reduction in revision surgeries and boost of MIS procedures.

Rank	First-listed OR procedure*	Aggregate costs for hospital stays, \$ in millions	Percent of aggregate costs for stays with OR procedures, %	Mean cost per hospital stay, \$	Number of stays, in thousands
First-listed OR procedures		180,335	100.0	16,600	10,867
1	Spinal fusion	12,837	7.1	27,600	465
2	Arthroplasty of knee	11,317	6.3	15,900	711
3	Percutaneous coronary angioplasty (PTCA)	9,730	5.4	18,800	517
4	Hip replacement, total and partial	7,962	4.4	17,200	464
5	Cesarean section	7,481	4.1	5,900	1,269
6	Colorectal resection	6,747	3.7	23,400	289
7	Coronary artery bypass graft (CABG)	6,411	3.6	38,700	166
8	Heart valve procedures	6,070	3.4	53,400	114
9	Cholecystectomy and common duct exploration	5,048	2.8	12,600	400
10	Treatment, fracture or dislocation of hip and femur	4,275	2.4	16,800	255
11	Procedures related to cardiac pacemaker or cardioverter/defibrillator	4,036	2.2	33,200	122
12	Hysterectomy, abdominal and vaginal	3,268	1.8	9,300	351
13	Debridement of wound, infection or burn	2,642	1.5	20,700	128
14	Amputation of lower extremity	2,568	1.4	21,200	121
15	Appendectomy	2,441	1.4	9,200	265
16	Small bowel resection	2,409	1.3	34,500	70
17	Laminectomy, excision intervertebral disc	2,347	1.3	11,500	203
18	Treatment, fracture or dislocation of lower extremity (other than hip or femur)	2,220	1.2	13,700	162
19	Lobectomy or pneumonectomy	1,940	1.1	23,000	84
20	Circumcision	1,885	1.0	2,000	955

* Clinical Classifications Software (CCS), which groups procedures into clinical categories, was used in this analysis.

TABLE 2.6: Most costly OR procedures performed in US hospitals in 2011.
Table from [135]

2.4.4 Design requirements

Based on the trade-offs discussed in the previous section of various technologies used in PSP, the ideal design requirements for a smart assistive device in aiding PSP are laid down, as shown in the table 2.7. These requirements are fundamentally divided into functional, ergonomic and economic, as each category of problems might have to be approached differently. Detecting the presence of a cortical breach and anticipating it, within a sufficiently large time frame is one of the most important functional requirements. The surgeon should be able to determine the location of the instrument or screw in real-time in order to ensure accurate and safe PSP.

The feedback system used to guide the surgeon should be highly specific and sensitive in breach detection.

The reliability of breach detection and anticipation should result in fewer fluoroscopy images being acquired thereby lowering the radiation dosage to the surgeon.

Some of the obvious ergonomic requirements are easy handling and usage. Short learning curve and seamless integration into traditional workflow will both allow faster adoption of the device.

Surgeons are often bothered by excessive amount of audio and visual alarms in the OR. Especially since alarm fatigue is the second most common health technology hazard [20]. The feedback system of the ideal device should not end up being a hindrance to the surgeon. Another important requirement is the setup time. Switching from inactive to active state of the device should be quick and easy.

The economic requirements are more of a concern from a commercial standpoint. The cost-effectiveness trade-off is an important requirement. This is often directly related to the probability of receiving reimbursement from insurance companies.

TABLE 2.7: Design requirements for smart assistive device

Functional	Ergonomic	Economic
<ul style="list-style-type: none"> • Breach detection and anticipation capability in real-time 	<ul style="list-style-type: none"> • Easy to use 	<ul style="list-style-type: none"> • Cost-effective
<ul style="list-style-type: none"> • Feedback system should allow for timely trajectory correction 	<ul style="list-style-type: none"> • Easy to handle 	<ul style="list-style-type: none"> • Reimbursed by insurance companies
<ul style="list-style-type: none"> • High sensitivity and specificity in breach detection 	<ul style="list-style-type: none"> • Short learning curve 	
<ul style="list-style-type: none"> • Lower radiation dosage 	<ul style="list-style-type: none"> • Seamless integration into traditional surgical workflow • Breach detection feedback signal should be non-obstructive. • Short set-up time 	

2.5 Discussion

As with products in a market, it has been shown that surgical techniques also have subtle trade-offs associated with them. Uninterrupted workflows and low procedural costs have encouraged surgeons to still prefer conventional techniques over navigation techniques. This is strongly reflected by the opinions of the surgeons via the interviews.

Navigations systems have proven to solve two of the most important disadvantages of the conventional techniques namely, inaccuracy in PSP and high intraoperative radiation dosage to surgeons. However, these advantages have come at a cost. There is a pretty radical shift in traditional workflow often requiring several steps to be followed before making the first incision. This and other host of issues such as limited field of view have led to the limited adoption of the 3D Computer-assisted technique. An extremely high initial capital investment of around half a million dollars has also proven to be an important factor.

Neurophysiological monitoring devices due to their extremely high specificity in detecting abnormality in nerve function will always remain an important tool for spine surgeons, given the proximity of nerves in the surgical area and the potential of life-threatening complications associated with the procedure. However, the low sensitivity especially of highly popular triggered EMG modality, remains a concern. The requirement of highly trained dedicated personnel to read the data, definitely adds to the service costs of the device.

The PediGuard[®] is a relatively new device which does seem to show some promise. It has been designed to be a smarter version of the traditional pedicle probe, which integrates well into the traditional workflow. However, literature on its efficacy are quite scarce and more studies are warranted to confirm its value proposition.

A brief look at the global spine market clearly signifies its exponential growth in the near future. Several factors such as increase in aging population, broad spinal fusion indications and high cost of surgery are pointing towards a need for better optimized and cost-effective devices.

Based on all the trade-offs, design requirements were created for the ideal device. These requirements serve as guidelines during the investigation of the viability of optical techniques such as Diffusive Reflectance Spectroscopy (DRS) in PSP.

It can thus be concluded that inaccuracy in pedicle screw placement is in fact a problem. There is a need for a simple device to assist the highly popular techniques such as free-hand and 2D fluoroscopy-guided in order to improve their clinical outcomes and make the procedure less technically demanding for the surgeons.

2.6 Conclusion

This report attempts to answer several secondary research questions which intern help answer the primary research question of Phase 1. In this conclusion, answer to each of them would be dealt with briefly.

2.6.1 Secondary clinical research questions

1. What are the current surgical techniques for pedicle screw placement?

An extensive workflow analysis of each of the techniques used in clinical practice was performed as illustrated from figure 2.9 to figure 2.27.

2. What is the definition of accurate pedicle screw placement?

At the moment there is no reliable, validated breach definition available in literature. However out of a total of 8 distinct definitions found, 2 of them were extensively cited leading to some consensus. The most cited definition is defined based on the 'anatomical safe zone' principle and should be used as a benchmark while developing experimental protocols for the new proposed solution.

3. How accurate are the current techniques in pedicle screw placement?

Based on the highest level of evidence available in literature it can be concluded that conventional techniques such as free-hand and 2D fluoroscopy-guided have high placement accuracy variability which is clearly indicative of the complexity and technically demanding nature of the procedure.

4. What is the complication rate associated with each technique?

The number of screw-related complications reported in literature are low but can be potentially life-threatening. Due to several reasons such as ambiguity in definition of screw-related complication and surgeons' reluctance to report complications due to medicolegal reasons, the low reported complication rate should be interpreted with caution and not underestimated.

2.6.2 Primary clinical research question

5. Is inaccuracy in pedicle screw placement a problem?

The high accuracy variability of conventional techniques coupled with their high popularity, as reflected by surgeons' interviews confirm the presence of a problem. The fact that spinal fusion surgery is one of the most frequently performed surgeries in the United States, which has the biggest spine market share in the world, points to the magnitude of the problem.

Part II

Phase 2 research: The technical investigation

Chapter 3

Fundamental background into Diffuse Reflectance Spectroscopy

Diffuse reflectance spectroscopy (DRS) is a method to analyze tissue components using broad-band light. In the setup of this study, wavelengths from 400 to 1600 nm are applied. Light is sent into the tissue via an emitting fibre that directly contacts the tissue. A second fibre collects the light that has travelled through the tissue. The collected spectrum signal depends on two fundamental photon-tissue interactions namely, absorption and scattering. Figure 3.1 shows schematically the photon-tissue interactions that results in the diffuse reflectance that is detected at the tissue surface. The distance between the emitting and detecting fibre is the fibre separation distance (FD). Larger FD results in larger penetration depths of the photons and a decrease in reflectance intensity [147].

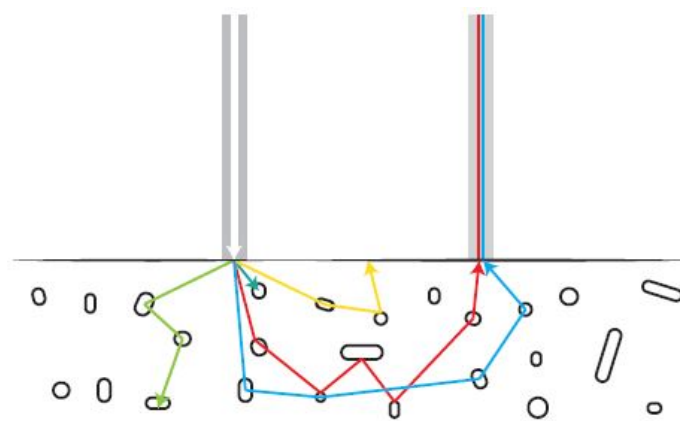


FIGURE 3.1: Schematic representation of photon scattering and absorption in tissue. The left fiber emits broad-band white light, the right fiber collects photons and transports them to the spectrometer. Each arrow represents a photon, the black shapes are chromophores. The green photon is absorbed after two scattering events whilst the yellow photon is scattered twice and then leaves the tissue. Both the red and blue photon undergo several scattering events until they are collected by the right fiber.

3.1 Absorption

Absorption of a medium is described by its absorption coefficient, μ_a , and depends on wavelength. μ_a represents the amount of absorption in units of inverse length (cm⁻¹). The most important absorbers in tissue are oxy- and deoxygenated haemoglobin (HbO₂ and Hb), water and fat. Haemoglobin is a strong absorber in the visible wavelength range (400 to 800 nm) whereas fat is a strong absorber in the near Infrared (NIR) range. Other tissue chromophores that absorb light in this range are for example bile, bilirubin, β -carotene and methaemoglobin which are organ dependent [17, 80, 79]. Absorption spectra of the chromophores in the visible

area of the spectrum are shown in figure 3.2 [148]. Water and fat absorb mainly in the near-infrared part of the spectrum (800-1600 nm), these absorption spectra are shown in Figure as well. Other chromophores absorbing light in the near-infrared part are collagen and elastin

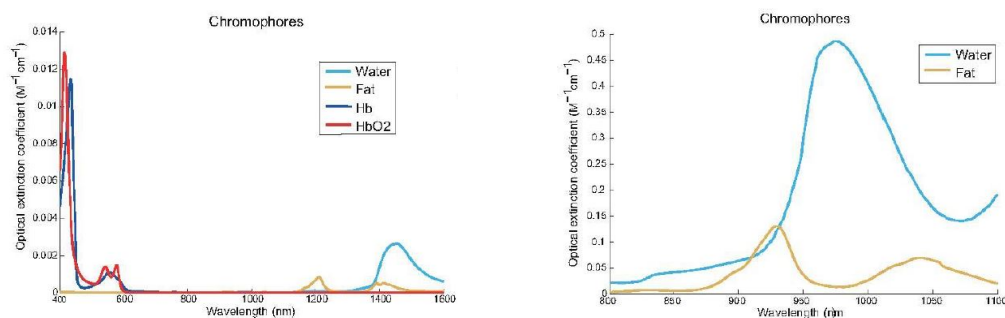


FIGURE 3.2: Absorption spectra of Hb, HbO₂, water and fat over the whole wavelength area (left) and absorption spectra of water and fat from 800 to 1100 nm (right).

3.2 Scattering

Scattering occurs when a photon hits a molecule and is not absorbed. In a scattering event, the propagation direction of the photon is changed. Scattering occurs due to structural heterogeneities or fluctuations in the refractive index of a medium, in tissue due to different particles, such as cells, collagen fibres and organelles. The scattering of a medium is described by its scattering coefficient μ_s . This coefficient represents the probability of a photon being scattered per unit length and is in units of inverse length (cm⁻¹).

Scattering depends on the wavelength of the light and on the size and refractive index of the particle that induces scattering. The direction of scattering events in a medium is represented by the anisotropy factor (g) of the medium. The factor g is the average cosine of the deflection angle (θ); for $g = 0$ scattering is isotropic and for $g = 1$ scattering is directed forwardly. In tissues the anisotropy factor ranges approximately from 0.8 to 1, indicating highly forward scattering. Generally, structures on the scale of photon wavelengths (i.e. 100-2000 nm) cause Mie scattering, which is directed very forwardly. Smaller structures cause Rayleigh scattering, which is isotropic. In tissue Mie scattering occurs mainly, because larger structures are the strongest tissue scatterers of visible and NIR light. For example, mitochondria inside cells and the collagen fibres outside cells are strong Mie scatterers.

Instead of μ_s and g , usually the reduced scattering coefficient (μ'_s) is used to describe tissue scattering in DRS applications, this parameter is derived from the similarity principles.³⁸ The reduced scattering coefficient can be derived from a diffuse scattering signal. The relationship between μ'_s , μ_s and g is:

$$\mu'_s = \mu_s(1 - g) \quad (3.1)$$

3.3 The measurement setup

The experimental setup consists of an optical probe with three optical fibers with a NA of 0.22, a spectrometer with a silicon detector (Andor Technology, DU420A-BRDD), a spectrometer with an InGaAs detector (Andor Technology, HL-2000-HP) as shown in 3.3. One optical fiber is connected to a light source. The second and third optical fibers are connected to the spectrometer with a silicon detector and to the spectrometer with an InGaAs detector, respectively. The silicon detector is a matrix of 1024 by 255 pixels with a pixel size of 26x26 microns whereas the InGaAs detector is a single array of 512 pixels with a pixel size of 500x50 microns. The spectral resolution for the silicon and InGaAs detectors are 4 and 10 nm, respectively. The fiber distance between the two optical fibers was fixed to a value of 1.2 mm. Before DRS measurements

are performed, the system has to be calibrated for wavelength and a white reference. The full calibration process is described by Nachabé *et al* [80] and is described shortly in this chapter.

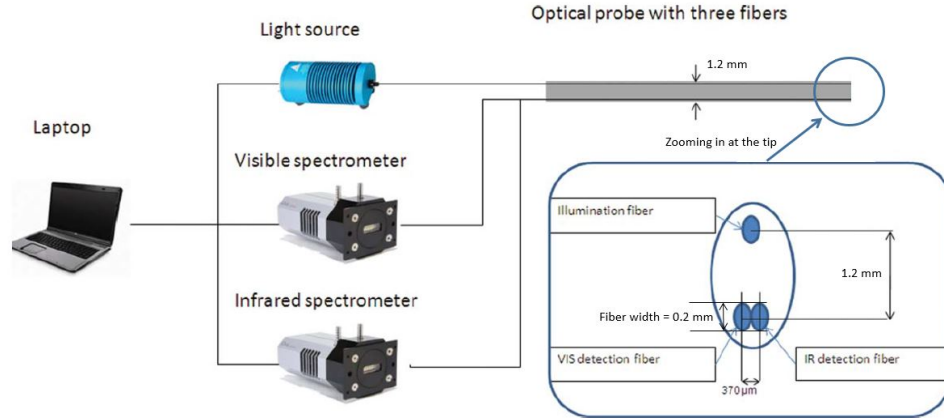


FIGURE 3.3: Schematic of the measurement setup of the optical probe

During the wavelength calibration, a wavelength value was assigned to each pixel of the spectrometers, by fitting a second-order polynomial to a set of atomic lines from an argon light source, of which the wavelengths of the peaks are known. The second calibration step is the white calibration. The optical probe was placed about 1.5 cm above a white reflectance standard (Spectralon SRS-99-020, Labsphere), which reflects the light uniformly. This calibration step compensates for the spectral shape of the light source, the light dependency of the probe and the wave-length dependent sensitivity of the spectrometers. To obtain a calibrated tissue spectrum, effective and background measurements of the tissue and the white reflectance standard are required. The calibrated spectrum ($S(\lambda_i)$) is calculated as

$$S(\lambda_i) = \frac{T(\lambda_i) - T_{dark}(\lambda_i)}{C(\lambda_i) - C_{dark}(\lambda_i)} \quad (3.2)$$

where $T(\lambda_i)$ and $C(\lambda_i)$ are the reflectance measurements of the tissue and the white reflectance standard, respectively. $T_{dark}(\lambda_i)$ and $C_{dark}(\lambda_i)$ are the background measurements of the tissue and white reflectance standard, respectively. These background measurements are obtained subsequently with the reflectance measurements. The integration times of the measurements were adjusted per spectrometer to obtain enough signal and prevent overflow. The maximum integration times were one second. One DRS measurement is the average of multiple subsequently acquired spectra of one measurement location. To obtain the measurement of a medium, the probe was in direct contact with the medium.

3.4 Analysis of the spectra

Analysis of the measured spectra can be performed by 1) evaluating the raw or filtered spectra directly, 2) evaluating the optical tissue properties derived from the diffuse reflectance spectra, and 3) evaluating biological parameters, such as blood or water content, derived from the spectra themselves. Both the second and third method requires a priori knowledge of the tissue-light interaction. The third method also requires knowledge of the optical properties of several wavelength-dependent tissue chromophores, such as blood, water, and lipid. This study analysis is performed on the raw and filtered spectra and by applying a fit model. This model is applied to derive biological (absorption related) and scatter parameters from the spectra and was developed by Rami Nachabé [80]. The model is based on the diffusion theory model described first by Farrell *et al* [29].

Diffusion theory fit model

The fit model utilizes an analytical solution of the diffusion theory model for light propagation in scattering media (e.g. tissue) [80]. This model holds only if the following assumptions are made [29].

Assumptions

1. In tissue scattering is generally highly forwarded peaked with the anisotropy factor is 0.8 or higher. Furthermore in most tissues many scattering events occur before an absorption event [136]. Therefore, individual scattering is less important and the averaged of g can define a scattering event and scattering can be described by the reduced scattering coefficient $\mu'_s = (1-g) \mu_s$.
2. The second assumption is that the diffuse approximation holds. This theory depends on the assumption that many scattering events have occurred before the light is detected. Therefore scattering should dominate absorption ($\mu'_s \gg \mu_a$) and the mean free path of a photon should be small compared to the fibre separation distance.
3. The third approximation is that the source can be described by single scatter source instead of a pencil beam. This single scatter source is the first scattering event on an axis that is perpendicular to the tissue surface and in line with the emitting fibre.
4. The model assumes that the measured tissue is homogeneous.

Diffusion theory model to fit spectra This model was first described by Farrell *et al* [29], and implemented by Nachabé *et al* [80, 79]. The model used in this fit model corresponds to the solution of the diffusion equation for a semi-infinite medium. The analytical expression for the diffuse reflectance (R) as a function of the distance between the emitting and collecting fibre (ρ), the absorption coefficient (μ_a) and the reduced scattering coefficient (μ'_s) are expressed as

$$R[\mu_s, \mu'_s, \rho] = \alpha \frac{\mu'_s}{4\pi\mu_t} \left[z_0 \left(\mu_{eff} + \frac{1}{r_1} \right) \frac{e^{-\mu_{eff}r_1}}{r_1^2} + (z_0 + 2z_b) \left(\mu_{eff} + \frac{1}{r_2} \right) \right] \quad (3.3)$$

Where α is a scaling factor, $\mu^t = \mu_s + \mu'_s$ is the total attenuation coefficient, $\mu_{eff} = \sqrt{3\mu_a\mu_t}$ is the effective attenuation coefficient and $z_0 = 1/\mu_t$ is the location of the virtual scattering source. $z_b = 2AD$ expresses the extrapolated boundary condition, here A depends on the relative refractive index of the tissue and the surrounding medium and the critical angle. In this model $A=1$, as it was assumed there is no refractive index mismatch between the tissue and the optical fibre. Furthermore, D is the diffusion constant. The separation distance between the fibres is expressed in $r_1 = \sqrt{z_0^2 + \rho^2}$ and $r_2 = \sqrt{(z_0 + 2z_b)^2 + \rho^2}$, which are the distance between the single scattering source and the collecting fibre and the distance between the image source and the collecting fibre, respectively.

Absorption The absorption coefficient is expressed as a function of the absorption coefficients of several tissue chromophores

$$\mu(\lambda) = \mu_a^{blood}(\lambda) + \mu_a^{w+f}(\lambda) + \mu_a^{other}(\lambda) \quad (3.4)$$

Where μ_a^{blood} , is the absorption of the chromophores oxygenated and deoxygenated haemoglobin, respectively HbO_2 and Hb, μ_a^{w+f} is absorption by water and fat and μ_a^{other} is absorption by other tissue chromophores, such as bile or β -carotene. Absorptions of blood, water and fat are required in the implementation of the model, other absorption parameters are optional β -carotene.

Absorption of water and fat is expressed as

$$\mu_a^{w+f} = f^{w+f} \left[f^{\frac{f}{f+w}} \mu_a^{fat}(\lambda) + \left(1 - f^{\frac{f}{f+w}} \right) \mu_a^{water}(\lambda) \right]. \quad (3.5)$$

Where μ_a^{fat} and μ_a^{water} are the absorption coefficients of fat and water, respectively.

Scattering The scattering coefficient is expressed in two components, the first representing Mie scattering and the second Rayleigh scattering:

$$\mu_s = S_{800} \left(f^{Mie} \left(\frac{\lambda}{\lambda_0} \right)^{-b} + (1 - f^{Mie}) \left(\frac{\lambda}{\lambda_0} \right)^{-4} \right) \quad (3.6)$$

The first component represents Mie scattering and the second Rayleigh scattering. λ_0 is a normalization wavelength, the reduced scattering at 800 nm. The b parameter corresponds to the Mie reduced scattering slope and correlates with the average particle size. When computing the reduced scattering with the Mie theory, it was observed that b decreases with the average diameter of the particles according to a Lorentzian cumulative function [149]. In a similar way as for the absorption coefficient, non wavelength dependent parameters such as reduced scattering amplitudes and slope are fitted from the estimated total reduced scattering μ'_s .

Generally, structures on the scale of photon wavelengths (i.e 100-1000) nm cause Mie scattering, which have a high probability of scattering in the forward direction [136].

Chapter 4

The experimental investigation

4.1 Geometry mapping experiment of *ex vivo* swine vertebral tissue

4.1.1 Abstract

BACKGROUND CONTEXT: The pedicle screw placement surgical procedure is technically demanding due to the risks associated with the malpositioned screw entering the spinal canal, which could lead to a neural injury. In order to investigate the applicability of DRS technology to reduce or eliminate this risk, the tissue types encountered by the screw tip needs to be investigated.

PURPOSE: The purpose of this study was to measure the average cortical thickness and to investigate the structural features of cancellous bone, cortical bone and the spinal canal on a *ex vivo* swine vertebra.

METHODS: Two thoracic vertebrae were extracted from the spinal column of a swine cadaver. The vertebra was divided into 6 regions. 10 cortical thickness measurements were acquired per region via an optical microscope of 40x magnification (Leica Microsystems, Germany). The structural features of the tissue were examined using the same optical microscope used for the thickness measurements.

RESULTS: A semi-fluidic substance with a whitish appearance was found in the spinal canal. The highly porous cancellous bone with trabeculae were clearly visible. The smooth textured cortical bone could be clearly distinguished from the cancellous bone. The average cortical bone thickness was found to vary between 0.5 to 0.85 mm.

CONCLUSIONS: The structural characteristics of cancellous bone was found to be different from cortical bone. There is a high probability that the semi-fluidic whitish material found in the spinal canal belongs to the contents of the epidural space.

4.1.2 Introduction

The pedicle screw placement workflow involves several steps before the actual insertion of screw into the vertebrae. Figure 4.4 shows an example of one of the most widely clinically adopted workflows. Step 4, step 6 and step 7 are the most crucial steps in the process. The instruments used at each of these steps are the pedicle probe, screw tap and the pedicle screw respectively. The risk of a neural or vascular injury is highest during these steps. There are three possible paths or trajectories that are most commonly encountered during each of the three steps mentioned earlier as depicted in figure 4.1. These are namely the lateral trajectory, medial trajectory and the normal trajectory. There is a non-zero risk of the lateral trajectory leading to a vascular injury, and the medial trajectory leading to a neural injury.

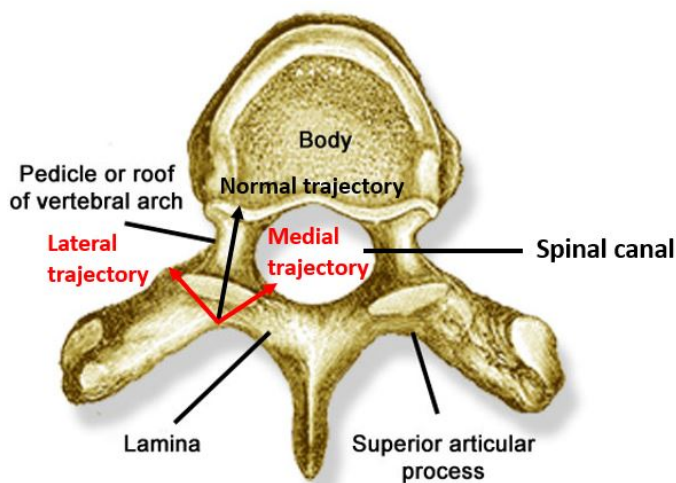


FIGURE 4.1: Axial view of thoracic vertebral bone. Figure from [89]

The scope of this thesis has been restricted to understanding the medial breach scenario in particular. A medial breach scenario occurs when the tip of the instrument follows the medial trajectory instead of the normal trajectory as shown in figure 4.1.

Figure 4.2 shows the axial cross-section of a human vertebra. The cortical bone can be seen surrounding the vertebral body and the spinal canal. The porous cancellous bone can be seen occupying the bulk of the vertebral body. If the instrument tip follows the medial trajectory, then it would first encounter the cancellous bone bulk, followed by the cortical shell surrounding the spinal canal and finally enter the spinal canal, which could be potentially life threatening.

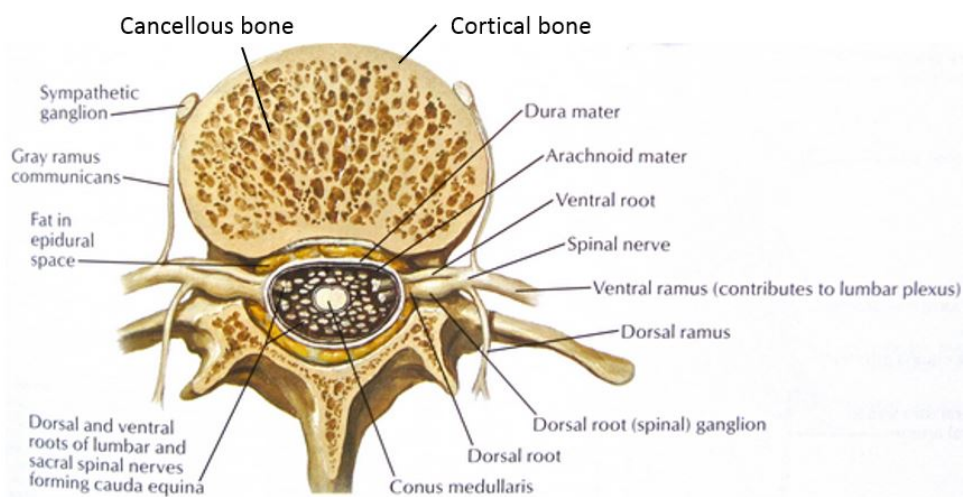


FIGURE 4.2: Axial view of thoracic vertebral bone. Cortical bone can be seen surrounding the vertebral body and the spinal canal

The spinal canal is particularly a difficult region for an anatomic study. As Hogan *et al* [47] notes that the flexible and semifluid tissues are held in place by a balance of subtle forces created by the CSF pressure and subatmospheric epidural space pressure. These are often disrupted upon exposure by dissection while entering into the spinal canal. Even then, several studies [47, 45, 137, 15, 32] have been published which have used various techniques to meticulously study the arrangement of soft tissues in the spinal canal. It must be pointed out that the geometry of

the soft tissues have slight variations across various levels of the spine. Also, the spinal cord terminates at lumbar level of one or two [137, 15].

Figure 4.3a shows the axial view of a cervical vertebral cross-section. From the dorsal side, it can be seen that the epidural space occupies the first layer of the spinal canal. An extensive study of the anatomy of the epidural space by Westbrook *et al* [137] explicitly confirms this fact. The lateral view of the vertebral cross-section as shown in figure 4.10b, clearly shows how the epidural space alternatively borders the laminae of the vertebra and the ligamentum flavum [15]. **This aspect confirms the fact that during a medial breach, the instrument tip would first enter the spinal canal via the epidural space.**

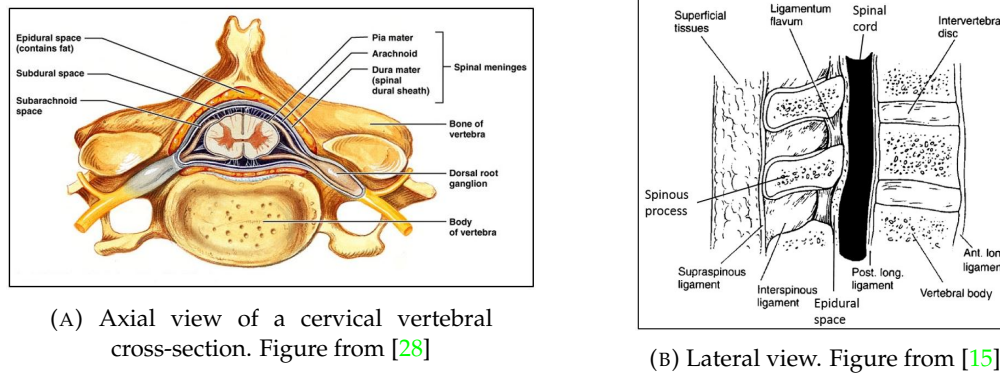


FIGURE 4.3: Various views showing the spinal canal cross-section and tissues surrounding it.

Nickallis *et al* [83] specifically measured the thickness of the epidural space in obstetric patients. He found that epidural space at the posterior space in an adult measures to about 0.4 mm at C7-T1, 7.5 mm in the upper thoracic region, 4.1 mm at the T11-12 region and 4-7 mm in the lumbar region.

From figure 4.2 it becomes clear that the cortical bone surrounding the spinal canal is of a finite thickness. Ritzel *et al* [108] measured the thickness of the cortical bone surrounding the vertebral body using hystometric analysis. The presented data revealed a mean cortical thickness of 0.285, 0.244 and 0.290 mm across cervical, thoracic and lumbar regions respectively. However, no study was found on the cortical thickness measurement surrounding the spinal canal. Knowledge of the cortical bone thickness is crucial in understanding the spectral sensing transitions during a medial breach, which would also serve as the basis of Monte-carlo simulations during the simulation investigations to follow.

Therefore, the purpose of this study is to measure the average cortical thickness and to investigate the structural features of cancellous bone, cortical bone and the spinal canal on a *ex vivo* swine vertebra.

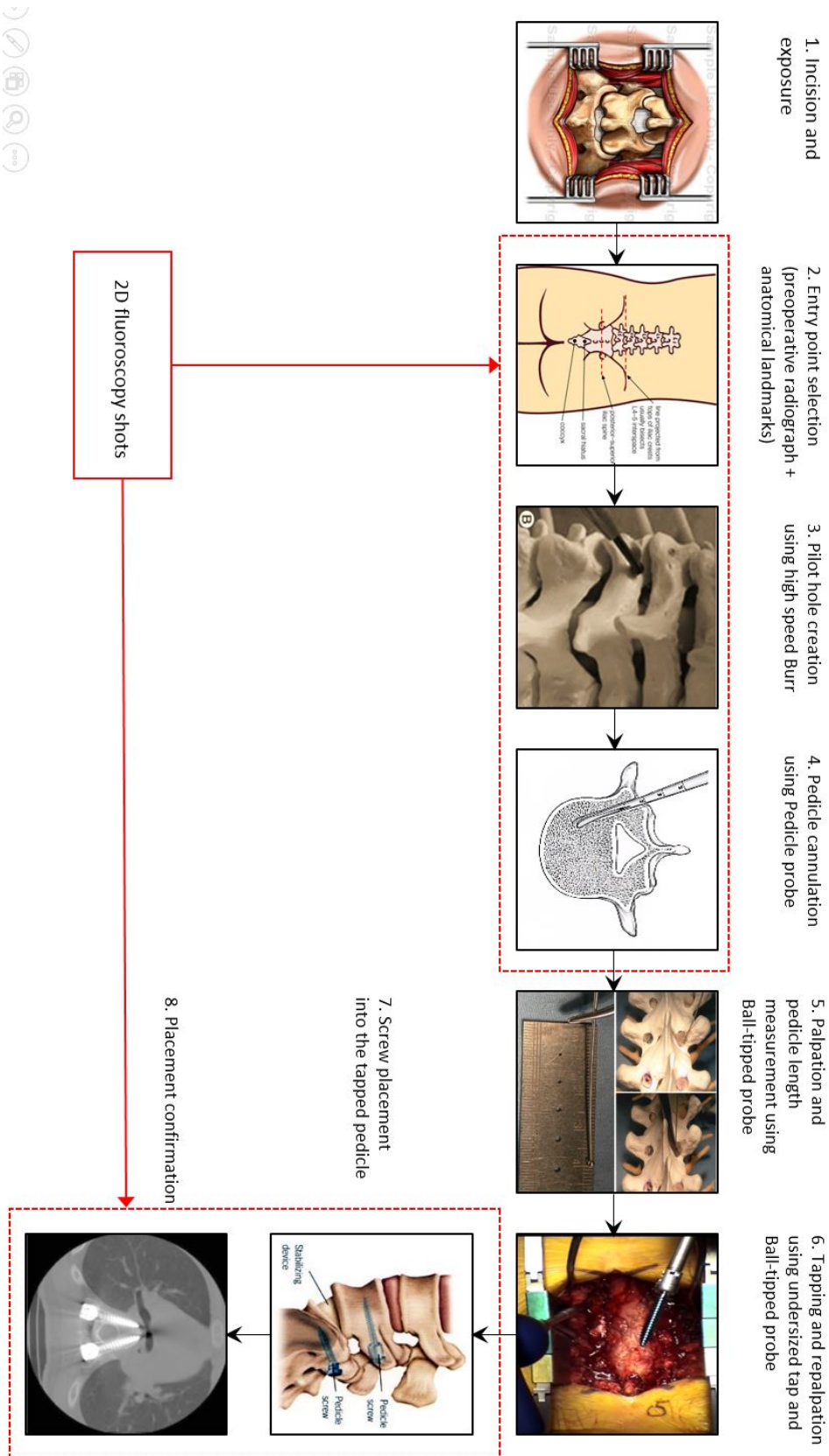


FIGURE 4.4: Surgical workflow of 2D fluoroscopic guided technique (Open)

4.1.3 Materials and methods

Figure 4.5 shows the entire extracted vertebral column. A total of two thoracic vertebrae were extracted from the spinal column of a swine cadaver using a hacksaw which was estimated to be deceased and stored in a frozen state for one year.



FIGURE 4.5: Vertebral column extracted from a swine vertebra

In order to measure the cortical bone thickness across different regions, the vertebra was divided into six intravertebral regions namely, pedicle left, pedicle right, left, right, top and bottom as shown in the axial view of 4.6. Cortical thickness measurements were performed using the optical microscope with a maximum magnification of 40x as shown in figure 4.7. The microscope images were recorded digitally and thickness measurements were acquired after performing calibration using a reference scale. A total of 10 measurements were acquired per region which accounts for a total of 60 measurement points per vertebra. All images analyzed for cortical thickness measurements were acquired using a maximum magnification of 40x.

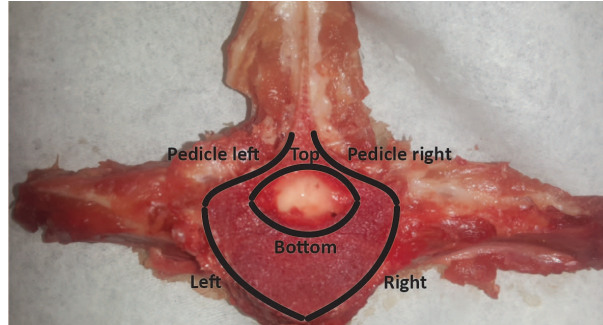


FIGURE 4.6: Dividing the swine vertebrae into 6 regions in the axial view

The structural features of various tissue types were observed using an optical microscope with a maximum magnification of 40x. Different regions of the vertebra were probed and images were then recorded digitally.



FIGURE 4.7: The available optical microscope was used to zoom-in into the tissue under investigation

4.1.4 Results

A semi-fluidic material with a whitish appearance was found in the spinal canal as shown in figure 4.8. Figure 4.9 shows the microscopic images acquired at various regions of the swine vertebra. In the right region, the pores of the cancellous (trabecular) are clearly visible. The smooth textured cortical bone is also visible.

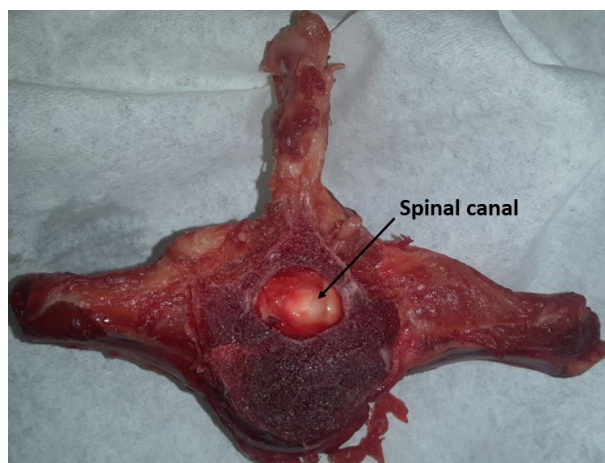


FIGURE 4.8: Whitish semi-fluidic material found in the spinal canal

Structural features of bone and spinal canal

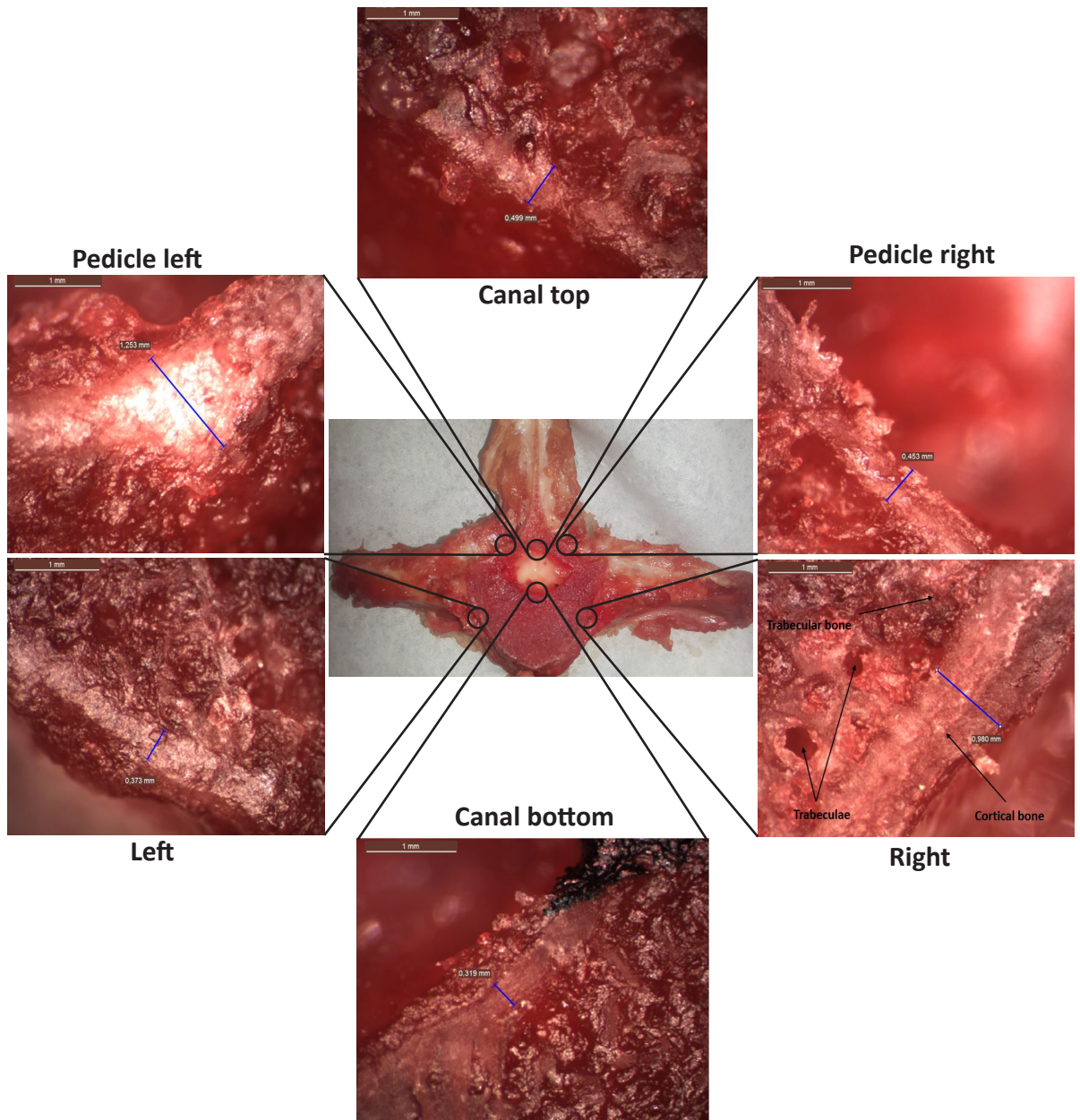


FIGURE 4.9: Microscopic images of various regions of the extracted swine vertebra

Thickness of cortical bone

In figure 4.10 boxplots of the spread of the cortical thickness measurements across the six vertebral regions are shown. Table 4.1 and 4.2 provides an overview of the descriptive statistics across the intravertebral regions for the two thoracic vertebra examined. Regions namely 'Canal top' and 'Canal bottom' are of particular interest in this study as they represent the average thickness of cortical bone found surrounding the spinal canal. The average thickness across the spinal canal was thus found to vary between 0.50 mm and 0.85 mm.

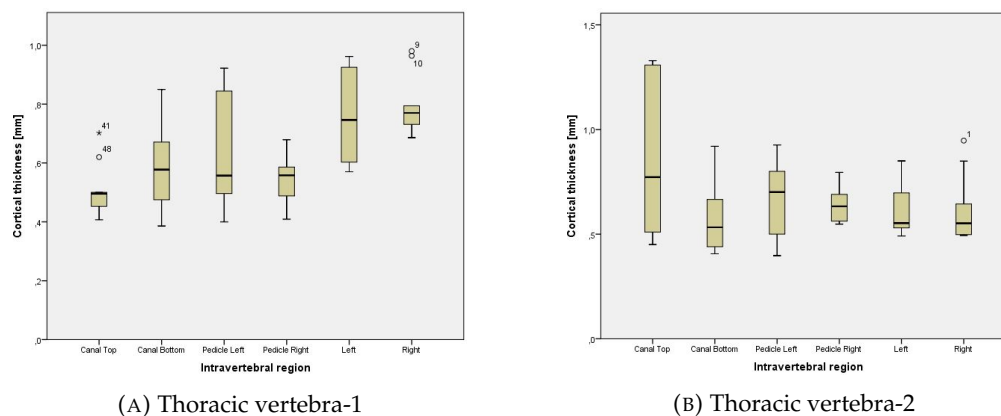


FIGURE 4.10: Box plots of cortical bone thickness measurements across intravertebral regions

TABLE 4.1: Thoracic vertebra-1

Cortical thickness [mm]	N	Minimum	Maximum	Mean	Std. Deviation
Canal bottom	10	0.38	0.85	0.59	0.14
Canal top	10	0.4	0.70	0.51	0.09
Left	10	0.57	0.96	0.76	0.16
Pedicle left	10	0.40	0.92	0.64	0.19
Pedicle right	10	0.41	0.68	0.55	0.07
Right	10	0.69	0.98	0.80	0.09

TABLE 4.2: Thoracic vertebra-2

Cortical thickness [mm]	N	Minimum	Maximum	Mean	Std. Deviation
Canal bottom	10	0.40	0.92	0.59	0.17
Canal top	10	0.45	1.33	0.85	0.36
Left	10	0.49	0.85	0.62	0.12
Pedicle left	10	0.40	0.93	0.66	0.19
Pedicle right	10	0.55	0.80	0.64	0.08
Right	10	0.50	0.95	0.62	0.16

4.1.5 Discussion

The focus of the geometry mapping study was to develop an intuitive visualization of the type of tissues which are encountered by the instrument tip during a medial breach scenario. To achieve this, two thoracic *ex vivo* swine vertebrae were closely examined to identify the structural features of bone and spinal canal. Apart from the instrument tip traversing the cancellous bone and cortical bone, it was unclear which type of tissue would be first encountered once the tip is within the spinal canal. An extensive search of scientific literature revealed that after the perforation of the cortical bone, the instrument tip would first come in contact with the epidural space. Thus, during a medial breach scenario, the instrument tip would traverse three distinct tissues namely the cancellous bone, cortical bone and the epidural space.

The geometry and optical properties of these three tissues would fundamentally influence the strategy which would be needed to be adopted to optimize the optical sensing algorithm.

Figure 4.9 shows the microscopic images of various regions of the swine vertebra. Even without using staining methods as used in histological studies, cancellous bone can be distinguished from cortical bone. The highly mineralized cortical bone is clearly distinguishable due to specular reflections from the optical microscope lamp. The pores in the cancellous bone termed as trabeculae are also visible in the right region as depicted in figure 4.9. The trabeculae

are usually occupied by red and yellow bone marrow [69], but as swine specimen used in this study is estimated to be deceased for over a year, it lacks perfusion. Thus, the *ex vivo* nature of the tissue would definitely have an influence on the overall generalizability of the results of the studies to follow.

Figure 4.8 illustrates a microscopic image of a spinal canal. This tissue has a whitish appearance with a semi-fluid consistency. Hogan *et al* [47] in his elaborate study of the soft tissues in the spinal canal found the epidural space to have a semi-fluidic consistency. This structural make-up could be to cushion and keep the spinal cord in place within the spinal canal. Therefore, there is a high probability that this whitish semi-fluid tissue found in the present study belongs to the contents of the epidural space. However, as Hogan *et al* [47] points out, the spinal canal is particularly a difficult region for an anatomic study. The flexible and semifluid tissues are carefully held in place by a balance of subtle forces created by the CSF pressure and subatmospheric epidural pressure. These are often disrupted upon exposure by dissection while entering the spinal canal. Thus, not only the tissue condition in terms of the *in vivo* and *ex vivo* nature, but also the dissection method would play an important role in the overall generalizability of results from such studies.

The boxplots in figure 4.10 indicate that there is variation of cortical thickness within each region as well as between intervertebral regions. Variation in cortical thickness was also found between the two thoracic vertebrae studied. Such variation is bound to be present when tissues are being investigated. Therefore, Monte-Carlo models of varying cortical thicknesses would have to be built in order to analyze their effect on photon-tissue interactions.

It must be noted that the cortical thickness data pertains to swine vertebrae. Human cortical bone thickness surrounding the vertebral body and the spinal canal could be significantly different. More reliable estimates of the cortical thickness can only be made by repeating the experiment on human specimens.

The measurement technique used in this study also adds a source of variability in the measurement. Researchers such as Ritzel *et al* [108] have used a more accurate method of measuring the cortical thickness by using a hystometric approach. Staining helps enhance the visual characteristic differences between cancellous and cortical bone thereby resulting in a more accurate measurement method. In the present study, no staining was performed and the measurements were made purely by visual inspection. However, due to use of the optical microscope, higher number of specular reflections seen due to the dense nature of cortical bone did indeed help distinguish the two bone tissues from one another. Also, since variation in cortical bone thickness is expected, such elaborate hystometric studies might not be necessary.

Table ?? indicates that the cortical thickness surrounding the spinal canal is comparable and in some cases lower than the thickness surrounding the vertebral body and the pedicle. However, several researchers such as Crostelli *et al* [21] and Lee *et al* [60] while performing pedicle screw insertions in humans have hypothesized that the medial canal wall is thicker than the lateral wall. This further illustrates the point that swine vertebral geometry might be significantly different from human vertebral geometry.

Apart from intravertebral and intervertebral cortical thickness variability, spinal region dependent differences in lumbar, thoracic and cervical only adds to the complexity of the problem while developing a universal solution for breach anticipation. The accommodation of the optical sensing to these different sources of variability is an extremely important challenge that must be tackled. This would need a careful analysis of the influence of parameters such as fiber distance, sensing depth and cortical thickness on the output spectra and/or other relevant parameters such as fat chromophore concentration.

4.1.6 Conclusion

- Structural characteristics of cancellous bone was found to be quite different from cortical bone as examined via an optical microscope.
- A whitish semi-fluidic material was found in the spinal canal. There is a high probability of this material being part of the contents of the epidural space.

- Average cortical bone thickness surrounding the spinal canal for the studied *ex vivo* swine vertebra was found to lie within the range of 0.50 to 0.85 mm.

4.2 Optical mapping experiment of *ex vivo* swine vertebral tissue

4.2.1 Abstract

BACKGROUND CONTEXT: DRS coupled with the fitting algorithm integrated into an instrument has the capability of differentiating tissue in front of the instrument tip. Such an optical sensing system could be valuable in warning a spine surgeon before a potential neural injury.

PURPOSE: The purpose of this study was to identify the important parameters of interest retrieved from DRS, by gauging their sensitivities across intravertebral regions.

METHODS: The experimental setup consists of an optical probe with three optical fibers, a spectrometer with a silicon detector (Andor Technology, DU420A-BRDD), a spectrometer with an InGaAs (Andor Technology, HL-2000-HP). The fiber distance was fixed at 1.2 mm. The integration time for each measurement is on average 0.5 s. The reflectance spectra obtained lied within the window of 400 to 1600 nm. The optical probe was placed perpendicular to the tissue surface during data acquisition. A total of 7 vertebrae were used in this study. Each vertebra was divided into 5 regions. 10 spectral measurements were acquired per region. The acquired spectral data was then quantified using the fitting algorithm which outputted a host of parameters such as chromophore concentrations and scattering parameter. Kruskal-Wallis test was used to establish statistical significance. A P-value of less than 0.01 was considered statistically significant.

RESULTS: Fat chromophore concentration was found to be significantly higher in the spinal canal as compared to cancellous and cortical bone ($H(1)=165.66, p<0.01$, $H(1)=164.25, p<0.01$). Fat chromophore concentration was found to be significantly higher in cancellous bone than in cortical bone ($H(1)=77.9, p<0.01$). The scattering parameter was found to be significantly higher in the spinal canal as compared to cancellous and cortical bone ($H(1)=141.96, p<0.01$, $H(1)=150.28, p<0.01$). The scattering parameter was also found to be significantly higher in cancellous bone as compared to cortical bone ($H(1)=77.9, p<0.01$).

CONCLUSIONS: Fat chromophore concentration and the scattering parameter were found to be significantly different across cancellous bone, cortical bone and spinal canal in the 7 vertebrae analyzed.

4.2.2 Introduction

Composition of bone

Bone is made up of both organic and inorganic components. The majority of bone tissue is made up of inorganic components. The inorganic mineralized part of bone gives it its mechanical strength [55]. This includes hydroxyapatites, mineral salts and needle-like crystals of calcium phosphates [69]. Kontoyannis *et al* [54] analyzed the bone composition in animal tissue using Raman Spectroscopy. He found that 70% of bone is made up of inorganic matrix, while organic matrix and water occupies the rest. Several authors have found that cortical bone is more mineralized than trabecular bone [54, 38].

The organic components of bone include organic molecules such as glycosaminoglycans, glycoproteins, lipids, peptides and enzymes [54]. Several studies state that the organic components of bone largely comprises of collagen and water [54, 86, 101] but solid scientific reference for this fact is yet to be established. One of the main functions of bones, especially trabecular bone is triglyceride (fat) storage, which is stored in the trabeculae of the cancellous bone [69]. Barber *et al* [24] examined the variation of fat to water ratio across intervertebral regions using magnetic resonance spectroscopy. He found a linear increase of fat content from L2 to L5. Li *et al* [63] found that fat content was significantly elevated in patients with osteoporosis. The author also observed a similar trend of increase of fat content from L1 to L4.

Contents of epidural space

The epidural space contains semi-liquid fat, lymphatics, arteries, loose areolar connective tissue, spinal nerve roots and extensive plexus of veins [32]. Hogan *et al* [47] extensively studies the anatomy of soft tissues in the spinal canal and found fat to be the principal occupant of the epidural space. Several other studies have confirmed this fact [32, 137, 15]. Fyneface-ogan [32] also observed that the distribution of fat is largely distributed across the dorsal margin of the space. Apart from fat, the anterior epidural space is perfused by veins and arteries [39]. Desjardins *et al* [23] probed the epidural space for tissue differentiation using optical spectroscopy. They found a 25-fold higher fat fraction in epidural space as compared to neighboring tissues such as ligamentum flavum and skeletal muscles. Another study [106] reflected a similar result, which fits the trends observed by previous studies.

Although there have been several studies which have attempted to individually quantify the components of bone and epidural space, only one study was found which has tried to analyze the variation of optical properties across different regions of the vertebra, in the context of the pedicle screw placement surgical procedure. Liu *et al* [65] monitored the reduced scattering coefficient across intravertebral regions using near-infrared spectroscopy. The author observed a significant change of the retrieved reduced scattering coefficients during a medial and lateral breach.

To the best of my knowledge, this is the first study in which spectroscopic differentiation of tissue has been performed in order to identify the important parameters of interest, by gauging their sensitivities across intravertebral regions, in the context of a medial breach.

4.2.3 Materials and methods

Experiment setup

The experimental setup consists of an optical probe with three optical fibers with a NA of 0.22, a spectrometer with a silicon detector (Andor Technology, DU420A-BRDD), a spectrometer with an InGaAs detector (Andor Technology, HL-2000-HP) as shown in figure 4.11. One optical fiber is connected to a light source. The second and third optical fibers are connected to the spectrometer with a silicon detector and to the spectrometer with an InGaAs detector, respectively. The silicon detector is a matrix of 1024 by 255 pixels with a pixel size of 26x26 microns whereas the InGaAs detector is a single array of 512 pixels with a pixel size of 500x500 microns. The spectral resolution for the silicon and InGaAs detectors are 4 and 10 nm, respectively. The fiber distance between the two optical fibers was fixed to a value of 1.2 mm. The integration time for each measurement is on average 0.5 s. The reflectance spectra obtained with both spectra are combined together to form one single reflectance spectrum ranging from 500 to 1600 nm, and is used in order to apply the mathematical modeling for the data analysis. The spectral data modelling algorithm used to quantify the reflectance spectra has been described in chapter 3.

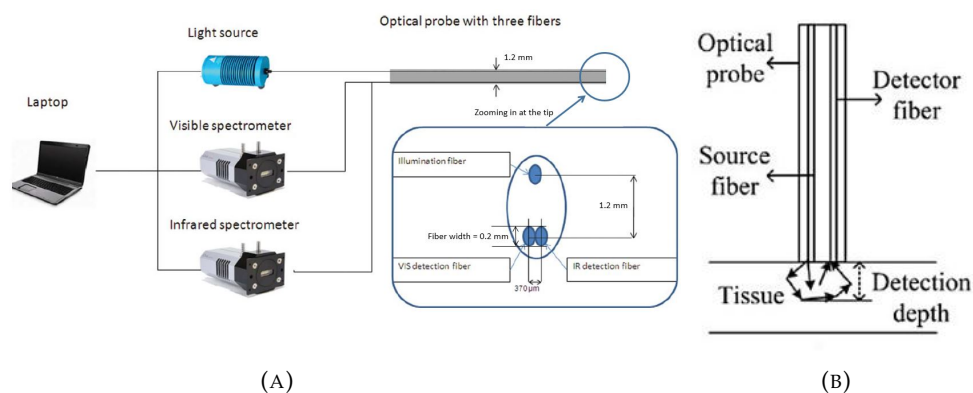


FIGURE 4.11: (A) Schematic representation of components of the measurement setup; (B) Front view of dual-fiber probe

Experiment methods

Vertebrae were extracted from the spinal column of a swine cadaver which was estimated to be deceased and stored in a frozen state for one year. The vertebra were divided into five regions namely pedicle cancellous, pedicle cortical, vertebral body cancellous, vertebral body cortical and spinal canal, as demarcated via the axial view of figure 4.12. During data acquisition, the optical probe was placed perpendicularly to the tissue surface with minimum pressure using a fixation system as shown in figure 4.13. Measurement locations were selected per region on a random basis. Three measurement spectra were acquired per measurement location. This data was then averaged which led to a total of 10 spectral data points per intravertebral region. The process was repeated for a total of 4 thoracic and 3 lumbar vertebra. The acquired data was then inputted into a spectral processing fitting algorithm which quantified the measurement spectra in order to provide a host of parameters which include chromophore concentrations and scattering parameters.

Statistical analysis

Kolmogorov-Smirnov and Shapiro-Wilk tests were first applied to check if the data is normally distributed. Kruskal-Wallis test which is a non-parametric equivalent of one-way independent ANOVA was thus applied to gauge the statistical significance of the results. This test as applied as a post-hoc test to compare each of the group means. Statistical analysis was performed using IBM SPSS Statistics 22 (IBM, New York). A P-value less than 0.01 was considered as statistically significant.

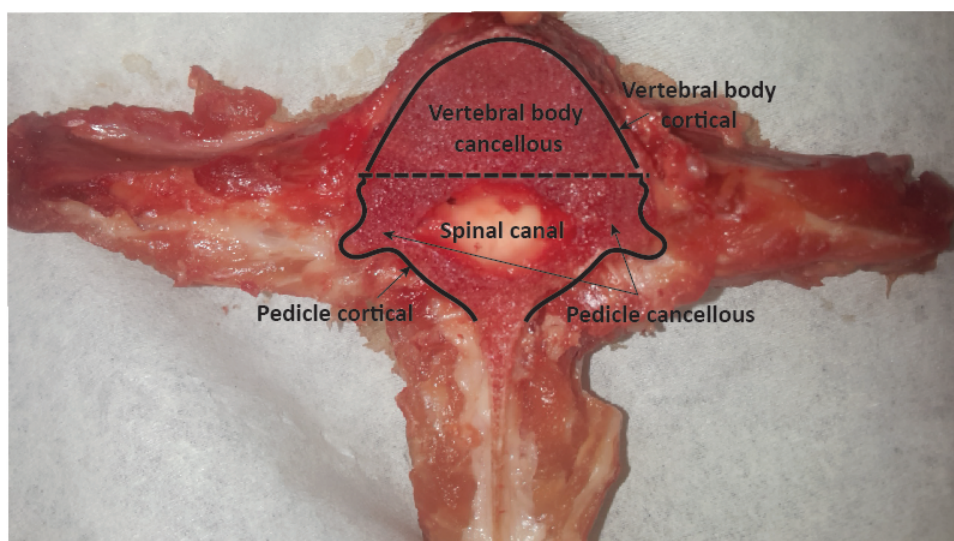


FIGURE 4.12: Axial view of a thoracic vertebra divided into five regions. Each region was mapped using the optical probe.

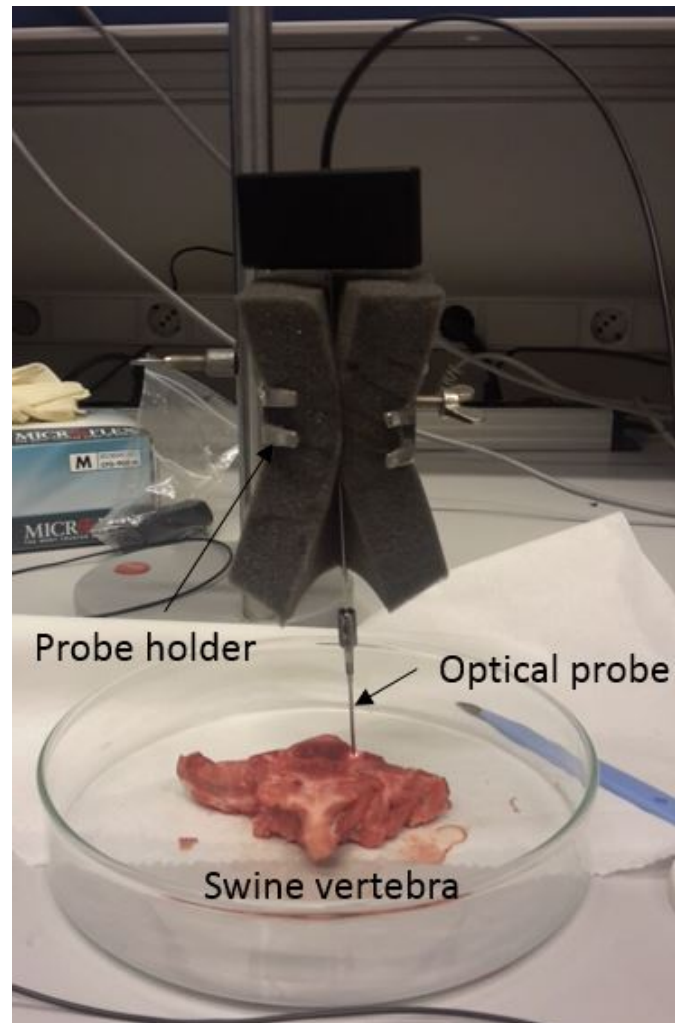


FIGURE 4.13: Optical probe placed perpendicular to the vertebral tissue surface during data acquisition.

4.2.4 Results

Out of the host of parameters analyzed, it was found that fat chromophore concentration and the scattering parameter normalized at 800 nm, varied statistically significantly across intravertebral regions. The change of fat chromophore concentration across intravertebral region can be visualized descriptively via figure 4.14. The boxplot does seem to indicate that the spinal canal has a higher fat content than other intravertebral regions.

The data was also pooled to analyze the change in fat concentration specifically across three main tissues namely cancellous bone, cortical bone and spinal canal. Figure 4.17 displays the trends.

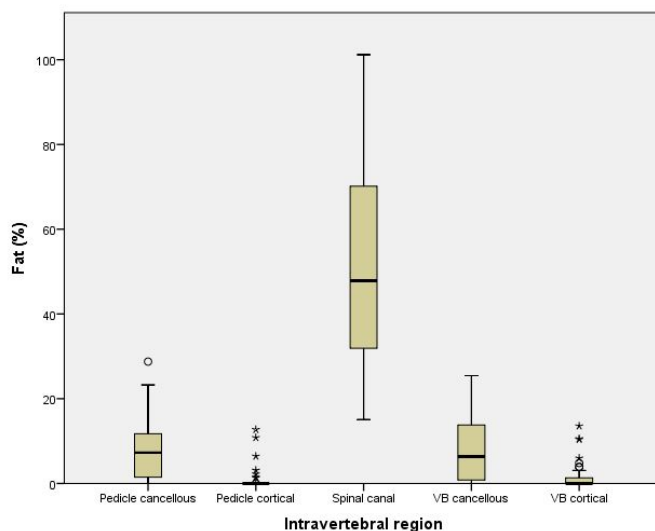


FIGURE 4.14: Boxplot depicting the change in fat concentration across the six intravertebral regions probed.

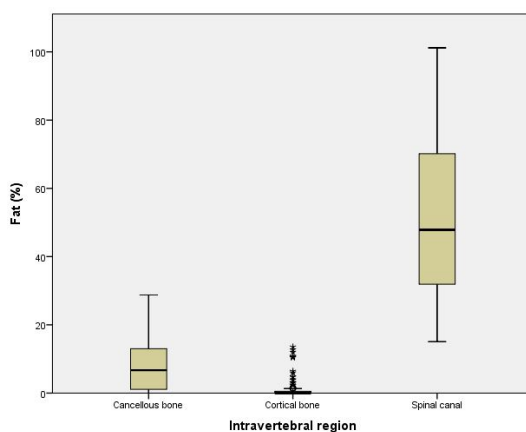


FIGURE 4.15: Boxplot depicting the pooled data of the change in fat concentration across intravertebral regions for the three principal tissues under investigation.

TABLE 4.3: Descriptive statistics of fat concentration data

Intravertebral region	N	Minimum	Maximum	Mean	Std. Deviation
Cancellous bone fat (%)	120	0.00	28.75	8.02	7.20
Cortical bone fat (%)	110	0.00	13.55	1.24	2.99
Spinal canal fat (%)	110	15.06	101.18	51.51	22.52

Fat chromophore concentration was found to be significantly higher in cancellous bone than in cortical bone ($H(1)=77.9, p < 0.01$). It was also found that the fat chromophore concentration was significantly higher in spinal canal as compared to cancellous and cortical bone ($H(1)=165.66, p < 0.01$, $H(1)=164.25, p < 0.01$).

Figure 4.16 shows the distribution of the scattering parameter across intravertebral regions.

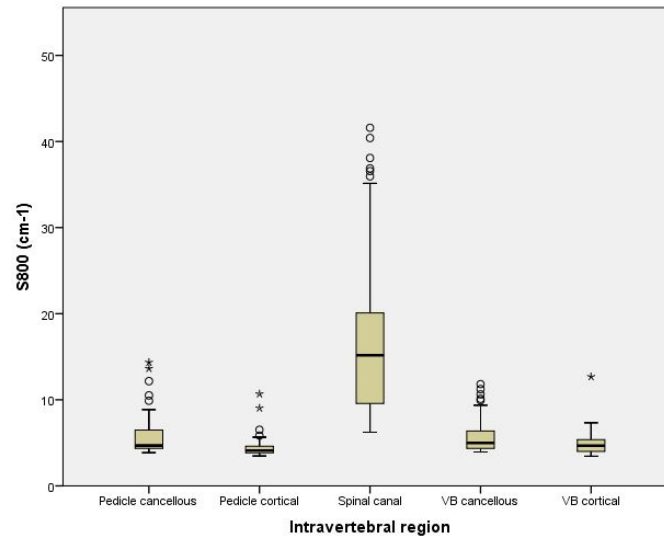


FIGURE 4.16: Boxplot depicting the change in the scattering parameter across the six intravertebral regions probed.

The data was also pooled to analyze the change in the normalized scattering parameter specifically across three main tissue types namely cancellous bone, cortical bone and spinal canal. Figure 4.17 displays the trends.

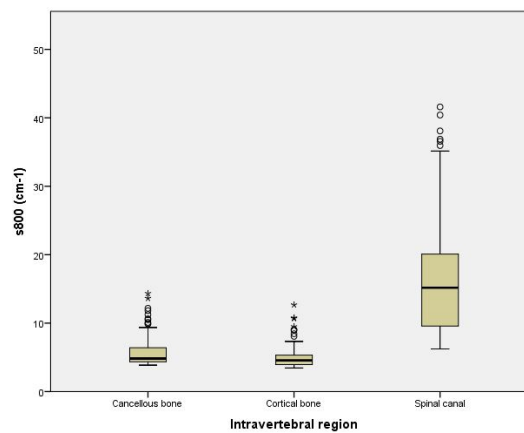


FIGURE 4.17: Boxplot depicting the pooled data of the change in scattering parameter across intravertebral regions for the three principal tissues under investigation.

TABLE 4.4: Descriptive statistics of scattering parameter data

Intravertebral region	N	Minimum	Maximum	Mean	Std. Deviation
Cancellous bone S800 (cm-1)	120	3.86	14.35	5.75	2.13
Cortical bone S800 (cm-1)	110	3.45	12.68	4.97	1.63
Spinal canal S800 (cm-1)	110	6.23	41.59	16.02	8.08

The scattering parameter was found to be significantly higher in cancellous bone as compared to cortical bone ($H(1)=14.54, p<0.01$). The scattering parameter was also found to be significantly higher in spinal canal as compared to cancellous and cortical bone ($H(1)=141.96, p<0.01$, $H(1) = 150.28, p<0.01$).

4.2.5 Discussion

This study was primarily tuned to spectroscopically map the various regions of the swine vertebrae. The spectra obtained at these regions was then quantified to identify the key parameters that significantly changed across the intravertebral regions. These parameters could then potentially be used to build an alarm system (sensing system) to warn the surgeon during an impending medial breach. Due to the fundamental capabilities of the DRS technology and the fitting algorithm discussed in chapter 3, the spectra retrieved from the various pure tissues was also used to derive their optical properties. These are then used to develop the Monte-Carlo model discussed in the subsequent study.

The boxplot shown in figure 4.15 shows that fat chromophore concentration is sensitive to intravertebral region being probed. This result was also found to be statistically significant. However, variation in the fat concentration even within pure tissue exists primarily due to the heterogeneity of the tissue and noise stemming from the spectral fitting algorithm (PNsas). This variation needs to be carefully analyzed especially since the aim of the proposed sensing system would be to provide real-time feedback to the surgeon. Relatively consistent fat chromophore concentration thresholds would need to be established for each of the three tissue types in order to build a reliable sensing system.

Figure 4.17 points out that the scattering of photons is much higher in the spinal canal. This is expected since the spinal canal was found to contain a semi-fluid substance within it as shown in figure 4.8 in the previous study. Equation 3.6 shows that the scattering is inversely dependent on average particle size via the Mie scattering slope. The semi-fluidic nature of the substance indicates lower particle size which in turn should induce higher photon scattering. Therefore, this is an expected result.

Scattering of photons was also found to be higher in cancellous bone as compared to cortical bone. Figure 4.9 part of the geometry mapping experiment clearly illustrates the porous nature of the cancellous bone. This type of bone also houses blood and fat deposits within its pores [69]. The high porosity coupled with differences in tissue types should contribute to the higher scattering of photons due to differences in refractive indices. The highly mineralized cortical bone was found to be much denser in structure. It is also relatively homogeneous due to the absence of perfusion and fat deposits. Thus, the higher value of scattering parameter in cancellous bone as compared to cortical bone as shown in the table 4.4 is an expected result.

The scattering parameter could therefore be used as a potential candidate to optimize the alarm system. However, even in the estimation of the scattering parameter from the retrieved spectra, variation exists. The factors causing the variation range from heterogeneity in tissue and noise arising from the spectral fitting algorithm, to name a few.

DRS and the PNsas spectral fitting software were built fundamentally to quantify the retrieved spectra in terms of organic chromophores such as fat, water and blood etc. Whereas, konstantinos *et al* [54] found that 70% of human bone is made up of inorganic matrix. Modifying the PNsas spectral fitting algorithm to quantify inorganic molecule concentrations could be useful. However, it is known that organic molecules are intrinsically larger in size as they form large number of hydrocarbon chains. This aspect makes them sensitive to photon interactions. There is a strong possibility that inorganic molecules do not contribute to a well defined reflectance spectra.

Given that researchers have found the epidural space to contain several other tissue types such as lymphatics, arteries and nerve roots, its influence on the fat chromophore concentration needs to be further investigated in an *in vivo* setting. The *ex vivo* swine vertebral bone used in this study also lacks perfusion. However, since the wavelength of light absorbed by fat and blood belong to seemingly independent diagnostic windows (fat chromophore is NIR sensitive and blood chromophore is visible light sensitive), the fat chromophore concentration trend found, might be less effected by the *ex vivo* nature of the tissue.

A possibility exists that new parameters which are also estimated by the spectral fitting algorithm become relevant during experiments conducted in an *in vivo* human vertebral tissue.

Reiterating the observation made in the previous geometry mapping study, generalizability of the results in such experiments is heavily influenced by the tissue quality and the dissection method used to probe the tissue. Refined experiments of needle insertion by keeping the vertebral column intact could help draw more concrete claims. In other words, acquiring data by

reproduction of the actual clinical environment is vital in optimizing the sensing algorithm in order to get one step closer to clinical adoption of the technology.

4.2.6 Conclusion

Fat chromophore concentration and the scattering parameter were found to be significantly different across cancellous bone, cortical bone and spinal canal in the 7 vertebrae studied in an *ex vivo* swine.

Chapter 5

The simulation investigation: Building the Monte-Carlo model

5.1 Effect of fat concentration on insertion depth of the optical probe in vertebral swine tissue

5.1.1 Abstract

BACKGROUND CONTEXT: Monte-Carlo methods are a broad class of computational algorithms that rely on repeated random sampling to obtain numerical results. This powerful method was leveraged by researchers to develop an algorithm to predict steady-state photon-tissue interactions for biomedical applications. The Monte-Carlo model was then adopted to understand photon interactions in a 3-layered tissue geometry consisting of cancellous bone, cortical bone and the spinal canal. The model provides the capability of modifying the tissue thickness in order to understand the change in the diffuse reflectance due to photon-tissue boundary interactions.

PURPOSE: The purpose of this study was to build a 3-layer Monte-Carlo model to understand the relationship of fat chromophore concentration on the insertion depth of a optical probe, during a medial breach scenario.

METHODS: Monte-Carlo model of steady-state light transport in multi-layered tissue (MCML) developed by Wang and Jacques was adopted in this study. Wavelengths were simulated at 10 nm intervals resulting in 121 datapoints over the range of 400 nm to 1600 nm. A refractive index of 1.44 and an anisotropy factor of 0.9 was chosen for all the three tissue types as input for the Monte-Carlo model. Wavelength-dependent absorption and reduced scattering coefficients were retrieved from the previous optical mapping study and used as input for the model. 10^6 photons were simulated in each simulation which led to one reflectance datapoint per wavelength. The fiber distance was chosen to be equal to 0.12 cm.

RESULTS: Fat concentration was found to change across different layers of tissues. The signal change was found before the optical probe tip came in contact with the tissue boundary, indicating a non-zero breach anticipation window.

CONCLUSIONS: This study demonstrated via a 3-layer Monte-Carlo model, the influence of fat chromophore concentration on insertion depth during a medial breach scenario. The presence of a non-zero breach anticipation window indicates that DRS in-principle, has the potential to anticipate medial breaches during a pedicle screw placement procedure.

5.1.2 Introduction

Fundamental background

Monte Carlo methods have been adopted to model reality in a wide range of fields right from scientific domains such as physics and engineering to even modeling systems in finance and business. The following section serves as a primer into the understanding of core Monte-Carlo algorithm used to model photon transport in tissues.

Monte Carlo simulations rely on the random sampling of variables from a probability density function. The model is based on a random walk, where a photon or a photon packet is

traced through the tissue until it exits or until it gets entirely absorbed. Figure 5.2 describes pictorially how the photon packet is traced right from launch to the termination.

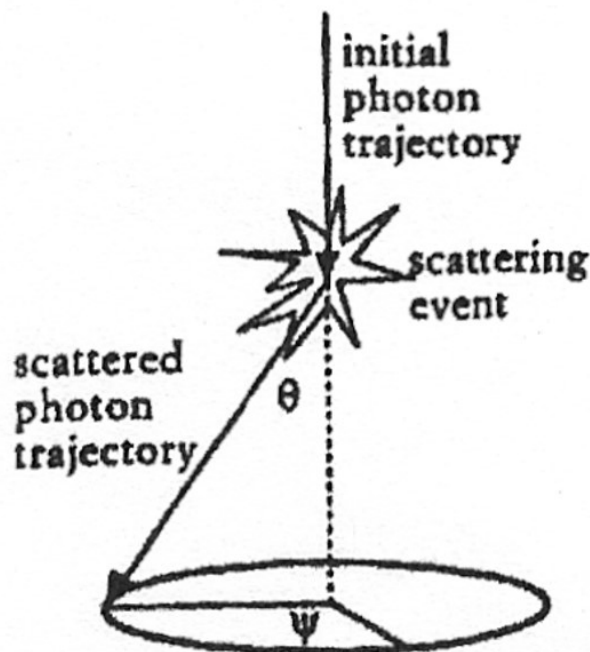


FIGURE 5.1: A scattering event is a function of deflection angle θ and azimuthal angle ψ

Photons are initially launched into the medium as shown in figure 5.1. This is done by assigning a weight W equal to unity, for each photon before injecting into the tissue. If there is a mismatched boundary between the outside medium (m) and tissue (t), then specular reflectance will occur according to Fresnel law:

$$R_{sp} = \frac{(n_t - n_m)^2}{(n_t + n_m)^2}. \quad (5.1)$$

In case the above event occurs, the resulting photon weight is reduced so that,

$$W = 1 - R_{sp}. \quad (5.2)$$

Assuming the photon packet has entered the tissue, photon propagation must occur. To do so, a path length or step size s is generated. A probability density function is first created which is in turn used to generate the path length. A random number is selected from a uniform probability density function between 0 and 1 so that,

$$\int_a^b p(k) dk = 1. \quad (5.3)$$

The path length is then generated as a function of the random number as,

$$s = \frac{-\ln(k)}{\mu_a + \mu_s}. \quad (5.4)$$

Once the photon packet has moved, it must experience an absorption event. However, in reality this is not completely true as will be made clear in the later section. This event would

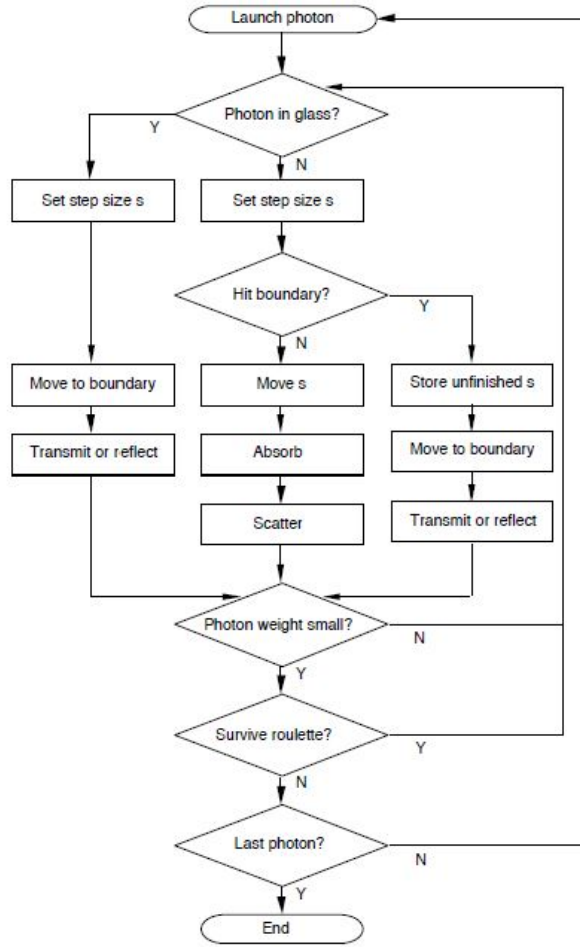


FIGURE 5.2: Flowchart depicting photon propagation in medium

lead to some attenuation of the photon weight ΔW given by,

$$\Delta W = \left(\frac{\mu_a}{\mu_a + \mu_s} \right) \times W. \quad (5.5)$$

Therefore, the new photon weight would be equal to

$$W_{new} = W_{old} - \Delta W. \quad (5.6)$$

Scattering of the photon is then modeled based on the deflection angle θ and azimuthal angle ψ as shown in figure 5.2. The deflection angle is calculated based on the expression by Henley-Greenstein for forward scattering ($g > 0$):

$$\theta = \cos^{-1} \left(\frac{1}{2g} \left(1 + g^2 - \left(\frac{1 - g^2}{1 - g + 2gk} \right)^2 \right) \right). \quad (5.7)$$

The azimuthal angle is also calculated according to

$$\psi = 2\pi k. \quad (5.8)$$

It must be noted here that equation 5.7 and 5.8 is driven by the same random number generator k created in equation 5.3. Once the photon has changed its direction, a new step size or path length is calculated. The photon weight is reduced yet again and the scattering interaction is accounted for. This process is repeated until the photon weight reduces to a value below a

threshold value specified. In order to obey the rules of conservation of energy, the photon is given one last shot to survive via a roulette. If it is unable to survive, the simulation for this photon ends.

Boundary events There is also a possibility when the photon reaches a boundary, which is signified by the change in refractive index. This phenomena is governed by Snell's law and Fresnell's equations. The former related to the direction of light to the refractive indices of the media given by:

$$\frac{\sin(\theta_1)}{\sin(\theta_2)} = \frac{n_2}{n_1}. \quad (5.9)$$

Light that hits the tissue with an angle equal to or greater than the critical angle is completely reflected. The critical angle is defined as:

$$\theta_c = \arcsin\left(\frac{n_2}{n_1}\right). \quad (5.10)$$

Fresnell's equations describe the amount of light that is transmitted and the amount of light that is refracted as a function of the angles determined by Snell's law and the polarisation of light. Finally, the internal reflectance is given by:

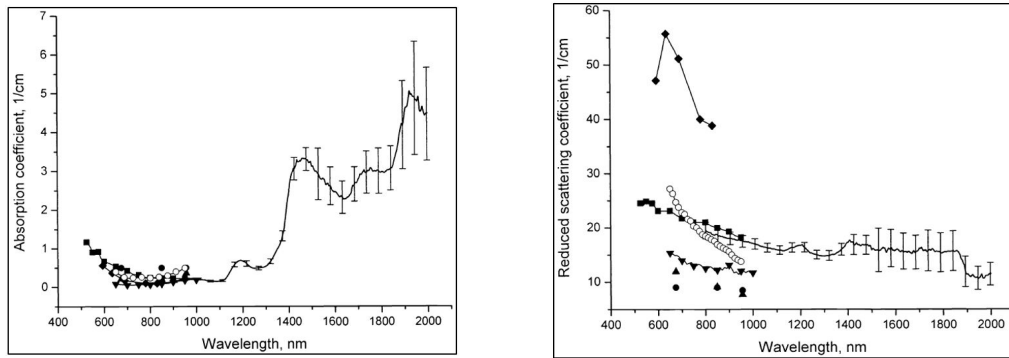
$$R(\theta_1) = \frac{1}{2} \left(\frac{\sin^2(\theta_1 - \theta_2)}{\sin^2(\theta_1 + \theta_2)} + \frac{\tan^2(\theta_1 - \theta_2)}{\tan^2(\theta_1 + \theta_2)} \right). \quad (5.11)$$

Due to statistical nature of this approach, the model accuracy is directly dependent on the number of photons simulated. Typically, a large number of photons in the order of 10^6 are required to obtain a useful simulation. Since, the validity of the model is heavily dependent on the optical properties inputted, the following sections delve deeper into the optical properties found by various researchers specifically of bone and spinal canal.

Optical properties of bone and spinal canal

Bashkatov *et al* [7] found the optical properties of human cranial bone in the spectral range between 800 and 2000 nanometers. All the measurements were performed for cortical bone samples. The anisotropy factor was assumed to be 0.9. This seems to be a standard assumption for tissues probed under visible and NIR spectral ranges [30],[124]. Figure 5.3a shows the dependence of the absorption coefficient on wavelength of light for cortical bone. Interestingly, Bashkatov *et al* [7] also compared the optical properties found by other researchers. The geometric symbols in the figures 5.3a and 5.3b elucidates these trends. It can be seen that while the absorption curves do seem to match across researchers, the reduced scattering coefficient data seems to vary quite significantly. The author attributes these discrepancies to the measuring techniques used, methods of tissue preparation and differences in bone types (cortical or cancellous) measured.

Bevilacqua *et al* [8] determined the optical properties of the human skull bone, apart from other tissues like white matter, scar tissue, optic nerve and tumors. The author adopted the refractive index of all tissues with a value of 1.4. Ting *et al* [123] has also suggested adopting a refractive index ranging from 1.3 to 1.5 for biological tissues. There were no studies found on the specific investigation of vertebral bone tissue.



(A) Wavelength-dependent absorption curve. Figure from [7]

(B) Wavelength-dependent reduced scattering curve. Figure from [7]

FIGURE 5.3: Wavelength-dependent optical properties found experimentally by Bashkatov *et al* [7]. The symbols correspond to averaged experimental data found in literature.

Monte-Carlo models have been used by several researchers to understand photon transport in tissues [131, 31, 113]. Li *et al* [62] specifically applied a Monte-Carlo model to define a detection depth during a pedicle wall breach in vertebral tissue. The researchers created a 2-layer model with a small fiber distance of 0.2 mm. However, the optical properties inputted into the model were derived from a phantom tissue model which raises questions regarding the validity of the model.

To the best of my knowledge, this is the first study in which a 3-layer Monte-Carlo model was built to understand the relationship of fat chromophore concentration on insertion depth during a medial breach scenario.

5.1.3 Materials and methods

In this study Monte-Carlo simulations of multiple tissue layers was applied in order to observe the spectral transitions during a medial breach scenario. For this purpose, the Monte Carlo model of steady-state light transport in multi-layered tissue (MCML) developed by Wang and Jacques [131] was applied, because this model has the ability to simulate photon propagation through multiple tissue layers.

Model input parameters

Wavelengths were simulated at 10 nm intervals, resulting in 121 datapoints over the range of 400 nm to 1600 nm. A refractive index of 1.44 and an anisotropy factor of 0.9 was chosen for all the three tissue types as input for the Monte-carlo model. Figure 5.6 displays the wavelength dependent absorption and reduced scattering coefficients used to build the model. Each simulation contains 100,000 photons which led to one reflectance datapoint per wavelength. The simulation was performed for the wavelength range of 400 to 1600 nm. Simulations were processed in parallel using the Linux cluster made available at Philips research, Eindhoven. The fiber distance was chosen to be equal to 0.12 cm.

Model geometry conventions

The cylindrical grid system adopted to model the geometry of a tissue layer is shown in figure 5.4. The geometry is a function of total depth z , total radius r and a total sweep angle equal to a . The geometry is subdivided into grid elements using distances dr , da and dz as shown in figure 5.4. In this study the radius grid width dr and the angular sweep width da were chosen to be equal to 0.002 cm and 3.6° respectively. A pencil beam of light enters the tissue layer at the center of the grid system C as denoted by the red arrow perpendicular to the top surface. The top layer with $dz = 0$ contains information about the amount of diffuse reflectance. Layer

depth is chosen as an integer multiple of dz , so that information within each grid element only pertains to one tissue type.

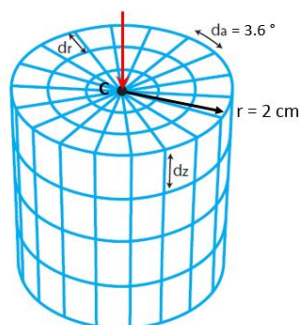


FIGURE 5.4: Cylindrical grid system used to model a tissue layer in Monte-Carlo simulations

Data Processing

Matlab was used to extract the diffuse reflectance spectra from the MCML output files. Figure 5.5 shows the top view of the top surface of the tissue geometry. Diffuse reflectance information was extracted by averaging information from all the grids swept by the receiving fiber of width 0.2 mm. This is depicted by the red region in figure 5.5.

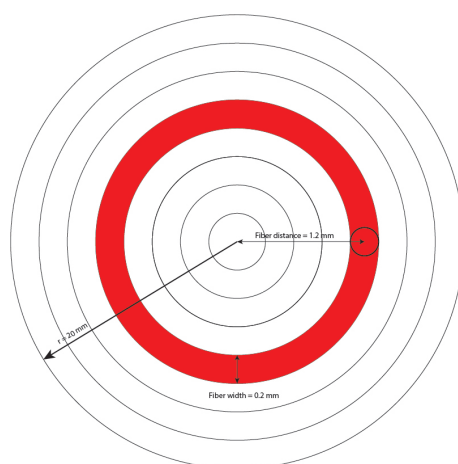


FIGURE 5.5: The diffuse reflectance information was extracted from the entire region represented in red (Figure not to scale).

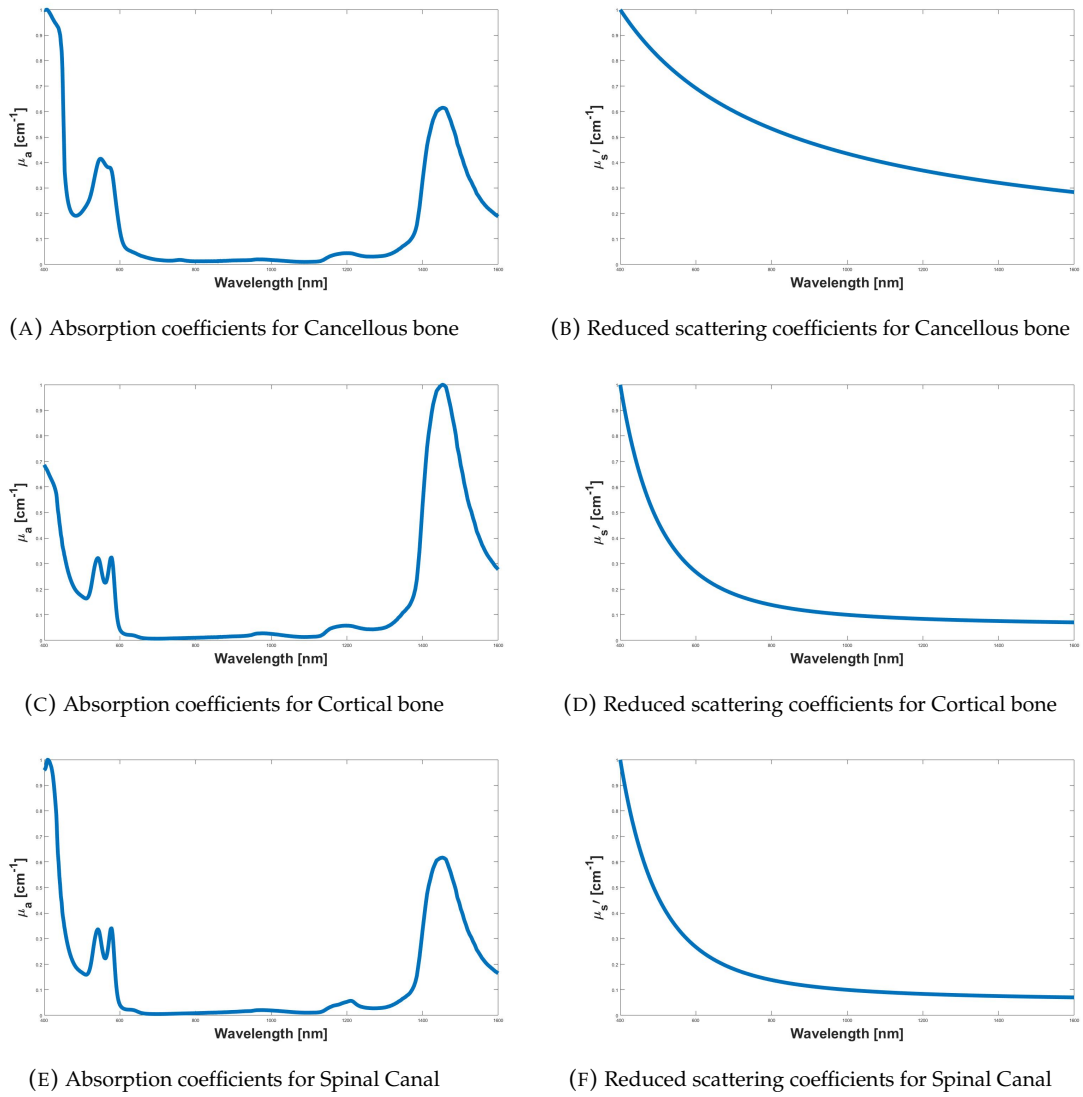


FIGURE 5.6: Absorption and reduced scattering coefficients for the Monte-Carlo model

Validation protocol

Figure 5.7 describes the workflow followed in order to validate the Monte-Carlo model. The measurement spectra was acquired from the optical mapping experiment performed during the previous study. The measurement spectra to be inputted into the inverse Farrell model was chosen based on the average fat chromophore concentration data as displayed in table 4.3. The three candidate measurement spectra corresponding to pure cancellous bone, cortical bone and spinal canal were then inputted into the inverse Farrell model to retrieve the wavelength dependent absorption coefficients (μ_a) and reduced scattering coefficients (μ_s') as shown in figure 5.6. The forward Monte-Carlo model was then executed to retrieve the simulated reflectance spectra at the specified fiber distance. The validity of the model spectra was then quantified by calculating the Variance-Accounted-For (VAF). The VAF can be described mathematically as follows:

$$VAF = \left(1 - \frac{\sum_{i=1}^N (y(t_i) - \hat{y}(t_i))^2}{\sum_{i=1}^N y(t_i)^2} \right) \times 100. \quad (5.12)$$

Where, $y(t_i)$ represents the measured spectral signal and $\hat{y}(t_i)$ represents the model spectral signal retrieved from the Monte-Carlo model. VAF provides a percentage value between 0 and

100. The higher the VAF, the lower the prediction error and better the model.

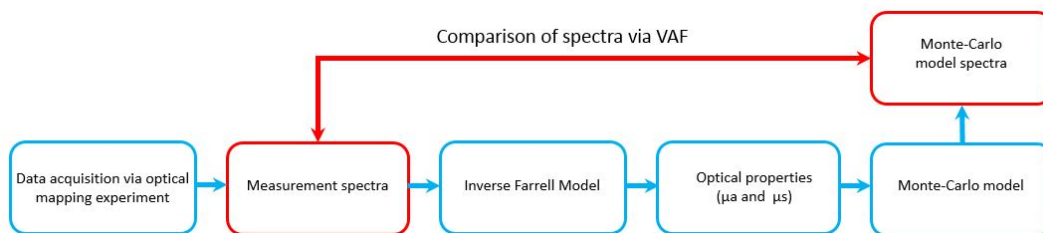


FIGURE 5.7: Workflow diagram of Monte-Carlo model validation protocol

Multilayer geometry development

The 3-layer Monte-Carlo model can be visualized with the help of figure 5.8 as shown. To simulate the traversing of the optical probe through the tissue layers, the thickness of the layer was reduced in steps of 0.2 mm. The outputted diffuse reflectance was obtained by averaging the reflectance measured by the regions swept in red as shown in figure 5.8. Diffuse reflectance spectra was acquired after each tissue thickness reduction. Quantification of the spectra to retrieve fat chromophore concentration was then performed. The data was then used to build the fat chromophore concentration vs insertion depth curves. The above process was repeated by varying the thickness of the cortical bone.

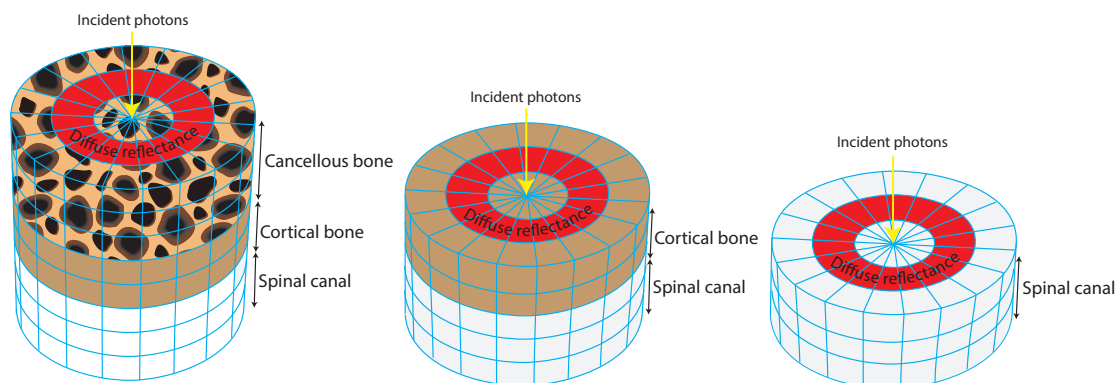


FIGURE 5.8: Cylindrical grid system used to model a tissue layer in Monte-Carlo simulations

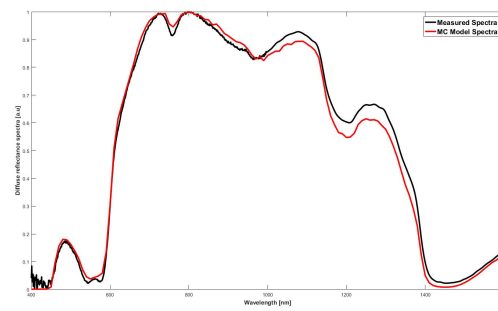
5.1.4 Results

Model Validation

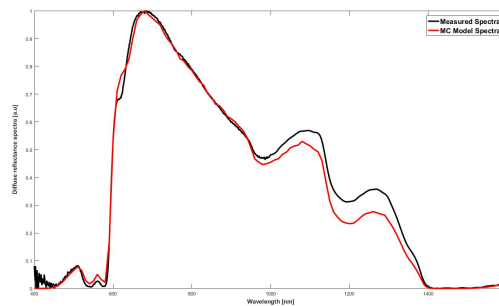
Figure 5.9a, 5.9b and 5.9c represent the reflectance spectra obtained for cancellous, cortical and spinal canal respectively. Each graph contains both the measured spectra from the optical mapping experiment and the spectra obtained from the Monte-Carlo simulations. Upon visual inspection it does seem to indicate that the Monte-Carlo model spectra does simulate reality rather well. The high values of VAF obtained in table 5.1 does indeed reflect this fact.

TABLE 5.1: Monte-Carlo validity checked via VAF

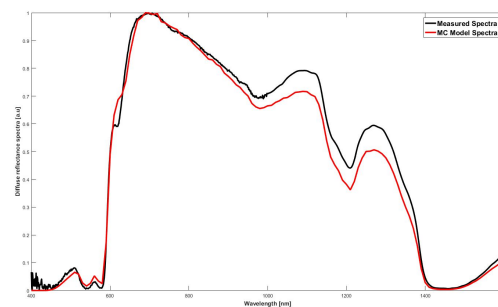
Tissue type	Variance-Accounted-For (VAF)
	[%]
Cancellous bone	99.4
Cortical bone	99
Spinal canal	98.9



(A) Cancellous bone reflectance spectra



(B) Cortical bone reflectance spectra



(C) Spinal canal reflectance spectra

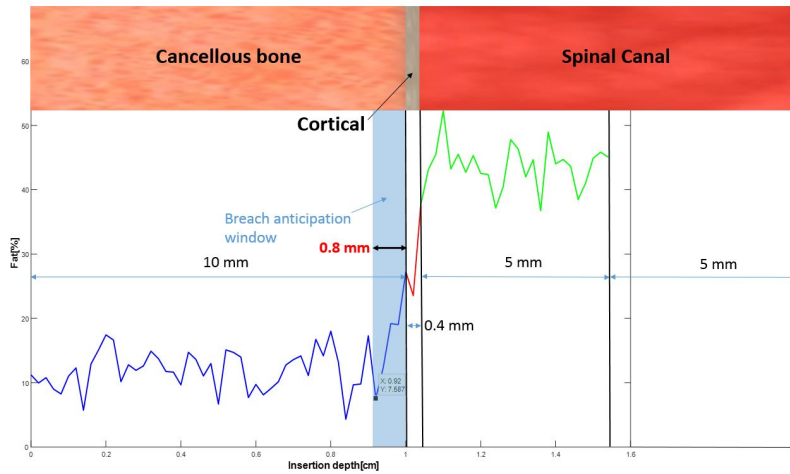
FIGURE 5.9: Comparison of experimentally measured spectra and Monte-Carlo model spectra for the three principal tissues under investigation.

Analysis of change in fat chromophore concentration during a medial breach scenario

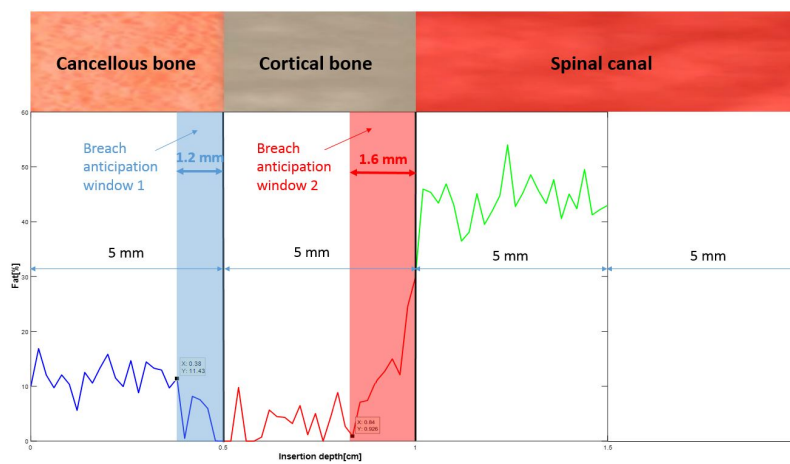
From the geometry mapping study it was found that the spinal canal thickness in an *ex vivo* swine was found to vary between 0.5 mm to 0.85 mm. Based on this result a conservative value of 0.4 mm was chosen as the thickness of the cortical bone surrounding the spinal canal as shown in the figure 5.10a. The fat chromophore concentration was found to have changed by 0.8 mm before the cortical bone boundary was reached.

When the cortical bone thickness was increased to 5 mm, the fat chromophore concentration was found to have decreased by 1.2 mm before cortical bone boundary was reached. This value increased to 1.6 mm during the transition from cortical bone to spinal canal as shown in figure 5.10b.

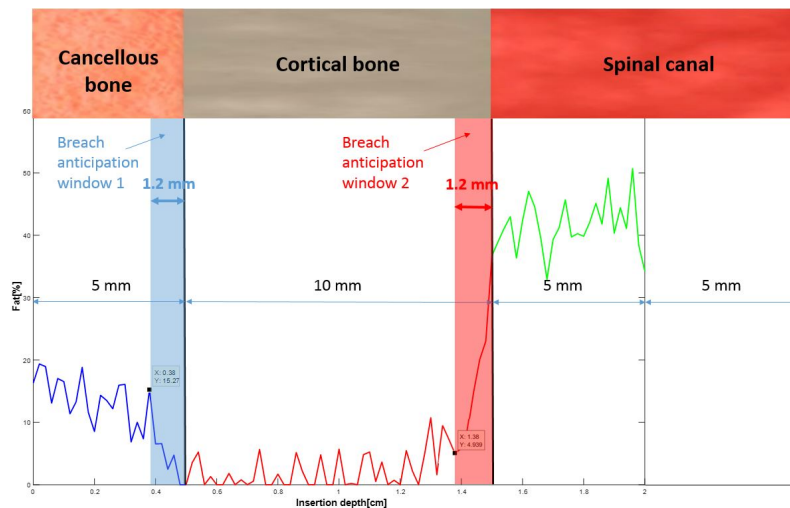
Similarly the downward trend of fat chromophore concentration during the transition of light source from cancellous bone to cortical bone was observed 1.2 mm before coming in contact with the cortical bone boundary as shown in figure 5.10c.



(A) Cortical bone thickness chosen as 0.4 mm



(B) Cortical bone thickness increased to 5 mm



(C) Cortical bone thickness increased to 10 mm

FIGURE 5.10: 3-layered Monte-Carlo model depicting the change in fat concentration with insertion depth during a medial breach scenario

5.1.5 Discussion

This study corresponds to the first of its kind in which a 3-layer Monte-Carlo model was developed to simulate a medial breach scenario during a typical pedicle screw placement procedure. More specifically, the behavior of a pencil beam of light exiting an optical fiber was modeled as the light source traverses through various tissue layers with different optical properties. The spectra obtained at each layer depth was then quantified in terms of fat chromophore concentration to obtain trends observed in figure 5.10.

Figure 5.10a indicates that the fat chromophore concentration drastic upward trend changes, 0.8 mm before the light source actually comes in contact with the cortical bone boundary. This breach anticipation distance of 0.8 mm was measured by selecting the data point after which a significant change in the fat chromophore concentration was observed. This early jump of the signal could be potentially used to alarm the surgeon before actually making a breach. However, whether the breach anticipation distance of 0.8 mm is sufficient from a clinical context needs further investigation via needle insertion experiments.

Interestingly, upon increasing the cortical thickness to 5 mm, the breach anticipation distance increased to 1.2 mm during the light source transition from cancellous to cortical bone as shown in figure 5.10b. This could be due to the fact that the ratio of fat content between cancellous and cortical bone increased due to the greater thickness of the cortical bone. In the previous case of 0.4 mm cortical thickness as shown in figure 5.10a, the emitted photons could be interacting with all the three layers assuming a detection depth of 0.5 mm (approximately half the chosen fiber distance). Whereas, in the second case it can be assumed that the emitting photons are only interacting with 2 layers at the first tissue boundary, namely cancellous and cortical bone. This observation could point to the fact that the breach anticipation distance is a function of fat chromophore concentration ratio of the layers across the boundary and the thickness of the layer in front of the light source.

Figure 5.10b also goes to show that a second breach anticipation window comes into existence with increase in cortical bone thickness. The breach anticipation distance was found to be 1.6 mm which could also be translated into an warning signal as the instrument tip has not entered the spinal canal yet. It must be noted that this fat chromophore concentration change is much more drastic due to fatty nature of the epidural space in the spinal canal. The low fat content of the cortical bone and relatively high fat content of the spinal canal was also seen during the optical mapping experiments as shown in the boxplots of the figure 4.15. It could be hypothesized that this high ratio of fat content of spinal canal to the fat content of the cortical bone led to the increase of the breach anticipation distance. However, 5.10c does not confirm this hypothesis.

The existence of two breach anticipation windows due to increase in the cortical bone thickness as shown in 5.10b and 5.10c could be optimized to warn the surgeon before the perforation of spinal canal. An anatomic study to measure the cortical thickness of the spinal canal in humans is needed further this claim.

There are several limitations in this study. The breach anticipation window chosen could be severely influenced by noise. Source of noise could be due to various factors. Some of them are linked to the model assumptions stated later. A source of noise arises from the fitting algorithm (PNsas) used to quantify the spectra in order to retrieve the fat concentration data. Another important source of noise is the number of photons used in the simulation. A million photons were used in this study. The model smoothness is inversely related to number of photons simulated. Unfortunately this heavily increases computation time. Thus, a trade-off exists and a host of parameters need to be carefully analyzed in order to reduce the dependence of noise on the breach anticipation window.

It must also be pointed out that the Monte-Carlo model output is inherently coupled to the optical properties inputted into it. The optical properties were in turn derived after quantifying a spectra retrieved from experiments as shown in the workflow diagram of figure 5.7. This could be a possible reason why the VAF is so high. In other words, the simulations and the real world experiments are coupled via optical properties.

Some of the key limitations are inherently linked to the assumptions which were made in order to tackle the problem.

Model Assumptions

Firstly, it is assumed that the geometry of the light source is a pencil beam. Which implies that a single stream of photons are entering the tissue layer. The model also assumes that this source is perpendicular to the tissue layer at all times as shown in figure 5.4. This might not hold true during the surgical procedure. The effect of light source geometry on the spectra and in turn on the fat chromophore concentration is an extremely important aspect that needs to be studied further in the near future.

The model treats photons as neutral particles without considering the wave nature of light. Therefore, the phase and polarization are assumed to be randomized and purposefully ignored. It is assumed that the photons are multiply scattered by tissues. This assumption works reasonably well when larger fiber distances are involved as the photons initial direction is in a sense forgotten due to large number of interaction events taking place before the photons enter the collection fiber. However, the effect of change in the fiber distance on the breach anticipation distance would be a vital study to conduct. Such a study could also shed light into the sensing depth of individual tissue types.

The model also assumes each tissue layer to be homogeneous in nature, which implies that the optical properties are uniformly distributed throughout each tissue layer. Given that the epidural space is made up of different types of tissues such as fat, blood, lymphatics and nerves, this assumption is violated. However, based on Hogan *et al* [47] study, if the bulk of the epidural space is occupied by fat, such an assumption seems reasonable.

From figure 5.5 it becomes clear that the diffuse reflectance exiting the top surface was calculated by averaging information from all the grids swept by the receiving fiber as shown by the red region. This was also done in order to reduce variability, given the statistical nature of the model. In practice, the surgeon might twist the instrument by various angles during the surgical procedure. This would mean that the geometry of light entering into the receiving fiber might also change. The effect of emitting light geometry on the breach anticipation distance is also quite a vital study which could provide new insights into various sources of noise that might be encountered during the clinical procedure.

The model tracks the photon path by assigning it a weight which is decreased after an absorption event occurs. In reality, an absorption event would lead to the termination of the photon. This is due to the fact that the energy of the photon is fundamentally quantized as found by Einstein. This is an inherent assumption in the model. But, as the model validity curves in figure 5.9 suggest, this assumption works quite well.

5.1.6 Conclusion

This study demonstrated via a 3-layer Monte-Carlo model, the influence of fat chromophore concentration on insertion depth during a medial breach scenario.

The significant change in the signal between various tissue boundaries as shown in figures 5.10a, 5.10b and 5.10c clearly indicates that DRS technology can in-principle be used to detect the presence of a tissue boundary. The existence of a non-zero breach anticipation window, suggests that DRS technology can in-principle be used to anticipate a medial breach.

Chapter 6

Overall Conclusion

The thesis has been modularized into two main investigations namely, the clinical and technical investigations. As stated in the research objectives in chapter 1, each investigation has been dealt with by answering several research questions. A brief summary of the answers pertaining to the clinical investigation would be elaborated first, followed by the answers to the technical investigation.

6.1 The clinical investigation

6.1.1 Secondary research questions

1. **What are the current surgical techniques for pedicle screw placement?**

An extensive workflow analysis of each of the techniques used in clinical practice was performed as illustrated from the workflow diagrams in the subsection 2.4.1.

2. **What is the definition of accurate pedicle screw placement?**

At the moment there is no reliable, validated breach definition available in literature. However out of a total of 8 distinct definitions found, 2 of them were extensively cited leading to some consensus. The most cited definition is defined based on the 'anatomical safe zone' principle and should be used as a benchmark while developing experimental protocols for the new proposed solution.

3. **How accurate are the current techniques in pedicle screw placement?**

Based on the highest level of evidence available in literature it can be concluded that conventional techniques such as free-hand and 2D fluoroscopy-guided have high placement accuracy variability which is clearly indicative of the complexity and technically demanding nature of the procedure.

4. **What is the complication rate associated with each technique?**

The number of screw-related complications reported in literature are low but can be potentially life-threatening. Due to several reasons such as ambiguity in definition of screw-related complication and surgeons' reluctance to report complications due to medicolegal reasons, the low reported complication rate should be interpreted with caution and not underestimated.

6.1.2 Primary research question

5. **Is inaccuracy in pedicle screw placement a problem?**

The high accuracy variability of conventional techniques coupled with their high popularity, as reflected by surgeons' interviews confirm the presence of a problem. The fact that spinal fusion surgery is one of the most frequently performed surgeries in the United

States, which has the biggest spine market share in the world, points to the magnitude of the problem.

6.2 The technical investigation

6.2.1 Primary research question

1. **Can DRS technology be used to detect and anticipate the presence of a tissue boundary during a medial breach scenario?**

Fat concentration versus insertion depth signals were found to change across different tissue types. This aspect indicates that DRS technology could in-principle be used to **detect** a tissue boundary during a medial breach scenario. The presence of a non-zero breach anticipation window suggests that the DRS technology could in-principle be optimized to sense the tissue boundary in advance. This information could be used by the surgeon to **anticipate** or prevent a medial breach from occurring.

Bibliography

- [1] Yasser Allam et al. "Computer tomography assessment of pedicle screw placement in thoracic spine: comparison between free hand and a generic 3D-based navigation techniques". In: *European Spine Journal* 22.3 (2013), pp. 648–653.
- [2] Vincenzo Amato et al. "Accuracy of pedicle screw placement in the lumbosacral spine using conventional technique: computed tomography postoperative assessment in 102 consecutive patients: Clinical article". In: *Journal of Neurosurgery: Spine* 12.3 (2010), pp. 306–313.
- [3] AMD. Needle, Jamshidi Needle Biopsy, 15G 100Mm. 2015. URL: <https://www.amdnext.com/jamshidi-needle-biopsy-15gax-100mm.html#.VqUd91KnH6k>.
- [4] Louis-Philippe Amiot et al. "Comparative results between conventional and computer-assisted pedicle screw installation in the thoracic, lumbar, and sacral spine". In: *Spine* 25.5 (2000), pp. 606–614.
- [5] Yu-Shu Bai et al. "Comparison of the pedicle screws placement between electronic conductivity device and normal pedicle finder in posterior surgery of scoliosis". In: *Journal of spinal disorders & techniques* 26.6 (2013), pp. 316–320.
- [6] James W Barber et al. "Biomechanical Study of Lumbar Pedicle Screws: Does Convergence Affect Axial Pullout Strength?." In: *Journal of Spinal Disorders & Techniques* 11.3 (1998), pp. 215–220.
- [7] Alexey N Bashkatov et al. "Optical properties of human cranial bone in the spectral range from 800 to 2000 nm". In: (2006), pp. 616310–616310.
- [8] Frederic Bevilacqua et al. "In vivo local determination of tissue optical properties: applications to human brain". In: *Applied optics* 38.22 (1999), pp. 4939–4950.
- [9] Rajesh K Bindal et al. "Surgeon and patient radiation exposure in minimally invasive transforaminal lumbar interbody fusion: Clinical article". In: *Journal of Neurosurgery: Spine* 9.6 (2008), pp. 570–573.
- [10] Gema de Blas et al. "Safe pedicle screw placement in thoracic scoliotic curves using t-EMG: stimulation threshold variability at concavity and convexity in apex segments". In: *Spine* 37.6 (2012), E387–E395.
- [11] Ciaran Bolger et al. "Electrical conductivity measurement: a new technique to detect iatrogenic initial pedicle perforation". In: *European Spine Journal* 16.11 (2007), pp. 1919–1924.
- [12] Austin C Bourgeois et al. "The evolution of image-guided lumbosacral spine surgery". In: *Annals of translational medicine* 3.5 (2015).
- [13] Bruno Perocco Braga, Josaphat Vilela de Moraes, and Marcelo Duarte Vilela. "Free-hand placement of high thoracic pedicle screws with the aid of fluoroscopy: evaluation of positioning by CT scans in a four-year consecutive series". In: *Arquivos de neuro-psiquiatria* 68.3 (2010), pp. 390–395.
- [14] Anna GU Brantley et al. "The Effects of Pedicle Screw Fit: An In Vitro Study." In: *Spine* 19.15 (1994), pp. 1752–1758.
- [15] M Brockway. "Anatomy of the epidural space". In: *Current Anaesthesia & Critical Care* 10.3 (1999), pp. 118–122.
- [16] David Burke and Richard G Hicks. "Surgical monitoring of motor pathways". In: *Journal of clinical neurophysiology* 15.3 (1998), pp. 194–205.

- [17] Torre M Bydlon et al. "Chromophore based analyses of steady-state diffuse reflectance spectroscopy: current status and perspectives for clinical adoption". In: *Journal of biophotonics* 8.1-2 (2015), pp. 9–24.
- [18] Mohamad Bydon et al. "Accuracy of C2 pedicle screw placement using the anatomic freehand technique". In: *Clinical neurology and neurosurgery* 125 (2014), pp. 24–27.
- [19] Christopher D Chaput et al. "Reduction in radiation (fluoroscopy) while maintaining safe placement of pedicle screws during lumbar spine fusion". In: *Spine* 37.21 (2012), E1305–E1309.
- [20] Renee Cocchi. *ECRI's Top 10 Health Technology Hazards for 2016*. 2015. URL: <http://www.healthcarebusinessstech.com/health-technology-hazards/> (visited on 01/04/2016).
- [21] Marco Crostelli, Osvaldo Mazza, and Massimo Mariani. "Free-hand pedicle screws insertion technique in the treatment of 120 consecutive scoliosis cases operated without use of intraoperative neurophysiological monitoring". In: *European Spine Journal* 21.1 (2012), pp. 43–49.
- [22] Guanyu Cui et al. "Morphologic evaluation of the thoracic vertebrae for safe free-hand pedicle screw placement in adolescent idiopathic scoliosis: a CT-based anatomical study". In: *Surgical and radiologic anatomy* 34.3 (2012), pp. 209–216.
- [23] Adrien E Desjardins et al. "Epidural needle with embedded optical fibers for spectroscopic differentiation of tissue: ex vivo feasibility study". In: *Biomedical optics express* 2.6 (2011), pp. 1452–1461.
- [24] Giovanni Di Leo et al. "Measurement of vertebral bone marrow lipid profile at 1.5-T proton magnetic resonance spectroscopy and bone mineral density at dual-energy X-ray absorptiometry: correlation in a swine model". In: *Skeletal radiology* 43.8 (2014), p. 1123.
- [25] Jeffrey C Dick et al. "Mechanical Evaluation of Cross-Link Designs in Rigid Pedicle Screw Systems". In: *Spine* 22.4 (1997), pp. 370–375.
- [26] Michael F Duffy et al. "Usefulness of electromyography compared to computed tomography scans in pedicle screw placement". In: *Spine* 35.2 (2010), E43–E48.
- [27] Nabil A Ebraheim et al. "Anatomic relations between the lumbar pedicle and the adjacent neural structures". In: *Spine* 22.20 (1997), pp. 2338–2341.
- [28] Pearson Education. *Gross Anatomy of the spinal cord*. 2004. URL: http://www.apsubiology.org/anatomy/2010/2010_Exam_Reviews/Exam_4_Review/CH_12_Gross_Anatomy_of_the_Spinal_Cord.htm.
- [29] Thomas J Farrell, Michael S Patterson, and Brian Wilson. "A diffusion theory model of spatially resolved, steady-state diffuse reflectance for the noninvasive determination of tissue optical properties invivo". In: *Medical physics* 19.4 (1992), pp. 879–888.
- [30] M Firbank et al. "Measurement of the optical properties of the skull in the wavelength range 650-950 nm". In: *Physics in medicine and biology* 38.4 (1993), p. 503.
- [31] Stephen T Flock et al. "Monte Carlo modeling of light propagation in highly scattering tissues. I. Model predictions and comparison with diffusion theory". In: *IEEE Transactions on Biomedical Engineering* 36.12 (1989), pp. 1162–1168.
- [32] Sotonye Fyनेface-Ogan. "Anatomy and clinical importance of the epidural space". In: *Epidural Analgesia-Current Views and Approaches* 12 (2012), pp. 1–12.
- [33] ROBERT W GAINES, C CRAIG SATTERLEE, GORDON I GROH, et al. "Experimental Evaluation of Seven Different Spinal Fracture Internal Fixation Devices Using Nonfailure Stability Testing: The Load-Sharing and Unstable-Mechanism Concepts." In: *Spine* 16.8 (1991), pp. 902–909.
- [34] Oliver P Gautschi et al. "Clinically relevant complications related to pedicle screw placement in thoracolumbar surgery and their management: a literature review of 35,630 pedicle screws". In: *Neurosurgical focus* 31.4 (2011), E8.

- [35] Florian T Gebhard et al. "Does computer-assisted spine surgery reduce intraoperative radiation doses?" In: *Spine* 31.17 (2006), pp. 2024–2027.
- [36] Ioannis D Gelalis et al. "Accuracy of pedicle screw placement: a systematic review of prospective in vivo studies comparing free hand, fluoroscopy guidance and navigation techniques". In: *European spine journal* 21.2 (2012), pp. 247–255.
- [37] GlobalData. *China's Spinal Fusion Market to Surge in Value and Double its Global Share by 2020*. 2014. URL: <http://healthcare.globaldata.com/media-center/press-releases/medical-devices/chinas-spinal-fusion-market-to-surge-in-value-and-double-its-global-share-by-2020-says-globaldata> (visited on 01/04/2016).
- [38] Simon R Goodyear et al. "A comparison of cortical and trabecular bone from C57 Black 6 mice using Raman spectroscopy". In: *Bone* 44.5 (2009), pp. 899–907.
- [39] Rob JM Groen and Hans Ponssen. "Vascular anatomy of the spinal epidural space: considerations on the etiology of the spontaneous spinal epidural hematoma". In: *Clinical anatomy* 4.6 (1991), pp. 413–420.
- [40] Phillip T Guillen et al. "Independent assessment of a new pedicle probe and its ability to detect pedicle breach: a cadaveric study: Laboratory investigation". In: *Journal of Neurosurgery: Spine* 21.5 (2014), pp. 821–825.
- [41] Alexander G Hadjipavlou et al. "Correlation of bone equivalent mineral density to pull-out resistance of triangulated pedicle screw construct." In: *Journal of Spinal Disorders & Techniques* 10.1 (1997), pp. 12–19.
- [42] Christopher L Hamill et al. "The use of pedicle screw fixation to improve correction in the lumbar spine of patients with idiopathic scoliosis: Is it warranted?" In: *Spine* 21.10 (1996), pp. 1241–1249.
- [43] WU Han et al. "Pedicle screw placement in the thoracic spine: a randomized comparison study of computer-assisted navigation and conventional techniques". In: *Chinese Journal of Traumatology (English Edition)* 13.4 (2010), pp. 201–205.
- [44] Maahir Ul Haque et al. "Radiation exposure during pedicle screw placement in adolescent idiopathic scoliosis: is fluoroscopy safe?" In: *Spine* 31.21 (2006), pp. 2516–2520.
- [45] Toru Hasegawa, Howard S An, and Victor M Hughton. "Imaging anatomy of the lateral lumbar spinal canal". In: 14.6 (1993), pp. 404–413.
- [46] Tonya Hines. *Anatomy of the Spine*. 2013. URL: <http://www.mayfieldclinic.com/PE-AnatSpine.htm#.VelCHZewtlk> (visited on 01/09/2015).
- [47] Quinn Hogan and Jeffrey Toth. "Anatomy of soft tissues of the spinal canal". In: *Regional anesthesia and pain medicine* 24.4 (1999), pp. 303–310.
- [48] Yoshihiro Hojo et al. "A multicenter study on accuracy and complications of freehand placement of cervical pedicle screws under lateral fluoroscopy in different pathological conditions: CT-based evaluation of more than 1,000 screws". In: *European Spine Journal* 23.10 (2014), pp. 2166–2174.
- [49] Yoshimoto Ishikawa et al. "Clinical accuracy of three-dimensional fluoroscopy-based computer-assisted cervical pedicle screw placement: a retrospective comparative study of conventional versus computer-assisted cervical pedicle screw placement: Clinical article". In: *Journal of Neurosurgery: Spine* 13.5 (2010), pp. 606–611.
- [50] Pierre Jérôme. *SpineGuard*. 2009. URL: <http://www.spineguard.com/company/> (visited on 01/04/2016).
- [51] Yongjung J Kim et al. "Free hand pedicle screw placement in the thoracic spine: is it safe?" In: *Spine* 29.3 (2004), pp. 333–342.
- [52] Young-Woo Kim et al. "Free-hand pedicle screw placement during revision spinal surgery: analysis of 552 screws". In: *Spine* 33.10 (2008), pp. 1141–1148.
- [53] Heiko Koller et al. "In vitro study of accuracy of cervical pedicle screw insertion using an electronic conductivity device (ATPS part III)". In: *European Spine Journal* 18.9 (2009), pp. 1300–1313.

- [54] Christos Kontoyannis, Malvina Orkoula, and Konstantinos Kalonakis. "Analysis of bone composition with Raman spectroscopy". In: *Πρακτικά 13ου Πανελληνίου Φαρμακευτικού Συνεδρίου* (2012).
- [55] Christos Kontoyannis, Malvina Orkoula, and Ioannis Karampas. "New methodologies for the quantification of the constituents of bone by Raman spectroscopy". In: *Η Φαρμακευτική στον 21ο αιώνα* (2012).
- [56] Victor Kosmopoulos and Constantin Schizas. "Pedicle screw placement accuracy: a meta-analysis". In: *Spine* 32.3 (2007), E111–E120.
- [57] Gerit Kulik et al. "A CT-based study investigating the relationship between pedicle screw placement and stimulation threshold of compound muscle action potentials measured by intraoperative neurophysiological monitoring". In: *European Spine Journal* 22.9 (2013), pp. 2062–2068.
- [58] T Laine et al. "Accuracy of pedicle screw insertion: a prospective CT study in 30 low back patients". In: *European Spine Journal* 6.6 (1997), pp. 402–405.
- [59] Melvin Law, Allan F Tencer, and Paul A Anderson. "Caudo-cephalad loading of pedicle screws: mechanisms of loosening and methods of augmentation." In: *Spine* 18.16 (1993), pp. 2438–2443.
- [60] Chang-Hyun Lee et al. "Can triggered electromyography thresholds assure accurate pedicle screw placements? A systematic review and meta-analysis of diagnostic test accuracy". In: *Clinical Neurophysiology* (2014).
- [61] Gang Li et al. "Complications associated with thoracic pedicle screws in spinal deformity". In: *European Spine Journal* 19.9 (2010), pp. 1576–1584.
- [62] Weitao Li, Yangyang Liu, and Zhiyu Qian. "Determination of detection depth of optical probe in pedicle screw measurement device". In: *Biomedical engineering online* 13.1 (2014), p. 1.
- [63] Xiaojuan Li et al. "Quantification of vertebral bone marrow fat content using 3 Tesla MR spectroscopy: reproducibility, vertebral variation, and applications in osteoporosis". In: *Journal of Magnetic Resonance Imaging* 33.4 (2011), pp. 974–979.
- [64] Cristian Linte, John Moore, Terry M Peters, et al. "How accurate is accurate enough? A brief overview on accuracy considerations in image-guided cardiac interventions". In: *Engineering in Medicine and Biology Society (EMBC), 2010 Annual International Conference of the IEEE. IEEE. 2010*, pp. 2313–2316.
- [65] Yangyang Liu et al. "Monitoring the reduced scattering coefficient of bone tissues on the trajectory of pedicle screw placement using near-infrared spectroscopy". In: *Journal of biomedical optics* 19.11 (2014), pp. 117002–117002.
- [66] John E Lonstein et al. "Complications associated with pedicle screws*". In: *The Journal of Bone & Joint Surgery* 81.11 (1999), pp. 1519–28.
- [67] Gary Lynn et al. "Mechanical stability of thoracolumbar pedicle screw fixation: The effect of crosslinks". In: *Spine* 22.14 (1997), pp. 1568–1572.
- [68] Amir Manbachi, Richard SC Cobbold, and Howard J Ginsberg. "Guided pedicle screw insertion: techniques and training". In: *The Spine Journal* 14.1 (2014), pp. 165–179.
- [69] Elaine Nicpon Marieb and Katja Hoehn. *Human anatomy & physiology*. Pearson Education, 2007.
- [70] Markets and Markets. *Spinal Implants and Spinal Devices Market worth 15.73 Billion USD by 2020*. 2014. URL: <http://www.marketsandmarkets.com/PressReleases/spine-surgery-devices.asp> (visited on 01/04/2016).
- [71] Alexander Mason et al. "The accuracy of pedicle screw placement using intraoperative image guidance systems: A systematic review". In: *Journal of Neurosurgery: Spine* 20.2 (2014), pp. 196–203.
- [72] F Mc Lain Robert, Timothy A Moseley, Neil A Sharkey, et al. "Lumbar pedicle screw salvage: pullout testing of three different pedicle screw designs." In: *Journal of Spinal Disorders & Techniques* 8.1 (1995), pp. 62–68.

- [73] A. McWilliams. *Medical robotics and computer assisted surgery, the global market*. 2011. URL: <http://www.bccresearch.com/market-research/healthcare/robotics-computer-surgery-market-hlc036d.html> (visited on 11/06/2015).
- [74] Houston Methodist leading medicine. *A Patients Guide to Intraoperative Monitoring*. 2009. URL: <http://www.houstonmethodist.org/orthopedics/where-does-it-hurt/back/intraoperative-monitoring/> (visited on 01/04/2016).
- [75] Medipoint. *Spinal Fusion – Global Analysis and Market Forecasts*. 2014. URL: <http://store.globaldata.com/market-reports/medical-devices/medipoint-spinal-fusion-global-analysis-and-market-forecasts#.VpgMz1KnH6k> (visited on 01/04/2016).
- [76] Grzegorz Miekisiak et al. "Accuracy of the Free-hand Placement of Pedicle Screws in the Lumbosacral Spine Using a Universal Entry Point: Clinical Validation". In: *Journal of spinal disorders & techniques* 28.4 (2015), E194–E198.
- [77] Hitesh Modi et al. "Accuracy of thoracic pedicle screw placement in scoliosis using the ideal pedicle entry point during the freehand technique". In: *International orthopaedics* 33.2 (2009), pp. 469–475.
- [78] Rouzbeh Motiei-Langroudi and Homa Sadeghian. "Assessment of pedicle screw placement accuracy in thoracolumbosacral spine using freehand technique aided by lateral fluoroscopy: results of postoperative computed tomography in 114 patients". In: *The Spine Journal* 15.4 (2015), pp. 700–704.
- [79] Rami Nachabé et al. "Estimation of biological chromophores using diffuse optical spectroscopy: benefit of extending the UV-VIS wavelength range to include 1000 to 1600 nm". In: *Biomedical optics express* 1.5 (2010), pp. 1432–1442.
- [80] Rami Nachabé et al. "Estimation of lipid and water concentrations in scattering media with diffuse optical spectroscopy from 900to1600nm". In: *Journal of biomedical optics* 15.3 (2010), pp. 037015–037015.
- [81] Christopher Nafis et al. "Method for estimating dynamic EM tracking accuracy of surgical navigation tools". In: *Medical Imaging*. International Society for Optics and Photonics. 2006, 61410K–61410K.
- [82] Edin Nevzati et al. "Accuracy of Pedicle Screw Placement in the Thoracic and Lumbar Spine Using a Conventional Intraoperative Fluoroscopy-Guided Technique: A National Neurosurgical Education and Training Center Analysis of 1236 Consecutive Screws". In: *World neurosurgery* 82.5 (2014), pp. 866–871.
- [83] RWD Nickalls and MS Kokri. "The width of the posterior epidural space in obstetric patients". In: *Anaesthesia* 41.4 (1986), pp. 432–433.
- [84] Eric W Nottmeier, Will Seemer, and Phillip M Young. "Placement of thoracolumbar pedicle screws using three-dimensional image guidance: experience in a large patient cohort: Clinical article". In: *Journal of Neurosurgery: Spine* 10.1 (2009), pp. 33–39.
- [85] nuvasive. *NVM5 nerve monitoring system*. 2016. URL: <http://www.nuvasive.com/patient-solutions/nuvasive-integrated-surgical-solutions/nvm5-nerve-monitoring-system/> (visited on 01/11/2016).
- [86] Jeffrey S Nyman et al. "Measuring differences in compositional properties of bone tissue by confocal Raman spectroscopy". In: *Calcified tissue international* 89.2 (2011), pp. 111–122.
- [87] Matthias F Oertel et al. "Clinical and methodological precision of spinal navigation assisted by 3D intraoperative O-arm radiographic imaging: technical note". In: *Journal of Neurosurgery: Spine* 14.4 (2011), pp. 532–536.
- [88] Medipark Omurga. *Medical devices*. 2013. URL: <https://www.linkedin.com/company/medipark-omurga-implantlar%C4%B1-d%C4%B1%C5%9F-tic-ltd-%C5%9Fti-> (visited on 01/10/2016).

- [89] OpenWetWare. *General depiction of an individual vertebra with labeled structures*. 2016. URL: http://openwetware.org/wiki/Artificial_Vertebrae,_by_Matthew_McNulty.
- [90] Dror Ovadia et al. "The contribution of an electronic conductivity device to the safety of pedicle screw insertion in scoliosis surgery". In: *Spine* 36.20 (2011), E1314–E1321.
- [91] Burak M Ozgur et al. "Automated intraoperative EMG testing during percutaneous pedicle screw placement". In: *The Spine Journal* 6.6 (2006), pp. 708–713.
- [92] Thomas N Pajewski, Vincent Arlet, and Lawrence H Phillips. "Current approach on spinal cord monitoring: the point of view of the neurologist, the anesthesiologist and the spine surgeon". In: *European Spine Journal* 16.2 (2007), pp. 115–129.
- [93] Daniel K Park et al. "Percutaneous lumbar and thoracic pedicle screws: a trauma experience". In: *Journal of spinal disorders & techniques* 27.3 (2014), pp. 154–161.
- [94] Paul Park et al. "Minimally invasive pedicle screw fixation utilizing O-arm fluoroscopy with computer-assisted navigation: Feasibility, technique, and preliminary results". In: *Surgical neurology international* 1.1 (2010), p. 44.
- [95] Yung Park and Joong Won Ha. "Comparison of one-level posterior lumbar interbody fusion performed with a minimally invasive approach or a traditional open approach". In: *Spine* 32.5 (2007), pp. 537–543.
- [96] Scott L Parker et al. "Accuracy of free-hand pedicle screws in the thoracic and lumbar spine: analysis of 6816 consecutive screws". In: *Neurosurgery* 68.1 (2011), pp. 170–178.
- [97] Purvi Shantilal Patel. "Screw fixation of implants to the spine". PhD thesis. University of Birmingham, 2010.
- [98] Chan Wearn Benedict Peng et al. "Clinical and radiological outcomes of minimally invasive versus open transforaminal lumbar interbody fusion". In: *Spine* 34.13 (2009), pp. 1385–1389.
- [99] A Pfuntner, LM Wier, and C Stocks. "Most frequent procedures performed in US Hospitals, 2010: Statistical Brief# 149". In: (2013).
- [100] Frank A Pintar et al. "Rotational stability of a spinal pedicle screw/rod system." In: *Journal of Spinal Disorders & Techniques* 8.1 (1995), pp. 49–55.
- [101] Mekhala Raghavan. "Investigation of Mineral and Collagen Organization in Bone Using Raman Spectroscopy". PhD thesis. University of Michigan, 2011.
- [102] Sean S Rajae et al. "Spinal fusion in the United States: analysis of trends from 1998 to 2008". In: *Spine* 37.1 (2012), pp. 67–76.
- [103] S Rajasekaran, P Rishi Mugesh Kanna, and Ajoy Prasad Shetty. "Safety of cervical pedicle screw insertion in children: a clinicoradiological evaluation of computer-assisted insertion of 51 cervical pedicle screws including 28 subaxial pedicle screws in 16 children". In: *Spine* 37.4 (2012), E216–E223.
- [104] Darryl A Raley and Ralph J Mobbs. "Retrospective computed tomography scan analysis of percutaneously inserted pedicle screws for posterior transpedicular stabilization of the thoracic and lumbar spine: accuracy and complication rates". In: *Spine* 37.12 (2012), pp. 1092–1100.
- [105] Y Raja Rampersaud et al. "Radiation exposure to the spine surgeon during fluoroscopically assisted pedicle screw insertion". In: *Spine* 25.20 (2000), pp. 2637–2645.
- [106] James P Rathmell et al. "Identification of the Epidural Space with Optical Spectroscopy-An In Vivo Swine Study". In: *The Journal of the American Society of Anesthesiologists* 113.6 (2010), pp. 1406–1418.
- [107] ReportsnReports. *Global Spine Surgery Market 2015-2019*. 2015. URL: <http://www.reportsnreports.com/reports/435886-global-spine-surgery-market-2015-2019.html> (visited on 01/04/2016).

- [108] Holger Ritzel et al. "The Thickness of Human Vertebral Cortical Bone and its Changes in Aging and Osteoporosis: A Histomorphometric Analysis of the Complete Spinal Column from Thirty-Seven Autopsy Specimens". In: *Journal of Bone and Mineral Research* 12.1 (1997), pp. 89–95.
- [109] Mark A Rivkin, Jessica F Okun, and Steven S Yocom. "Novel free-hand T1 pedicle screw method: Review of 44 consecutive cases". In: *Journal of neurosciences in rural practice* 5.4 (2014), p. 349.
- [110] CHARLES M RULAND et al. "Triangulation of Pedicular Instrumentation: A Biomechanical Analysis." In: *Spine* 16.6S (1991), S270–S276.
- [111] Amer F Samdani et al. "Triggered electromyography for placement of thoracic pedicle screws: is it reliable?" In: *European Spine Journal* 20.6 (2011), pp. 869–874.
- [112] Matthew R Sanborn et al. "Cost-effectiveness of confirmatory techniques for the placement of lumbar pedicle screws". In: *Neurosurgical focus* 33.1 (2012), E12.
- [113] C Rebecca Simpson et al. "Near-infrared optical properties of ex vivo human skin and subcutaneous tissues measured using the Monte Carlo inversion technique". In: *Physics in medicine and biology* 43.9 (1998), p. 2465.
- [114] Harvey E Smith et al. "Comparison of radiation exposure in lumbar pedicle screw placement with fluoroscopy vs computer-assisted image guidance with intraoperative three-dimensional imaging". In: *The journal of spinal cord medicine* 31.5 (2008), p. 532.
- [115] L. Solomon. *Spinal surgical devices: technologies and global markets*. 2010. URL: <http://www.bccresearch.com/market-research/healthcare/spinal-surgical-devices-hlc075a.html> (visited on 11/06/2015).
- [116] Ameliyat Sonras, Çekilen Bilgisayarl, and Tomografi Görüntülerinde Pedikül. "Postoperative computed tomography assessment of pedicle screw placement accuracy". In: *Turkish neurosurgery* 20.4 (2010), pp. 500–507.
- [117] Virginia spine specialists. *How to make your spinal fusion surgery a success*. 2015. URL: <http://www.virginiaspinespecialists.com/make-spinal-fusion-surgery-success/> (visited on 01/10/2016).
- [118] Kathryn J Stevens et al. "Comparison of minimally invasive and conventional open posterolateral lumbar fusion using magnetic resonance imaging and retraction pressure studies". In: *Journal of spinal disorders & techniques* 19.2 (2006), pp. 77–86.
- [119] F Tabaraud et al. "Monitoring of the motor pathway during spinal surgery." In: *Spine* 18.5 (1993), pp. 546–550.
- [120] Jinshan Tang et al. "Position and complications of pedicle screw insertion with or without image-navigation techniques in the thoracolumbar spine: a meta-analysis of comparative studies". In: *Journal of biomedical research* 28.3 (2014), p. 228.
- [121] Nai-Feng Tian and Hua-Zi Xu. "Image-guided pedicle screw insertion accuracy: a meta-analysis". In: *International orthopaedics* 33.4 (2009), pp. 895–903.
- [122] Nai-Feng Tian et al. "Pedicle screw insertion accuracy with different assisted methods: a systematic review and meta-analysis of comparative studies". In: *European Spine Journal* 20.6 (2011), pp. 846–859.
- [123] Chien-Kun Ting and Yin Chang. "Technique of fiber optics used to localize epidural space in piglets". In: *Optics express* 18.11 (2010), pp. 11138–11147.
- [124] Valerii Tuchin. *Tissue optics: light scattering methods and instruments for medical diagnosis*.
- [125] Peter Ullrich. *Scoliosis Surgery*. 2004. URL: <http://www.spine-health.com/conditions/scoliosis/scoliosis-surgery> (visited on 01/10/2016).
- [126] unknown. *What is Scoliosis?* 2015. URL: <https://thelifeweliveandeverythingelseinbetween.wordpress.com/2015/02/11/what-is-scoliosis/>.
- [127] Jed S Vanichkachorn et al. "Potential large vessel injury during thoracolumbar pedicle screw removal: a case report". In: *Spine* 22.1 (1997), pp. 110–113.

- [128] Rajeev Verma et al. "Functional outcome of computer-assisted spinal pedicle screw placement: a systematic review and meta-analysis of 23 studies including 5,992 pedicle screws". In: *European Spine Journal* 19.3 (2010), pp. 370–375.
- [129] A Voloshin and J Wosk. "An in vivo study of low back pain and shock absorption in the human locomotor system". In: *Journal of biomechanics* 15.1 (1982), pp. 21–27.
- [130] Hung-Chen Wang et al. "Computer-assisted pedicle screw placement for thoracolumbar spine fracture with separate spinal reference clamp placement and registration". In: *Surgical neurology* 69.6 (2008), pp. 597–601.
- [131] Lihong Wang, Steven L Jacques, and Liqiong Zheng. "MCML—Monte Carlo modeling of light transport in multi-layered tissues". In: *Computer methods and programs in biomedicine* 47.2 (1995), pp. 131–146.
- [132] Vincent Y Wang et al. "Free-hand thoracic pedicle screws placed by neurosurgery residents: a CT analysis". In: *European Spine Journal* 19.5 (2010), pp. 821–827.
- [133] Yingsong Wang et al. "Computed tomography assessment of lateral pedicle wall perforation by free-hand subaxial cervical pedicle screw placement". In: *Archives of orthopaedic and trauma surgery* 133.7 (2013), pp. 901–909.
- [134] Robert Green Watkins IV, Akash Gupta, and Robert Green Watkins III. "Cost-effectiveness of image-guided spine surgery". In: *The open orthopaedics journal* 4 (2010), p. 228.
- [135] Audrey J Weiss, Anne Elixhauser, and Roxanne M Andrews. "Characteristics of operating room procedures in US hospitals, 2011". In: (2014).
- [136] Ashley J Welch and Martin JC Van Gemert. *Optical-thermal response of laser-irradiated tissue*. Vol. 2. Springer, 2011.
- [137] Jon L Westbrook. "Anatomy of the epidural space". In: *Anaesthesia & Intensive Care Medicine* 13.11 (2012), pp. 551–554.
- [138] YMD Wicharn, H Narapong, and L Sukalaya. "The Accuracy of Pedicle Screw Placement in Thoracic Spine Using the Funnel Technique in Idiopathic Scoliosis". In: *J Med Assoc Thai* 90.1 (2007).
- [139] Andrew D Wiles, David G Thompson, and Donald D Frantz. "Accuracy assessment and interpretation for optical tracking systems". In: *Medical Imaging 2004*. International Society for Optics and Photonics. 2004, pp. 421–432.
- [140] Martin James Wood and Jason McMillen. "The surgical learning curve and accuracy of minimally invasive lumbar pedicle screw placement using CT based computer-assisted navigation plus continuous electromyography monitoring—a retrospective review of 627 screws in 150 patients". In: *International journal of spine surgery* 8 (2014), p. 1.
- [141] Benson P Yang, Melvin M Wahl, and Cary S Idler. "Percutaneous lumbar pedicle screw placement aided by computer-assisted fluoroscopy-based navigation: perioperative results of a prospective, comparative, multicenter study". In: *Spine* 37.24 (2012), pp. 2055–2060.
- [142] Kazunori Yone et al. "Indication of fusion for lumbar spinal stenosis in elderly patients and its significance". In: *Spine* 21.2 (1996), pp. 242–248.
- [143] Sharon C Yson et al. "Comparison of cranial facet joint violation rates between open and percutaneous pedicle screw placement using intraoperative 3-D CT (O-arm) computer navigation". In: *Spine* 38.4 (2013), E251–E258.
- [144] MI Yusof, LK Ming, and MS Abdullah. "Computed tomographic measurement of cervical pedicles for transpedicular fixation in a Malay population". In: (2007).
- [145] Reinhard Zeller et al. "Technique for drilling instrument monitoring electrical conductivity in pediatric cervical spine screw insertion: a preliminary report". In: *Journal of Pediatric Orthopaedics* 29.7 (2009), pp. 760–764.
- [146] Ying Zhang et al. "Thoracic pedicle classification determined by inner cortical width of pedicles on computed tomography images: its clinical significance for posterior vertebral column resection to treat rigid and severe spinal deformities—a retrospective review of cases". In: *BMC musculoskeletal disorders* 15.1 (2014), p. 278.

-
- [147] Changfang Zhu et al. "Diagnosis of breast cancer using fluorescence and diffuse reflectance spectroscopy: a Monte-Carlo-model-based approach". In: *Journal of biomedical optics* 13.3 (2008), pp. 034015–034015.
- [148] Willem Gerrit Zijlstra, Anneke Buursma, and Onno Willem van Assendelft. *Visible and near infrared absorption spectra of human and animal haemoglobin: determination and application*. VSP, 2000.
- [149] George Zonios and Aikaterini Dimou. "Light scattering spectroscopy of human skin in vivo". In: *Optics Express* 17.3 (2009), pp. 1256–1267.